
Master Thesis

Detection and quantification of blast-induced cracks in small scale bench blasting

This project develops a methodology for the detection and quantification of blast-induced cracks in small scale bench blasts.

Juan Navarro Miguel

Date(30/01/2015)



Chair of Mining Engineering and Mineral Economics
Department Mineral Resources and Petroleum Engineering
Motanuniversitaet Leoben

A-8700 LEOBEN, Franz Josef Straße 18
Phone: +43/(0)3842-402-2001
Fax: +43/(0)3842-402-2002
bergbau@unileoben.ac.at

Declaration of authorship

„I declare in lieu of oath that this thesis is entirely my own work except where otherwise indicated. The presence of quoted or paraphrased material has been clearly signaled and all sources have been referred. The thesis has not been submitted for a degree at any other institution and has not been published yet.”

Preface, Dedication, Acknowledgement

First at all, I would like to acknowledge this Master Thesis to Montanuniversität Leoben, and especially Prof. Peter Moser, for the opportunity of being part of this research project promoted by the Chair of Mining Engineering and Mineral Economics, from which this Master Thesis was developed.

I would like to express my sincere gratitude to Prof. Finn Ouchterlony, my supervisor in this thesis, for his help and advice for the development of this Thesis and especially his great contribution on the day to day, teaching me and forming me.

I also wish to acknowledge to Peter Schimek and Radoslava Ivanova for their advice and teaching transmitted during this time.

I would like to thank José Ángel Sanchidrián, Pablo Segarra, Lina María Lopez and Ricardo Castedo for their help in the development of the damage maps calculation.

Finally, I would like to thank Diego Herrera for his help with grammatical advice during this Thesis and my friends and family for their constant support during the writing of this document.

Abstract

In order to understand how the cracks are generated in the surrounding rock during a bench blast, it is important to classify and quantify them. This thesis is developing a 3D model of the cracks generated in small scale blasting tests. By a visualization of the internal crack network it becomes possible to describe how and where the cracks are created.

To obtain the 3D model, the blasted specimen is cut into several slices. Then dye-penetrant is applied to the cut surfaces and the crack trace patterns are photographed. Each slice represents a vertical or horizontal cut through the specimen. These trace patterns are then used to create digital 3D models in AutoCAD.

From the AutoCAD models trace, angles and lengths can be measured and trace connections between the different levels drawn. Crack families can be identified based on angles, lengths and origin and characteristics in terms of crack density and intersection densities e.g. can be determined.

The proposed crack quantification method and the results obtained with it will be combined with the fragmentation and surface roughness results in other projects where model scale blasting was used to verify how crack development from previous blast influences rock fragmentation in subsequent blasts.

Results show that if blocks are blasted with different delay time between rows and holes, the longer the delay time, the higher the number of cracks, the more homogenous the distribution of radial cracks around the borehole and the greater damage in the block. In addition, an influence on the number of cracks has been shown, if different delay times are used only in the first row.

Zusammenfassung

Um den Prozess der durch Sprengungen ins anstehende Gebirge induzierten Risse verstehen zu können, ist es wichtig diese entstehenden Risse zu quantifizieren. Diese Master-Arbeit entwickelt ein 3D-Modell der bei kleinmaßstäblichen Sprengversuchen im anstehenden Gebirge entstehenden Risse. Durch diese Visualisierung der internen Riss-Netzwerke ist es möglich die Ursachen sowie räumlichen Anordnungen der Risse zu ermitteln.

Um das 3D-Modell zu generieren wird der gesprengte Probekörper in mehrere verschiedene Scheiben aufgeschnitten. Auf diesen erhaltenen Oberflächen, welche horizontale oder vertikale Schnitte durch den Probekörper darstellen, werden durch das Aufbringen von Penetriermittel die eingetragenen Risse sichtbar. Mithilfe von AutoCAD wird in weiterer Folge ein digitales 3D-Modell der Risse im Probekörper erstellt.

Aus diesen digitalen Modellen kann der Verlauf, der Winkel und die Länge der Risse sowie deren Verbindungen zwischen den verschiedenen Ebenen ermittelt werden. Daraus kann eine Einteilung in Rissfamilien bezüglich der unterschiedlichen Winkel, Längen und deren Ursprung erfolgen sowie Kennwerte bezüglich der Rissdichte und der Schnittpunkte der Risse ermittelt werden.

Die entwickelte Methode zur Quantifizierung von induzierten Rissen sowie die Ergebnisse daraus werden in weiterer Folge mit den Resultaten von Zerkleinerungs- und Oberflächenanalysen anderer Projekte kombiniert, um den Einfluss der induzierten Risse von vorangegangenen Sprengungen auf die Zerkleinerung der weiteren Sprengungen detektieren zu können.

Als Ergebnis zeigte sich bei Sprengungen in Betonblöcken, dass je länger die Verzögerungen zwischen den Bohrlöchern sind, desto größer ist die Anzahl der induzierten Risse, die Homogenität der Verteilung der Radialrisse um die Bohrlöcher und auch die Schädigung in den Blöcken. Weiters zeigte sich auch, dass bereits lediglich eine Veränderung der Verzögerung der ersten Reihe einen erheblichen Einfluss auf die Anzahl der entstehenden Risse hinter der dritten Reihe erwirkt.

Table of contents

Declaration of authorship.....	II
Preface, Dedication, Acknowledgement.....	III
Abstract.....	IV
Zusammenfassung.....	V
Table of contents.....	VI
1 INTRODUCTION.....	1
2 TEST SET UP.....	2
2.1 Testing blocks.....	3
2.1.1 Sequence of shots.....	4
2.1.2 Preparation of testing blocks after blasting.....	6
3 CRACK DETECTION METHODS.....	7
3.1 3D tomography.....	7
3.2 Crack detection analysis: 3D model.....	10
3.2.1 Documentation of crack detection analysis.....	11
3.2.2 Dye penetrant method.....	14
3.2.3 Preparation of data for 3D model design.....	15
3.2.4 3D model design.....	19
4 ANALYSIS OF DATA.....	24
4.1 Objective network measures for horizontal section.....	24
4.1.1 Crack families.....	24
4.1.2 Comparison between documented cracks types in section 3.2.1 and crack types found in section 4.1.1.....	31
4.2 Objective network measures for vertical section.....	32
4.2.1 Crack Types.....	32
4.3 Crack density analysis.....	35
4.3.1 Design of the grid.....	35
4.3.2 Criteria to choose the crack density values.....	36
4.3.3 Design of damage map from crack density.....	37
4.3.4 Comparison between different sizes of grid.....	39
4.3.5 Classification of slices according to the damage map.....	41
4.3.6 Crack intersection density analysis.....	42
5 RESULTS.....	43

5.1	Data analysis criteria	43
5.2	Crack development comparison using different delay time	44
5.3	Data analysis.....	45
5.3.1	Crack family analysis between slices surfaces and blocks.....	45
5.3.2	Crack family analysis between blocks	50
5.3.3	Radial crack distribution	61
5.3.4	Damage map analysis.....	68
6	CONCLUSIONS.....	74
7	Bibliography	78
8	List of figures.....	80
9	List of tables.....	91
	Annex table of contents.....	I
	ANNEX I: Crack patterns pictures	II
	ANNEX II: Digital picture of horizontal sections of slice surfaces.	VI
	ANNEX III: Digital picture of vertical sections of slice surfaces.	XVII
	ANNEX IV: Crack families detection.....	XXI
	ANNEX V: Crack density damage maps	XXVII
	ANNEX VI: Intersection crack density damage maps.....	XXXVI
	ANNEX VII: ANOVA F-Test an Kruskal Wallis methods.....	XLV
	ANNEX VIII: Data crack detection families.....	LI
	ANNEX IX: Comparison between data when using all the crack information from the slice and when using only cracks inside the edges	LVII

1 INTRODUCTION

During the last few years several scale blasting tests have been done at the Chair of Mining Engineering (Schimek et al. 2012). According to that project, the first part was a comparison of the fragmentation of shots in a row with finite delay (whole row shot in one blast) with that of shots in a row with infinite delay (a succession of single hole shots). Both types of shots were done in virgin material (first row) and in already damaged material (second row). The fragmentation was quantified by doing a sieving analysis of the blasted material from each shots sequence and the determination of sieving parameters and sieving curves.

The second part was the comparison of cracks induced by blasting. The comparison was done by surface observations and by post-blast sampling of drill-cores of the interesting parts of the material. In addition, thin sections were cut to analyze radial crack development.

Following the same methodology in both parts, new specimens were blasted during 2013. In this case a comparison of fragmentation using different delay times in the sequence for each row (blasting one row at a time) was done.

As an extension to the testing plan during 2013, the goal of the current thesis is then to analyze the induced cracks in the new specimens with an alternative procedure, in order to study and compare the damage by crack development created in the remaining (non-blasted) part of the testing blocks.

2 TEST SET UP

As explained in Schimek et al. (2012), the blasting site of the Chair of Mining Engineering at the Styrian Erzberg was developed during a master thesis (Maierhofer 2011). In it, a yoke within the walls of the blasting site was used, to allow waves to escape from test specimen (figure 2.1)



Figure 2.1: Yoke within the walls of the blasting site.

The gap between the yoke and the walls was filled with compacted sand, which transmitted about 70 % of the blasting waves into surrounding rock. The yoke also has space where the smaller testing blocks fit into. These small testing blocks, which are made of magnetic mortar (magnetite concrete), are placed on a mat cut out from a used conveyor belt. At the sides and at the back the block is grouted into the yoke by using fast hardening cement, which has the similar material properties as those of the blocks.

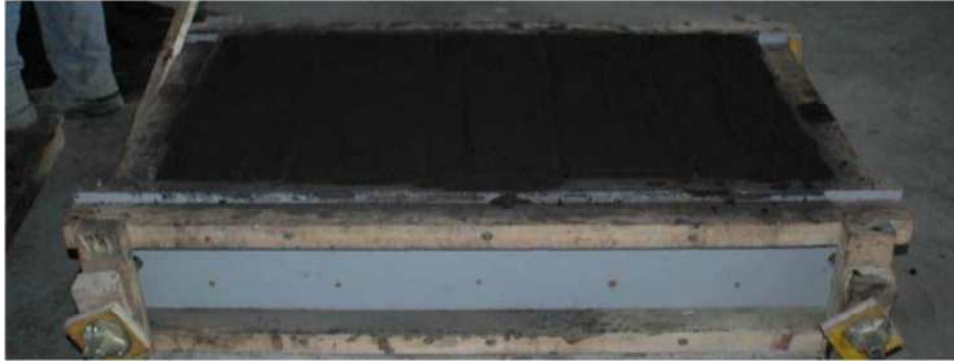


Figure 2.2: Sample blocks formwork (Schimek, 2012)

2.1 Testing blocks

The basic ingredients and proportions of the magnetite mortar from which testing blocks were cast can be seen in table 2.2. As is explained in Schimek et al. (2012), the recipe had the same proportions as used for small-scale tests at the Luleå Univ. Techn. (Johansson 2008) but used magnetite from Ferroxon instead of Minelco.

Ingredient	[%]
Portlandcement CEM II/A-M 42.5 N	25.60
Water	12.65
Glenium 361 (Plasticizer)	0.256
DCC-Entlüfter (Defoamer)	0.129
Magnetite powder (Ferroxon 618)	29.65
Quartz sand 0.1-0.5 mm (Me 31)	31.70

Table 2.1: Ingredients and proportions of magnetite mortar

The magnetite mortar was produced by a precast concrete plant because they were able to produce large batches of the concrete, about 680 kg. Therefore, within each batch, the produced samples should have the same properties.

The dimensions of the testing blocks used in this project were 660x280x210 mm (*LxHxW*) – The same as Johansson & Ouchterlony (2012). The blast holes were

drilled in the laboratory. The equipment used was a core-drill and the diameter was 10 mm. The reason to use this equipment was that the spalling effect at the bottom of the blocks and the deviation of the blastholes were minimized, compared with hammer drilling.

2.1.1 Sequence of shots

From the specimens blasted during year 2013, eight were analyzed during this project. As is shown in the table 2.1, the specimens were drilled with five boreholes per row. There is also one block with 7 boreholes per row, which belongs to a different project. The side-spacing of the blastholes was 110 mm (5 holes per row. Figure 2.3) and 95 mm (7 holes per row. Figure 2.4). The burden between rows was 70 mm. This arrangement gives a ratio of side-spacing to burden (S/B) of 1.57 and 1.36 respectively.

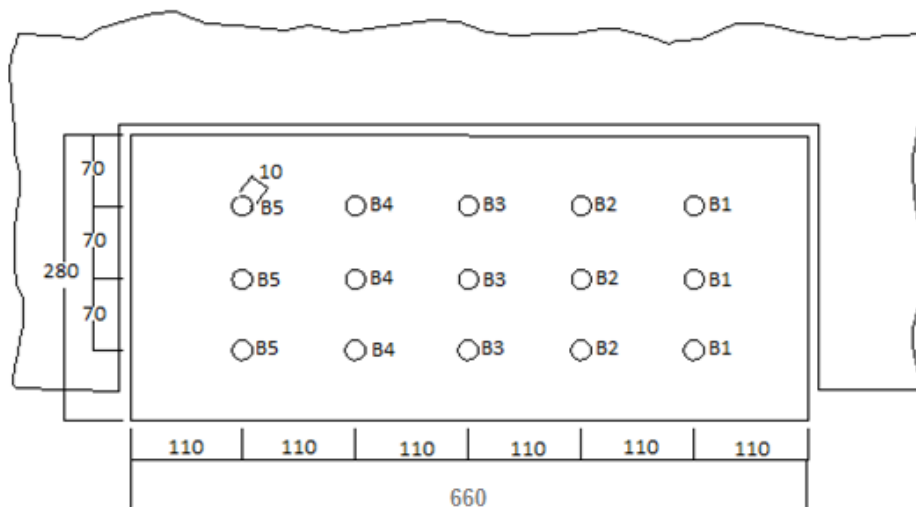


Figure 2.3: Design of the block for 5 blastholes

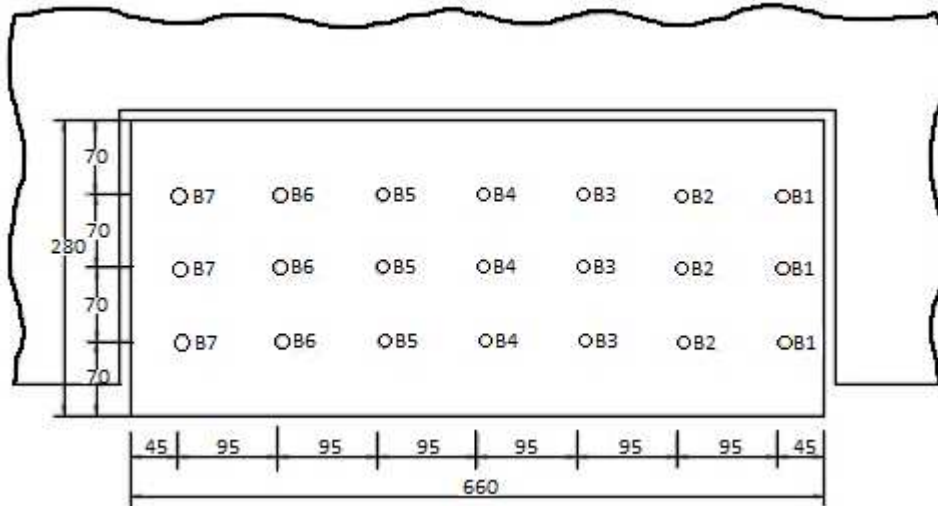


Figure 2.4: Design of the block for 7 blastholes

The specimens were blasted row per row, collecting the fragments blasted of each shot before blasting the following row. The delay time used between holes for each row was different (table 2.2), allowing the study of the influence of delay time on fragmentation.

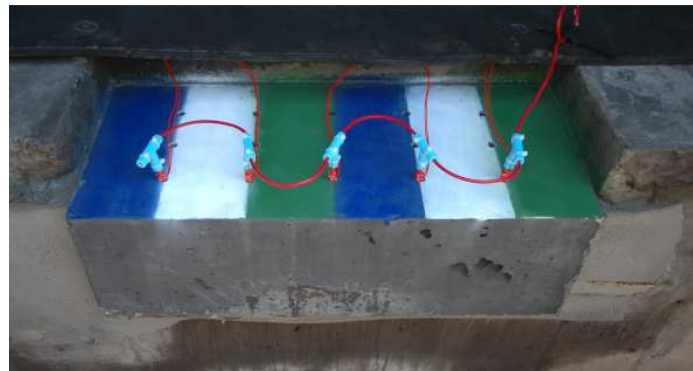


Figure 2.5: Initiation from top



Figure 2.6: Front view after blasting of: a) 1st row; b) 2nd row; c) 3rd row

The initiation was done from the top to the bottom of the borehole and from right to left (table 2.2; figures 2.3, 2.4). The explosive used for blasting the specimens was 20 g/m detonating cord. Knowing the transmission velocity of detonating cord is constant; to achieve different delay time it was necessary change the length of a 5 g/m cord which connects the boreholes.

Specimen	Rows	Holes per row	Delay time per hole and row (μ s)	Type of initiation
CH01B01	3	7	140-140-140	Right to left
CH02B01	3	5	0-0-0	Right to left
CH02B02	3	5	28-28-28	Right to left
CH02B03	3	5	140-0-0	Right to left
CH02B04	3	5	73-73-73	Right to left
CH02B05	3	5	28-140	Right to left
CH03B04	3	5	28-73-73	Right to left
CH03B05	3	5	28-0-0	Right to left

Table 2.2: Information about testing blocks

The assigned name to each block means:

- CH0 n^o: batch of the concrete block made by the precast concrete plant.
- B0 n^o: order in which the block was cast

2.1.2 Preparation of testing blocks after blasting

Once all three rows were blasted, there was a remaining part of the testing block: the backside of the last row (row 3). This part was influenced by cracks developed during the blasting of previous rows: in the work called blast induced cracks.

To study the properties of these induced cracks, this remaining part of the specimen had to be removed from the yoke. For that, and due to its high degree of damage, part of the already blasted volume in front of the remaining part was filled with fast hardening cement (figure 2.7).



Figure 2.7: Testing block filled with fast hardening cement in front.

3 CRACK DETECTION METHODS

To study induced crack by blasting, several methods were used. Each of them will be described in the following sections.

3.1 3D tomography

According to tomography principles explained by the company NANOXCT (www.nanoxct.eu), laboratory 3D X-ray computed tomography (XCT) is the most promising method for nondestructive and fully three dimensional characterizations of nanostructures. However due to conceptual limitations, commercial laboratory XCT devices are still an order of magnitude or more above the desired specifications in order to characterize 100 nm or smaller structures within a sufficient field of view.

The principle of common industrial XCT, also referred to as cone beam XCT, is explained as follows: At each angular position of a 360 degree turn, a 2D projection image of the specimen is obtained, which represents the X-ray attenuation of the specimen in the form of grey value images. The complete series of projection images allows to reconstruct the three dimensional distribution of the spatial X-ray attenuation, resulting in a volumetric grey value dataset of the scanned area.

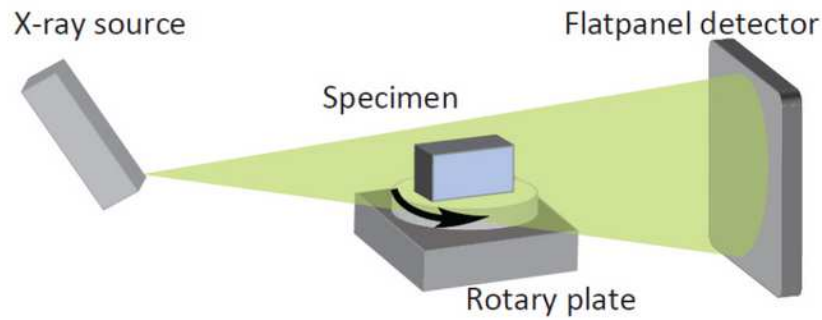


Figure 3.1: Explanation 3D X-ray Tomography method

Researchers of the Österreichisches Gießerei-Institut at the Montanuniversität Leoben, use this technology in their research, so taking advantage of this possibility, a first try to analyze the crack development inside the testing blocks was made. According to this, the plan was to analyze slices from a reference specimen, both horizontal and vertical from the block of 0.11 mm thickness. In figure 3.2.a and 3.2.b two pictures taken from this analysis are shown.

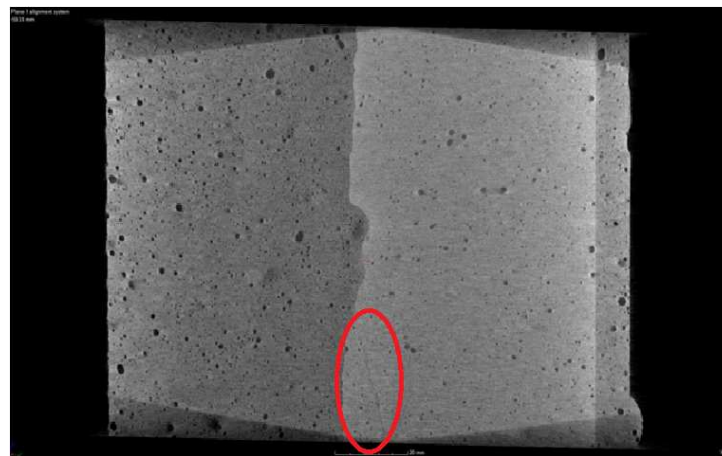


Figure 3.2.a: Induced Cracks (1) in testing blocks. 3D Tomography method

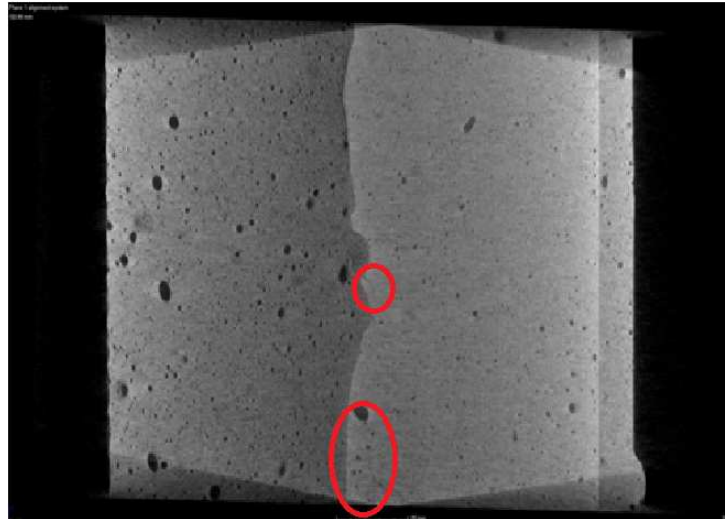


Figure 3.2.b: Induced Cracks (2) in testing blocks. 3D Tomography method

Figure 3.2.a and 3.2.b show two pictures taken using 3D tomography. There, few and small cracks were detected around the boreholes. The detected number of cracks is much lower than was expected in the beginning; perhaps, because the chosen specimen was not representative.

3D tomography presents some inconveniences for the current research:

- Costly analysis in this test with unsatisfactory results;
- Small sample size: Limitations of 3D tomography installations require cutting small samples of testing block before the analysis.
- Once a series of analyses is finished, the large amount of data it produces is time consuming to process.

For those reasons, this method was rejected to study the crack development. It is important to say that in the future, this analysis may become useful for studying specific parts of the testing blocks.

3.2 Crack detection analysis: 3D model

Several image-based methods to detect cracks on testing blocks have been proposed:

- Yamaguchi & Hashimoto (2010) introduced a high-speed crack detection method that employs *percolation-based image processing*.
- Fujita & Hamamoto (2011) proposed an automatic crack-detection method from noisy concrete surface images.
- Nishikawa et al. (2012) presented a two-step automated image processing method for detecting cracks in surface images of concrete structures: development of an image filter for detecting major cracks using *genetic programming (GP)* and *elimination of residual noise after filtering*.
- Su (2013) proposed a computer vision technique based on *charge coupled devices (CCD)* images to automatically detect cracks in concrete structures.
- Ehrig et al. (2011) in the International Symposium on Digital Industrial Radiology and Computed Tomography, used three different crack detection methods to implement 3D tomography: template matching, a sheet filter based on Hessian eigenvalues, and percolation.
- Olsson & Bergqvist (1996) at SveBeFo studied crack lengths from explosives in multiple holes blasting by cutting blocks and spraying them with penetrants.
- Ouchterlony et al. (1999) explained the SveBeFo dye penetrant technique of crack detection based at Svenneby where the emerging crack patterns are photographed and sketched.
- Ouchterlony et al. (2000) introduced new crack patterns to those found in Ouchterlony et al. (1999).
- Mogi et al. (2000) gave a similar explanation about the use of dye penetrant technique and crack patterns sketched as Ouchterlony & Olsson (2000).

- Saiang (2008) presented a summary of the blast damage investigation done by SveBeFo (Swedish Rock Engineering Research) during the period 1991 to 2003 in Sweden.

Those of the above methods that use an automated crack detection method were not possible to use because they require high image programming skills. As an alternative, and to compensate the lack of such an expertise, a 3D digital scale model method for each testing block was developed for the current project. It visualizes the internal crack network and describes how and where the cracks are created inside the blocks.

To carry out this alternative method, a blasted specimen is cut into several slices. Then, dye-penetrant is applied to the cut surfaces and the crack trace patterns that appear after dyeing are photographed (Ouchterlony et al. 2000). Each slice represents a vertical or horizontal cut through the specimen. These trace patterns are finally used to create digital 3D models in a computer-aided design (CAD) software, such as AutoCAD, to facilitate further crack analyses.

3.2.1 Documentation of crack detection analysis

Several crack detection analyses have been done in order to get a better understanding about the influence of blasting in crack development, which means, to get better tools to design blasting for the purpose of achieving a higher quality of the remaining rocks surfaces.

In the granite quarry tests at Svenneby, Ouchterlony et al. (1999) explained a technique for crack detection based on the use of dye penetrant that make cracks more visible (see section 3.2.2 for this procedure) and photographed and sketched the emerging cracks. Tests with water filled holes and dry holes were done. Different cracks patterns were found in both tests, but mainly six types of cracks were observed. See ANNEX I: figures I.1 to I.6.

- Radial cracks: crack emanating from the hole with axial notches. See figures I.2, I.3, I.4 and figure 3.3.
- Crushing cracks: diffuse zone with intense cracking. See figure I.1

- Arc shaped cracks: radial crack that is directed within 15° - 25° from the hole and which trend to curve toward the face. See figures I.2, I.4.
- Cone cracks: crack underneath the slot in the hole. See figure I.5.
- Notch root cracks: crack heading into the rock, angled 90° to the face. See figure I.6.
- Bench face cracks: branching crack from the bench face that interferes with the root notch cracks. See figure I.6.

Additionally, in the gneiss at Jakobsdal/Moraberg, Ouchterlony et al. (2000), five new crack types were detected (see figure 3.3 and 3.4).

- Foliation cracks: cracks that run along the weaker foliation planes.
- Structural cracks: Cracks related to the structure of the rock mass; i.e. the joints and sheeting planes.

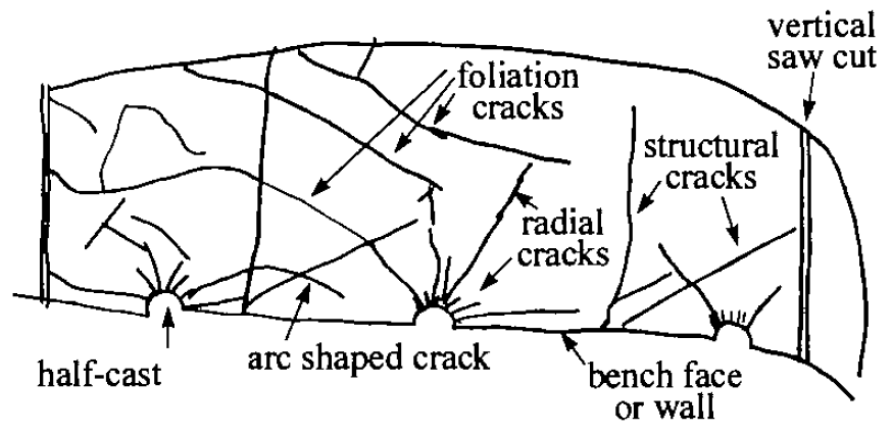


Figure 3.3: Crack detection in horizontal cut. Ouchterlony et al (2000).

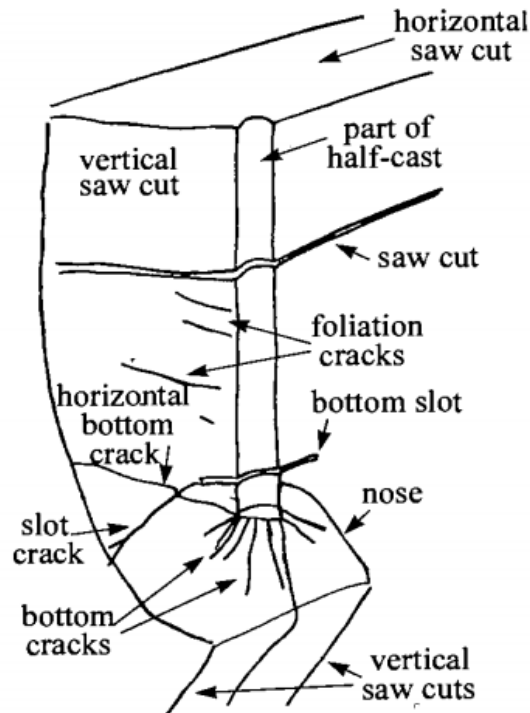


Figure 3.4: Crack detection in vertical cut. Ouchterlony, Olsson and Båvik (2000)

According to figure 3.4, three new crack types are found in the vertical cut:

- Bottom cracks: cracks that grow conically downward from the bottom corners of the blast holes.
- Slot cracks: cracks that emanate from the slot root.
- Horizontal bottom cracks: cracks that emanate from the bottom corners of the blast-holes.

In Saiang (2008), another crack pattern classification is made depending on factors such as: explosive parameters, blast-hole geometry and rock mass properties. Some examples of those patterns are seen in ANNEX I: figures I.7 to I.12. These pictures were taken from the works of Olsson and co-workers (Olsson and Bergqvist, 1995).

- A large number of short radial cracks close to the hole with maximum length of about 25 cm. See figure I.7.
- Bow-shaped tangential cracks formed as result when blasting was done with wider hole spacing. The maximum crack length was about 40 cm. See figure I.8.

- Long cracks with maximum length about 55 cm when using Emulet 20 as the explosive and the holes were completely filled. See figure I.9.
- A different crack pattern using a $\varnothing 24$ mm blast-hole charged with 22 mm Gurit is found. Crack lengths of up to 90 cm were observed. See figure I.10.
- A pre-existing crack inhibiting the growth of blast induced cracks is shown in figure I.11.
- A natural crack enhancing the growth of blast-induced cracks is represented in figure I.12.

3.2.2 Dye penetrant method

Dye Penetrant Testing examines the surface of an item (non destructively) for surface-breaking flaws, such as cracks. The test methodology is as follows:

- 1- Clean thoroughly the part to be tested.
- 2- Apply dye penetrant to the part surface and leave it to soak. The application can be made by spraying, brushing, dipping, etc. The liquid is drawn into any cracks via capillary action.
- 3- After the soaking time has expired (a minimum of 10 minutes) and the liquid becomes dry, allowing the penetrant material to sit, excess penetrant is wiped from off using a cleaner product. Remove as much penetrant as possible using a cloth or a piece of paper.
- 4- Once the cleaner has dried (after 10 minutes of waiting), the developer is applied. The developer is usually a dry white powder (for example chalk powder) suspension that is sprayed on the component. The developer is drawn out of the crack by reverse capillary action, resulting in a colored indication on the surface that is broader than the actual flaw, and therefore, much more visible.

Three products were used for the realization of this test: Dye-penetrant, cleaner and developer; of brand “Rocol”, manufacturer of Industrial Lubricants, Cutting Fluids & Line Marking Systems.

3.2.3 Preparation of data for 3D model design

The first step to create the 3D model is to rebuild the contour of the testing block in 3D with a similar shape as the real block.

The process is as follows:

- 1- Visual cracks detection on the surface has to be carried out. Trace out the cracks with a pen.

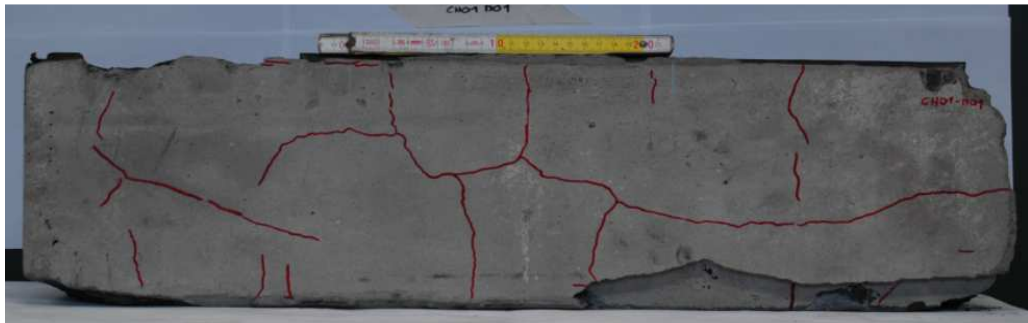


Figure 3.5: Surface cracks detection. Back side block CH01B01

- 2- Take pictures from each side of the block. Position the camera perpendicularly to the block. Use a length reference as a scale, such as a ruler, since every picture will be digitally rescaled to match actual measurements.
- 3- Apply dye penetrant on the back, up and down the surfaces of the testing block. This will allow detecting a larger number of cracks than in the previous visual analysis.

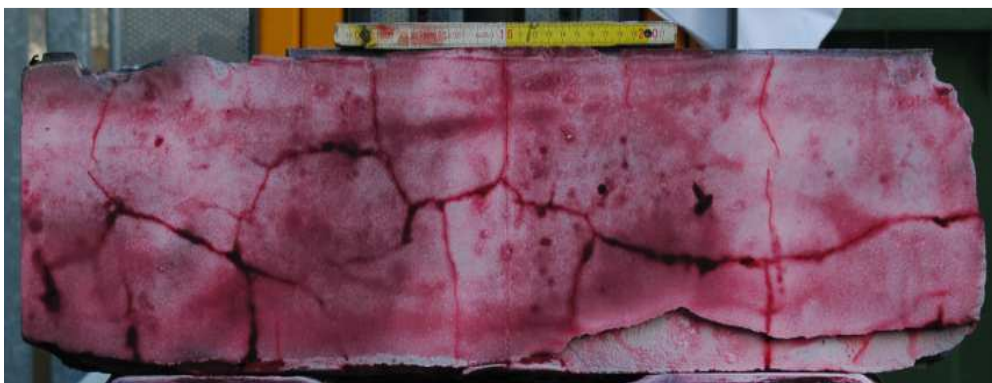


Figure 3.6: Dye penetrant application. Back side block CH01B01

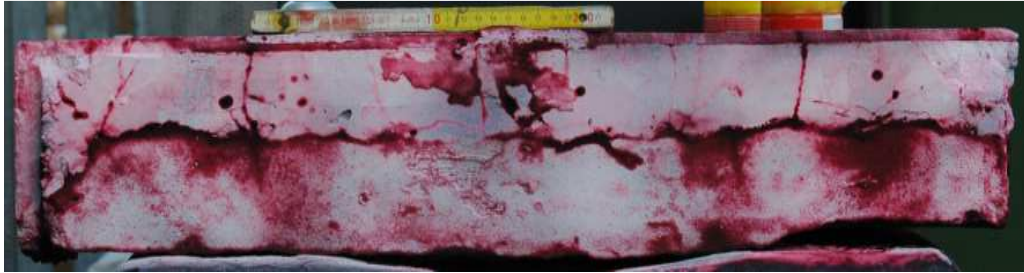


Figure 3.7: Dye penetrant application. Bottom side block CH01B01

- 4- Again, take pictures of the colored sides. Remember to position the camera correctly and to use a reference scale.

Once the block processing is finished, the detection of internal cracks in the testing block is carried out. The block is cut in 5 horizontal slices and then each slice is further cut into two parts by a vertical cut, achieving, in this way, an analysis of horizontal and vertical cracks within the block. During this process, the steps below are followed:

- 1- Cut the testing block in 5 slices. The distance between slices must be the same in every block to compare cracks at the same level of the specimen. A normal cutting machine from the laboratory equipment is used for cutting. From these 5 slices, 4 horizontal cutting faces, corresponding with the cut between slices, are used for the crack detection. Top and bottom of the specimen is not used for this purpose.

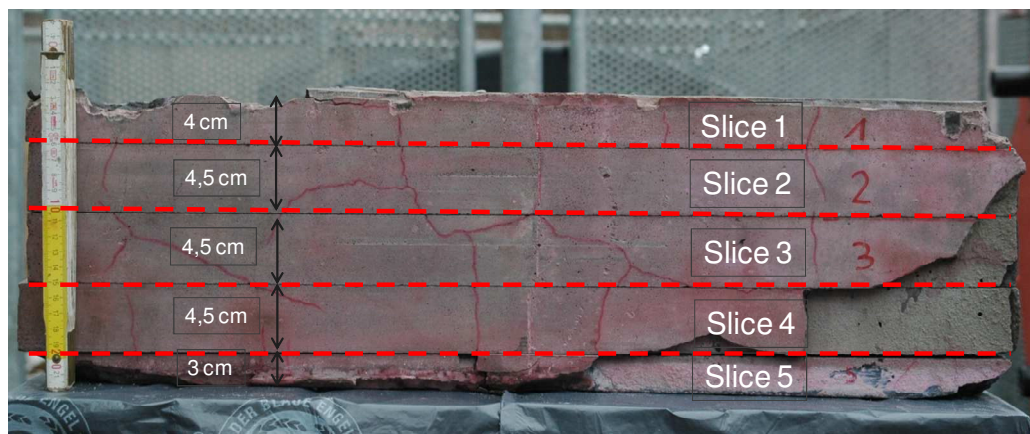


Figure 3.8: Distance between slices to cut the testing block.

- 2- Apply Dye Penetrant on the surface of each slice. Each slice has top and bottom faces that should almost coincide with the top and bottom faces of the next or previous slices respectively. Since the thickness of the cutting machine saw is 5 mm, the separation between adjacent faces is small compared to the lengths of most measured cracks; therefore the face in the better condition can be used for the analysis.

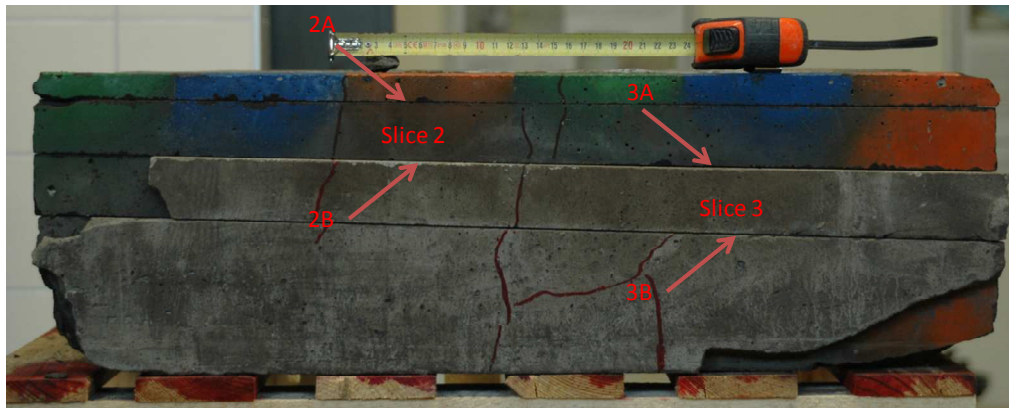


Figure 3.9: Clarification about the faces of the slices

- 3- Take photos of the slices. In this case, photos are taken when the cleaner is applied to observe cracks on the wet surface of the slice, and when the developer has been used. Adjust the camera exposure, to account for light changes, since these changes have influence the detection of cracks. With the purpose to visualize in greater detail cracks on the slice, more pictures were taken by adjusting the camera zoom. Due to the limitations of camera focus by zoom adjusting, the whole block can't be covered in one picture. Therefore, surface of the slice was covered by three different pictures, dividing the surface in three sections (figure 3.12).



Figure 3.10: Photo of the slice after using cleaner. Slice 3 block CH02B04

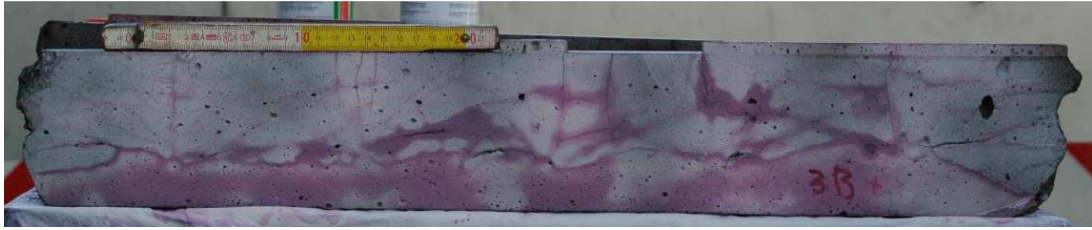


Figure 3.11: Photo of the slice after using developer. Slice 3 block CH02B04



Figure 3.12.a, b, c: Photos by zoom adjusting. Slice 3 block CH02B04

- 4- Once horizontal slices are processed, cut vertically each slice by 3 cm width, starting from the back side of the concrete part.



Figure 3.13: Distance vertical cut. Slice 3 block CH01B01

- 5- Apply dye penetrant over the new vertical surface as in steps 2.



Figure 3.14: Vertical slice after use developer. Slice 3 block CH01B01

- 6- Take photos of the vertical surface as in step 3.

3.2.4 3D model design

With the pictures taken, the trace patterns of the testing block are used to create digital 3D models in AutoCAD, following the procedure below:

- 1- Insert each photo in a new AutoCAD sheet. The chosen photo should be the one that most clearly represents the traces.
- 2- Every picture and every drawing should represent real measures of the testing blocks; therefore the inserted photo must be scaled using the reference length placed when the photo was taken. A good image scaling is important, because the 3D model must incorporate every drawing. As an experience: a 2 mm difference between the drawing and the traces in the picture is inadmissible.
- 3- Draw the contour and crack traces of the pictures using a different color. To organize the design of the 3D model, start drawing pictures taken from the side of the block, rebuild the 3D model by joining every side in 3D (as in step 4), and then the horizontal and vertical slices.



Figure 3.15: Back side testing block drawing using AutoCAD. Block CH01B01

To draw crack traces on the picture, the following criteria must be followed:

- a) Trace cracks or red lines visible on the slice. Different thickness of cracks can be found in the slice; therefore, emerging cracks with different color intensity by effect of dye-penetrant can be distinguished. All of them are considered cracks.

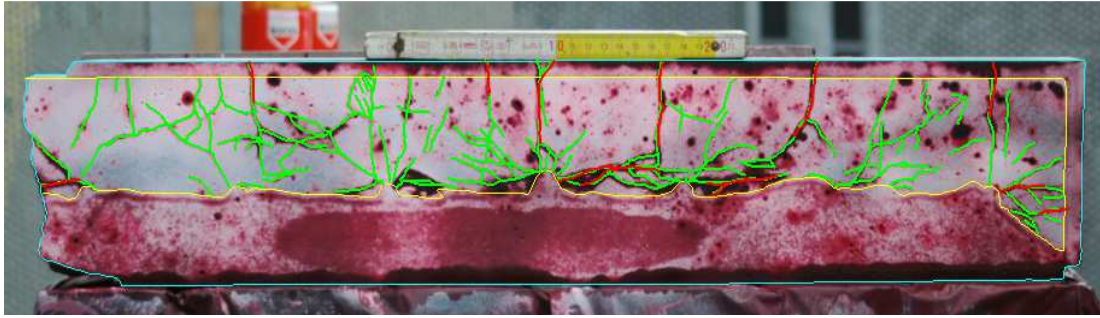


Figure 3.16: Drawing of crack traces on horizontal slice. Slice 3 Block CH01B01

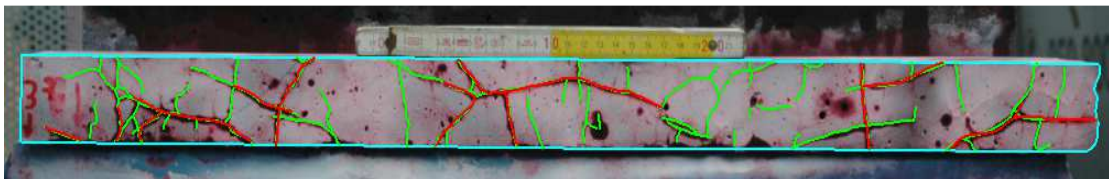


Figure 3.17: Drawing of crack traces on vertical slice. Slice 3 Block CH01B01

In figures 3.16 and 3.17, blue lines represent contour lines; red lines the main cracks observed without using dye-penetrant; green lines the crack traces detected using dye penetrant and yellow lines the boundary between magnetite mortar and fast hardening cement.

- b) Pay attention to the direction and continuity of the cracks in case there is a connection.
- c) In case of not seeing clearly the trace of a crack, use the zoomed in photos and those taken once the cleaner was applied.
- d) Once the crack traces and the contour of the slice are drawn, copy the drawing and paste it on one of the photos taken once the cleaner was applied. For that, this photo should be inserted on another AutoCAD sheet and scaled following the previous steps. The purpose of this step is to check that cracks traced in the first photo coincide with those traced in the second one. In case of mismatch, the drawing should be checked to figure out mistakes or add new crack traces from the second picture to the drawing.
- e) Finally, for horizontal slices, once the drawing was compared between both pictures, the boundary between magnetite concrete and fast hardening cement parts is drawn (see figure 3.16). The fast hardening

cement must be checked for crack traces, which may have been created after blasting. This may mean that cracks could be created in the concrete block after blasting, due to the removal of the testing block from the yoke or during transportation.

- 4- Design 3D model. To carry out this step, create a new AutoCAD sheet and set it to 3D modeling and draw a 3D rectangle. The process to design the contour of the 3D model is to copy drawings from each side of the block and paste them on this new sheet. Each slice has to be rotated to achieve the position in which they belong referring to the actual testing block. Finally, the new rotated drawings are fit to the rectangle previously drawn.

Once the side block drawings are fitted, it is necessary to design the shape of the block by paying attention to contour lines and changes of levels on the surface, trying to achieve a 3D model similar to the actual block.

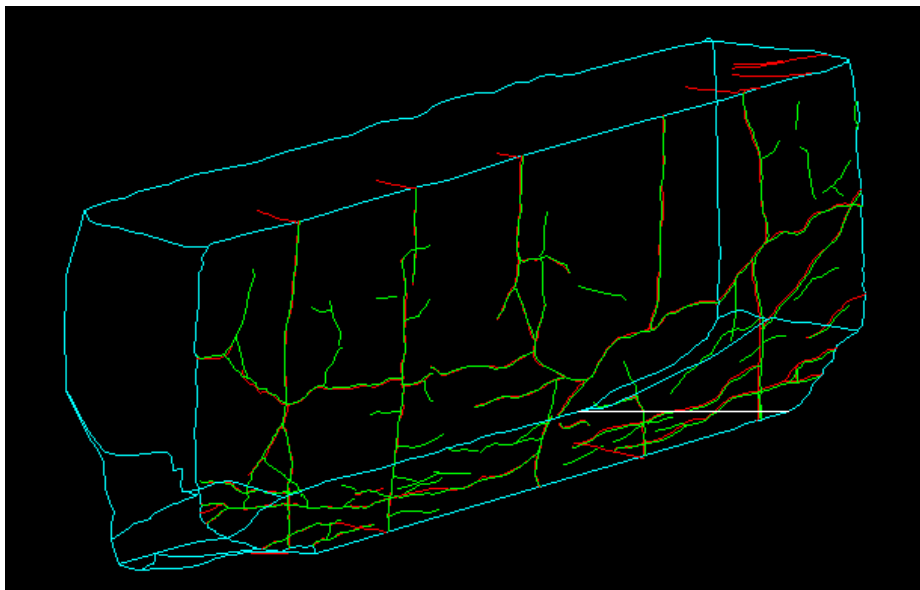


Figure 3.18: Contour 3D model. Block CH03B05

- 5- When the 3D model is created and the horizontal and vertical slices are drawn, they are introduced in the 3D model following the following order:
 - a) Copy and paste horizontal slice drawing in AutoCAD sheet where the 3D model is rebuilt. To facilitate slice drawing movement, group them.

- b) Rotate the slice to give it the right position in the block, depending on whether the slice drawn is the top or the bottom one.
- c) Introduce in the 3D model the height in which it was cut in the actual block by matching the contour of the slice with the outline of the block.

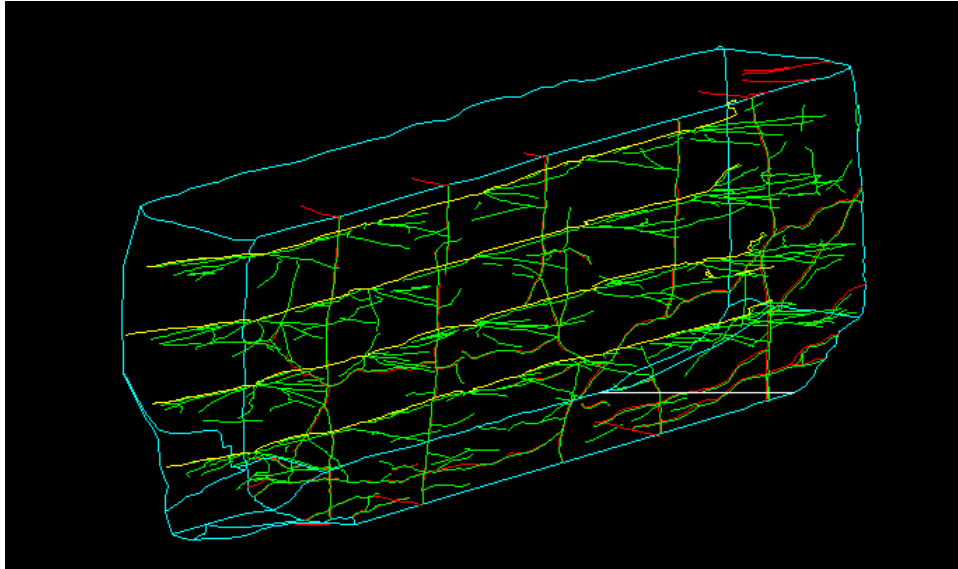


Figure 3.19: 3D model with horizontal Slices. Block CH03B05

- d) Repeat the procedure with vertical slice drawings by matching connections between cracks of both horizontal and vertical slices.
- 6- Draw boreholes inside the 3D model following the half circumference drawn in all horizontal slices created by effect of the blasting.
 - 7- Draw crack connections between levels. This is only possible when horizontal cracks of two slices and vertical cracks from the back side of the model and a vertical slice are aligned and both horizontal and vertical cracks connected.

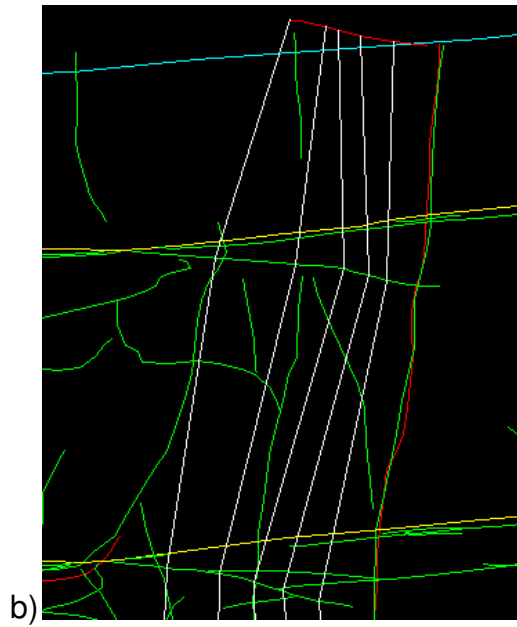
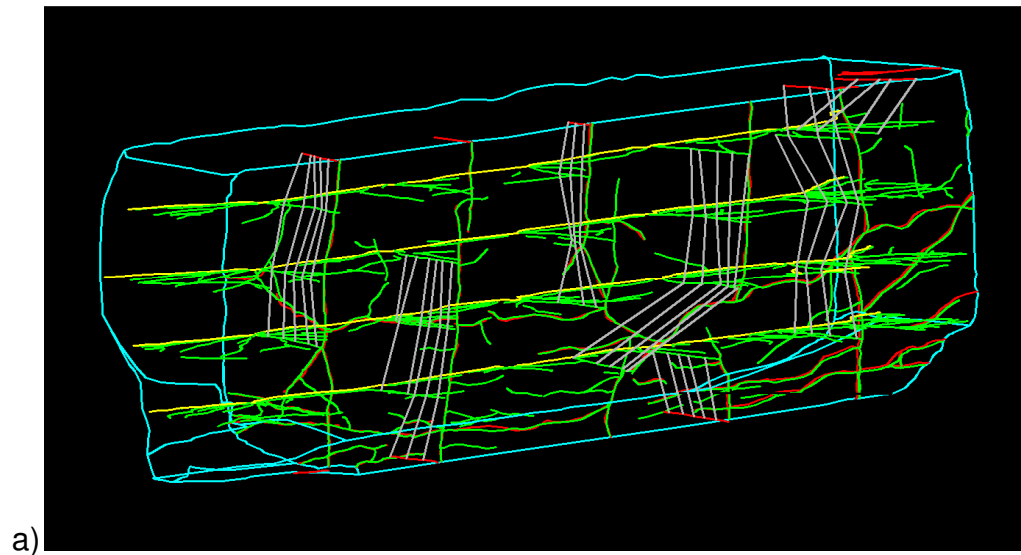


Figure 3.20. a, b: a) 3D model with connections between levels. Block CH03B05; b) Zoom 3D model with connections between levels. Block CH03B05

4 ANALYSIS OF DATA

4.1 Objective network measures for horizontal section

Using the CAD 3D models, a division of crack patterns based on angles and lengths in slice surfaces was made. ANNEX II shows examples of digitized cracks on the horizontal sections of the testing blocks. These sections correspond to the bottom side of the slice surface or the top side of next slice surface, depending on which horizontal section presents a better crack definition.

4.1.1 Crack families

Different cracks types were detected on the slices of all testing blocks. The cracks were grouped in ten different crack families. As is shown in table 4.1 crack families were defined according to the angle and length of the crack, their starting point and direction.

The crack detection analysis is shown in Annex IV, where the cracks of the slice surfaces depicted in Annex II are grouped in crack families using the color and the criteria established in this section.











Color	Name	Abbreviation
	Cracks from borehole in sectors between 90° - 80°	CB 90-80
	Cracks from borehole in sectors between 80° - 30°	CB 80-30
	Cracks from borehole in sectors between 30° - 0°	CB 30-0
	Straight cracks from back side	SCB
	Connections between boreholes	Connection
	Parallel cracks to the surface	Parallel
	Cracks with direction to the boreholes in sectors 90° - 80°	Dir 90-80
	Cracks with direction to the boreholes in sectors 80° - 30°	Dir 80-30
	Cracks with direction to the boreholes in sectors 30° - 0°	Dir 30-0
	Short cracks from borehole	Shorts

Table 4.1: Color coded families of crack traces in horizontal slices

Below, a detailed description of each family is given:

- 1- *Cracks from boreholes in sectors between 90° - 80°* : cracks that start from the borehole and develop a trajectory limited by sectors between 90° - 80° counted from both sides of the free face, i.e. sector 80° - 100° counted from one side. These cracks are divided according to their lengths from the center of the blast hole: long (> 3 cm) and short (between 1 cm and 3 cm). Cracks shorter than 1 cm belong to family no. 10, see below.

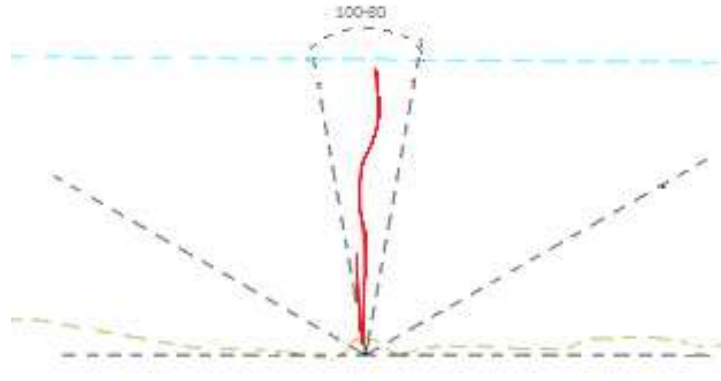


Figure 4.1: Cracks from borehole in sectors between 90° - 80°

- 2- *Cracks from borehole in sectors between 80° - 30°* : cracks that start from the borehole and develop a trajectory limited by sectors between 80° - 30° at both sides of the borehole. These cracks are divided according to their lengths from the center of the blast hole: long (> 3 cm) and short (between 1 cm and 3 cm). Cracks shorter than 1 cm belong to family no. 10, see below.

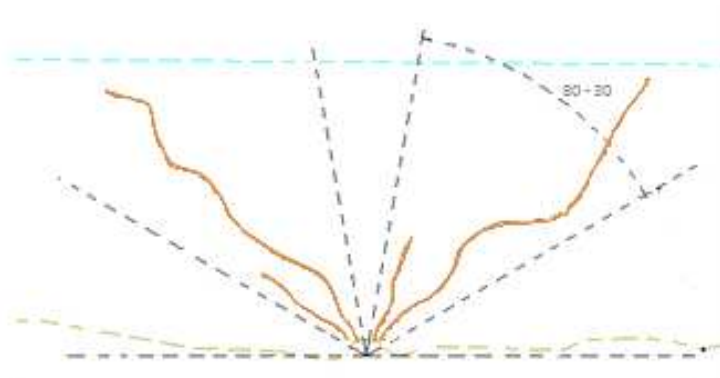


Figure 4.2: Cracks from borehole in sectors between 80° - 30°

- 3- *Cracks from borehole in sectors between 30° - 0°* : cracks that start from the borehole and develop a trajectory limited by sectors between 30° - 0° at both sides of the borehole. These cracks are divided according to their lengths from the center of the blast hole: long (> 3 cm) and short (between 1 cm and 3 cm). Cracks shorter than 1 cm belong to family no. 10, see below.

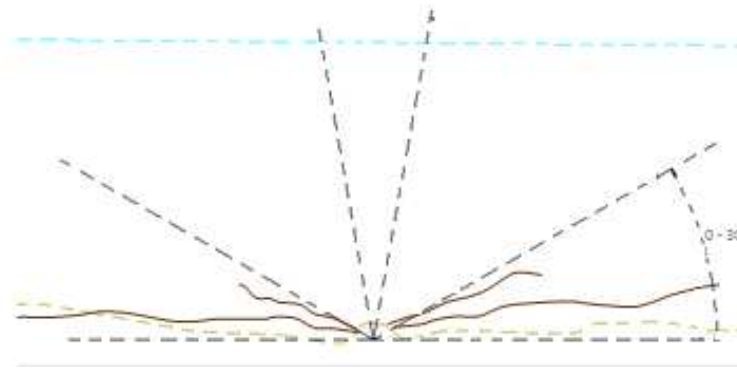


Figure 4.3: Cracks from borehole in sectors between 30° - 0°

- 4- *Straight cracks from back side*: cracks which seem to start from the back side of the slice and that follow a trajectory not directed towards the boreholes. These cracks are also divided according to their lengths: long (> 3 cm) and short (between 1 and 3 cm). Cracks shorter than 1 cm are not included in this family, because they are not representative considering the dimensions of the specimens.

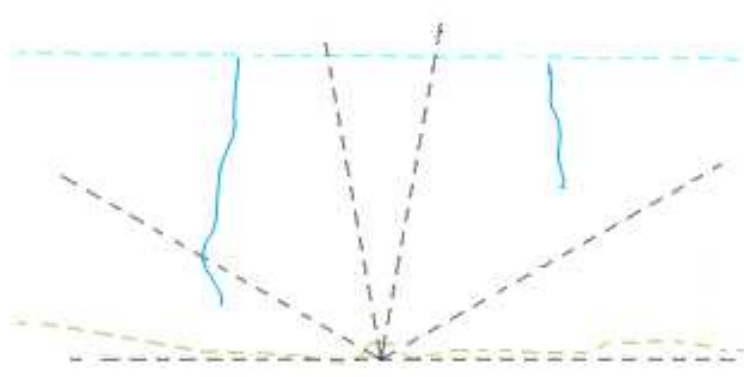


Figure 4.4: Straight cracks from back side

- 5- *Connections between boreholes*: sometimes cracks with an angle between 30° - 0° starting from two neighboring boreholes are connected, creating an arc shaped connection between boreholes, roughly with the shape of a banana.

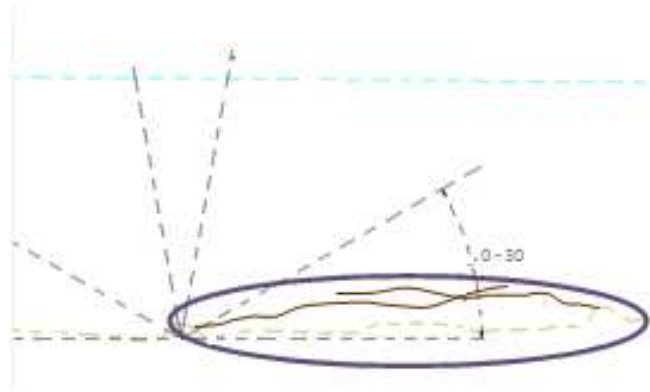


Figure 4.5: Connections between boreholes

- 6- *Parallel to the surface*: parallel cracks which are created along the slice. These cracks are also divided according to their lengths: long (> 3 cm) and short (between 1 and 3 cm). Cracks shorter than 1 cm are not included in this family, because they are not representative considering the dimensions of the specimens.

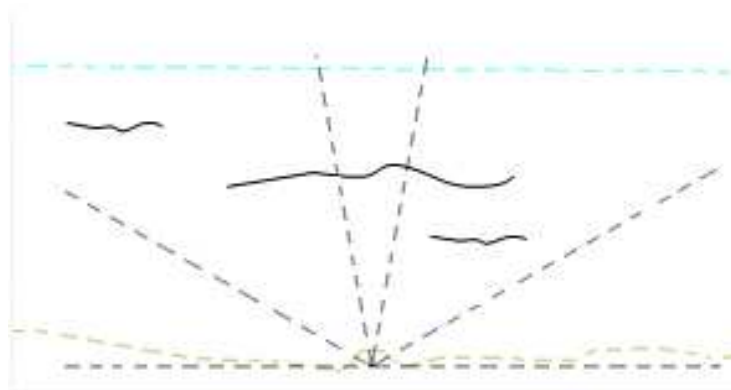


Figure 4.6: Parallel cracks to the surface

- 7- *Cracks with direction to the boreholes in sectors between 90° - 80°* : These cracks do not start from the borehole but develop a trajectory with a direction towards the hole and are limited by a sector between 90° - 80° from both sides of the borehole. These cracks are also divided according to their lengths: long (> 3 cm) and short (between 1 and 3 cm). Cracks shorter than 1 cm are not included in this family, because they are not representative considering the dimensions of the specimens.

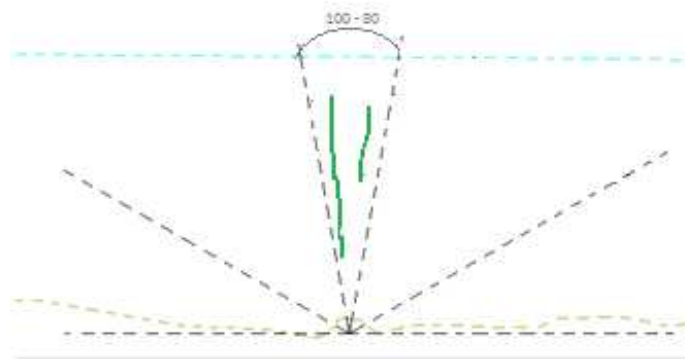


Figure 4.7: Cracks with direction to the boreholes in sectors between 90° - 80°

- 8- *Cracks with direction to the boreholes in sectors between 80° - 30°* : These cracks do not start from the borehole but develop a trajectory with a direction towards the hole and are limited by a sector between 80° - 30° from both sides of the borehole. These cracks are also divided according to their lengths: long ($> 3\text{cm}$) and short (between 1 and 3 cm). Cracks shorter than 1 cm are not included in this family, because they are not representative considering the dimensions of the specimens.

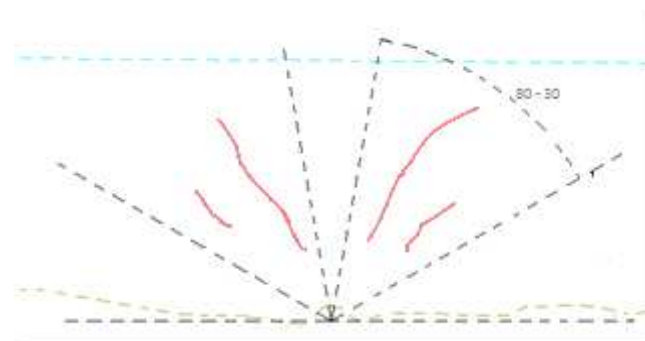


Figure 4.8: Cracks with direction to the boreholes in sectors between 80° - 30°

- 9- *Cracks with direction to the boreholes in sectors between 30° - 0°* : These cracks do not start from the borehole but develop a trajectory with a direction towards the hole and are limited by a sector between 30° - 0° from both sides of the borehole. These cracks are also divided according to their lengths: long ($> 3\text{cm}$) and short (between 1 and 3 cm). Cracks shorter than 1 cm are not included in this family, because they are not representative considering the dimensions of the specimens.

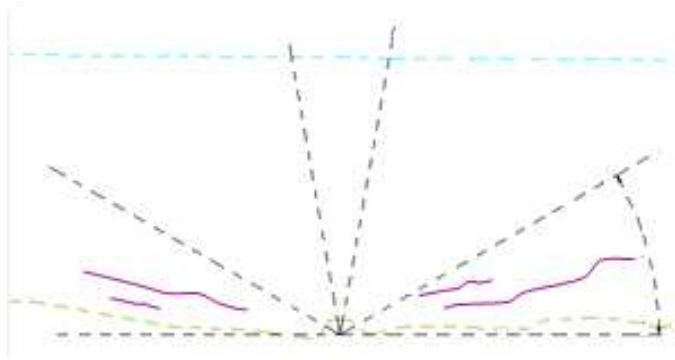


Figure 4.9: Cracks with direction to the boreholes in sectors between 30° - 0°

10- *Short cracks from borehole*: short cracks which start from the borehole. The lengths of these cracks are smaller than 1 cm and can appear in all directions.

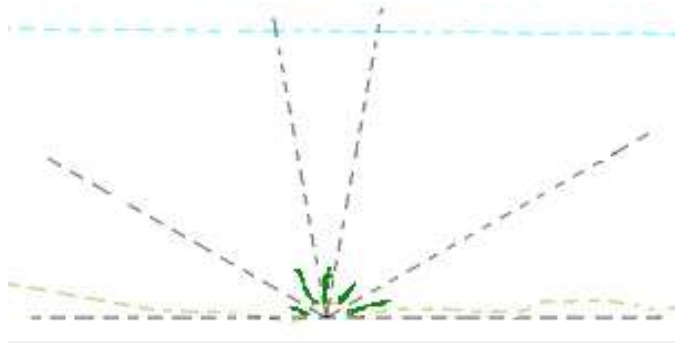


Figure 4.10: Short cracks from borehole

4.1.2 Comparison between documented cracks types in section 3.2.1 and crack types found in section 4.1.1

Several similitudes are found between crack types described by Ouchterlony et al. (1999 & 2000) and Saiang (2008) and crack families analyzed in the horizontal sections (section 4.1.1):

- a) Long and short radial cracks are found in both the Ouchterlony et al. (1999 & 2000) and Saiang (2008) analyses. In section 4.1.1, six different radial crack families divided in 3 sectors are described: 3 starting from the borehole and 3 that develop a trajectory with a radial direction away from the hole:
 - A notch *root crack*, defined in Ouchterlony et al. (1999) (see figure I.6) is the crack family defined as: *Cracks from boreholes in sectors between 90° - 80°*.
 - *Arc shaped cracks* defined by Ouchterlony et al. (1999) and *Bow-shaped tangential cracks* described by Saiang (2008) may be comparable with *Cracks from boreholes in sectors between 30° - 0°*. In addition, when a long crack (longer than 3 cm) of this family connects two boreholes, *Connections between boreholes* can be included in this classification.
- b) *Foliation cracks* and *Bench face cracks* are quite similar to *Parallel cracks* found but there are no foliation planes in our specimens.
- c) *Structural cracks* are also very similar to crack family: *Straight cracks from back side*. However, since our studied blocks are made without foliation planes or joints, other generating mechanisms must have caused them.
- d) *Short cracks from borehole* are also found in every picture from ANNEX I.

Crack patterns described in Saiang (see ANNEX I, figures I.7 to I.12) show a combination of the crack families digitized in the horizontal sections (see ANNEX II and ANNEX IV).

4.2 Objective network measures for vertical section

Analogously to section 4.1, crack families based on angles and lengths in vertical slices were defined. An example of digitized cracks of the vertical sections of the testing block is shown in ANNEX III.

4.2.1 Crack Types

Following the same methodology as in section 4.1.1, several crack types were detected on the slices of all testing blocks. In this way, 5 different families of cracks collect all the cracks created. As shown in table 4.2 cracks families are defined according to the angle and length of the crack and their starting point and direction.






Color	Name	Abbreviation
	Cracks following a direction in sectors between 90° - 80°	CD 90-80
	Cracks following a direction in sectors between 80° - 30°	CD 80-30
	Cracks following a direction in sectors between 30° - 0°	CD 30-0
	Parallel to the surface	Parallel
	Connections between slices	Connection

Table 4.2: Color coded families of crack traces in vertical slices

A detailed description of each family is shown below:

- 1- *Cracks following a direction in sectors between $90^\circ - 80^\circ$* : cracks which start from one of the surfaces of the slice and that develop a trajectory limited by an angle between $90^\circ - 80^\circ$ with both surfaces of the slice. These cracks are divided according to a new definition of their lengths (l): long (> 3 cm) and short (between 1 and 3 cm). Cracks shorter than 1 cm are not included in this family, because they are not representative considering the dimensions of the specimens.

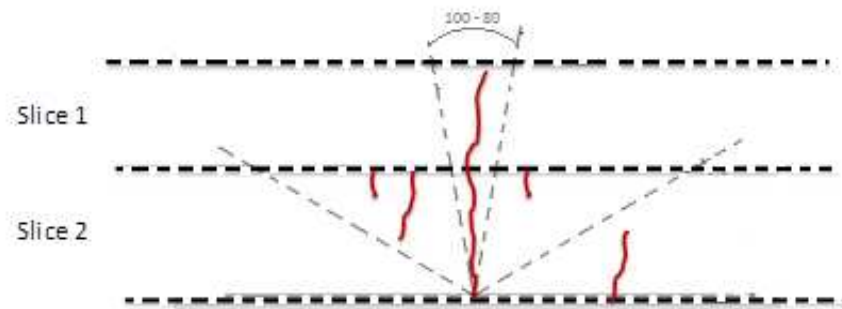


Figure 4.11: Cracks following a direction with angle between $90^\circ - 80^\circ$

- 2- *Cracks following a direction in sectors between $80^\circ - 30^\circ$* : cracks which start from one of the surface of the slice and that develop a trajectory limited by an angle between $80^\circ - 30^\circ$ with both surfaces of the slice. These cracks are divided according to according to a new definition their lengths (l): long (> 3 cm) and short (1 - 3 cm). Cracks shorter than 1 cm are not included in this family, because they are not representative considering the dimensions of the specimens.

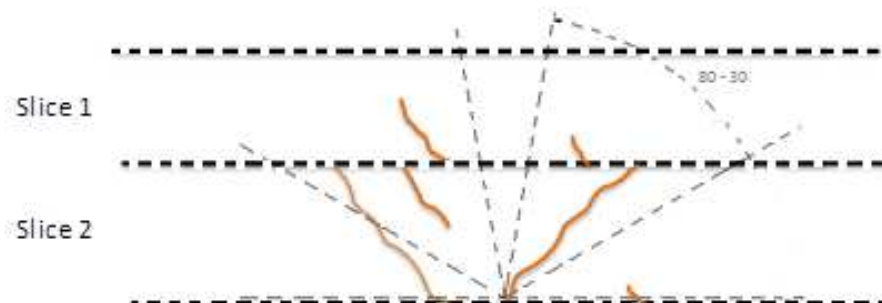


Figure 4.12: Cracks following a direction with angle between $80^\circ - 30^\circ$

- 3- *Cracks following a direction in sectors between 30° - 0°* : cracks which start from one of the surface of the slice and that develop a trajectory limited by an angle between 30° - 0° both surfaces of the slice. These cracks are divided according to according to a new definition their lengths (l): long (> 3 cm) and short (1 - 3 cm). Cracks shorter than 1 cm are not included in this family, because they are not representative considering the dimensions of the specimens.

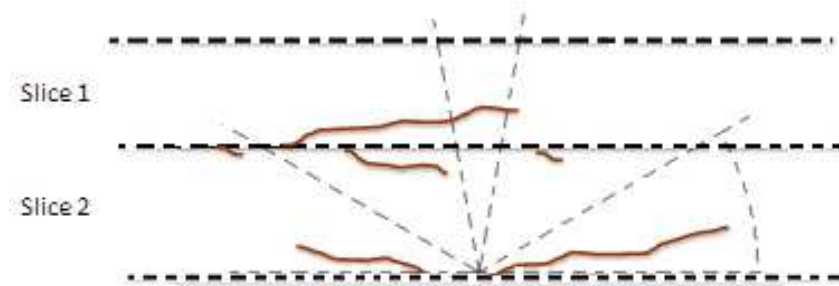


Figure 4.13: Cracks following a direction with angle between 30° - 0°

- 4- *Parallel crack to the surface*: parallel cracks which are created along the slice. These cracks are divided according to according to a new definition their lengths (l): long (> 3 cm) and short (1 - 3 cm). Cracks shorter than 1 cm are not included in this family, because they are not representative considering the dimensions of the specimens.

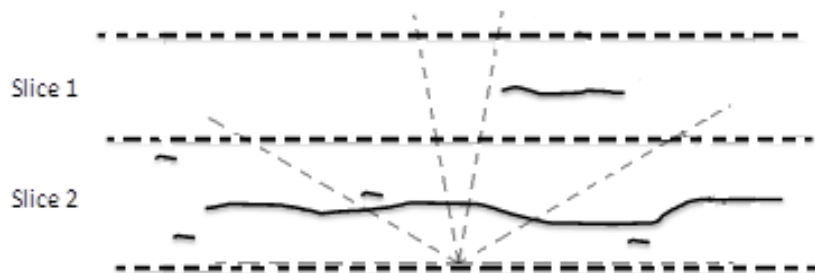


Figure 4.14: Parallel crack to the surface

- 5- *Connections between slices*: connections of cracks between two adjacent slices.

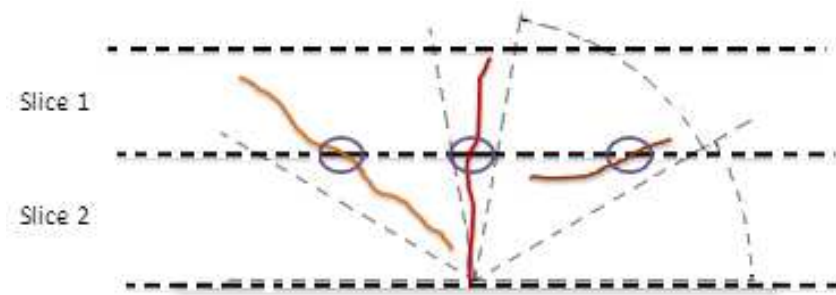


Figure 4.15: Connections between slices

4.3 Crack density analysis

The concentration of cracks along the slice is one measure of the amount of damage that was created, the more cracks in a specific region, the more damage created. Taking this idea into account, a study of crack density was made, in order to detect where the damage (greater amount of cracks) is concentrated within the slice.

4.3.1 Design of the grid

To carry out this analysis, the digital slice model was divided by a grid (figure 4.16), in which every cell receives a value according to the number of cracks within its borders.

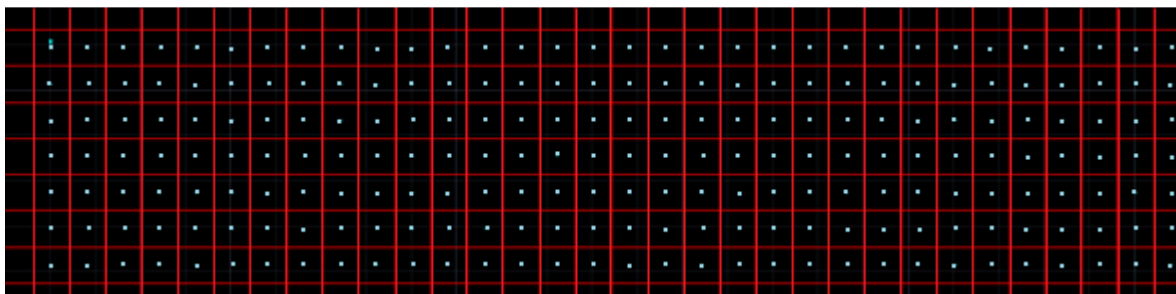


Figure 4.16: Grid 2x2 cm.

The size of the cells of the grid is 2 x 2 cm. In section 4.3.4, the reason for this choice is explained.

To create a damage map to represent crack density in the slices, a Matlab code, explained in section 4.3.3, was written. Three values are necessary as input for the code: X and Y coordinates of representative points; and a value containing the number of cracks. These named points are located in the center of each cell of the grid as is shown in figure 4.16.

4.3.2 Criteria to choose the crack density values

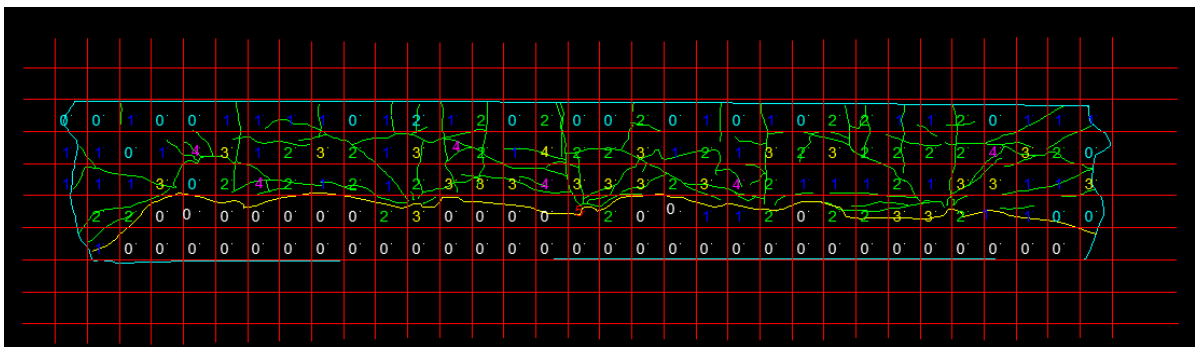


Figure 4.17: Grid 2x2 cm. Slice 2 block CH02B04

To quantify crack density in the grid, one counts the number of cracks within each cell and records this number.

Since there are sometimes complicated situations, knowing if a crack is considered or not to be inside the cell, the following procedures was followed:

- a) *Length of the crack*: The length of a crack to be considered within the grid must be larger than $\frac{1}{8}$ times the length of the cell size (length > 2.5 mm). Smaller cracks are not representative for the crack density representation, considering the size of the cell.
- b) In case that a crack runs through several cells of the grid, then it is counted in all cells where it meets the requirements a), c) and d).
- c) *Crack in the corners of the cells*: Cracks that can be seen in the corners are not taken into account if they lie outside the four corner limiting lines of length 2.5 mm (white line), see Figure 4.18.

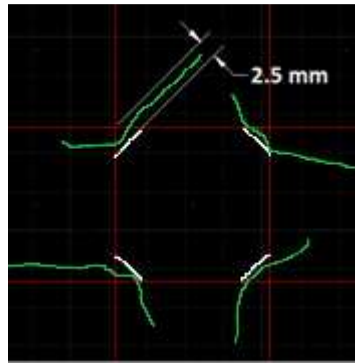


Figure 4.18: Imaginary lines (white color) which limit when a crack (green line) is valid or nor.

d) *Connections between cracks separated by the grid:* Connections of cracks separated by the cells of the grid where a short part of these cracks, that meets the requirements a), b) and c), belongs to another cell (white lines). In this case the crack is counted within the cell where the larger part of the crack is situated, giving it the corresponding value. See figure 4.19.

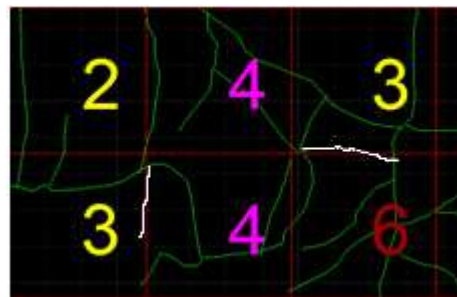


Figure 4.19: Connections between cracks separated by the grid.

4.3.3 Design of damage map from crack density

To construct a damage map, a Matlab code was written. The purpose is to visualize the crack density in the slice using isolines and areas drawn with different colors around the peak values of density. In this way, an approximate identification of where the damage is concentrated in the slice and the associated degree of damage therein is possible to make.

To prepare the data for running the Matlab code, several steps must be followed:

- a) Once the detection of crack density in the grid is finished, a different color must be associated with each number (figure 4.17). Since it is not possible to export text from AutoCAD, the different colors will represent the values of number of cracks detected in each cell. For that, the text and the drawn points should be painted with the color associated to the number.
- b) Export the characteristics of the drawn points (X and Y coordinates and color of each point) to an Excel file.
- c) In Excel, reference the (X, Y) coordinates to the coordinate origin (0, 0) and assign a number for each color.

To represent damage map in Matlab, use the (two) functions:

- a) *Griddata*: according to the Matlab manual, $vq = \text{griddata}(x, y, v, xq, yq)$ fits a surface of the form $v = f(x, y)$ to the discrete data in the vectors (x, y, v) . The *griddata* function interpolates the surface at the query points specified by (xq, yq) and returns the interpolated values, vq . The surface always passes through the data points defined by x and y . To interpolate values, a cubic interpolation was used.
- b) *Contourf*: in the manual this function is defined as: a filled contour plot that displays isolines calculated from a matrix $Z(x, y, vq)$ and fills the areas between the isolines using constant colors corresponding to the current figure's colormap.

Using these functions and identifying the data in the code, the damage map can be plotted. The damage map representation of figure 4.17 is shown in figure 4.20. The range of values is between -1, representing the fast hardening cement, to 6, representing the maximum crack density (six cracks). A value of 0 represents the concrete part without cracks.

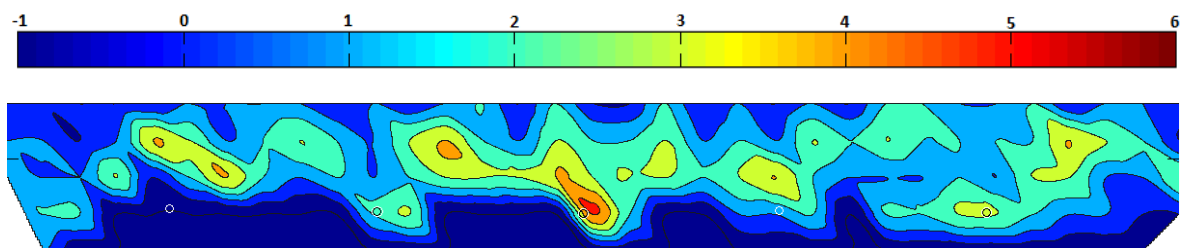


Figure 4.20: Damage map Slice 2 block CH02B04

4.3.4 Comparison between different sizes of grid

Grids with different sizes were analyzed in order to achieve the best representation possible of crack density. In this section, three different sizes were compared. Slice 2 from Block CH02B04 was taken as example.

- a) *Grid with cells of 2 x 2 cm:* Slice 2 from Block CH02B04 is represented in figures 4.17 and 4.20.
- b) *Grid with cells of 1 x 1 cm:* The same slice as above is represented in figures 4.21 and 4.22 using a grid with a cell size of 1 x 1 cm.

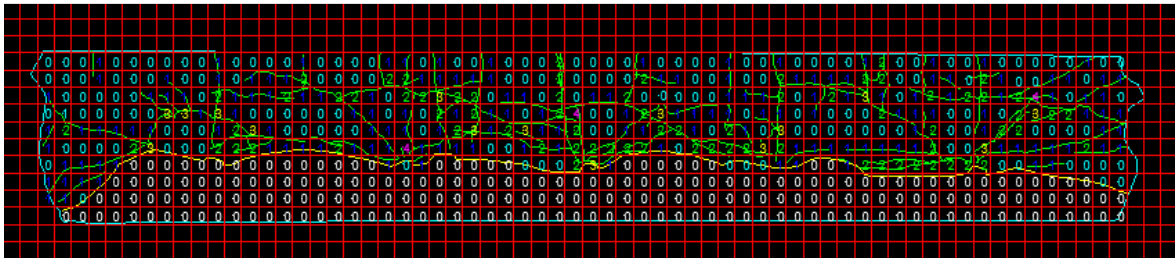


Figure 4.21: Grid 1x1 cm. Slice 2 block CH02B04

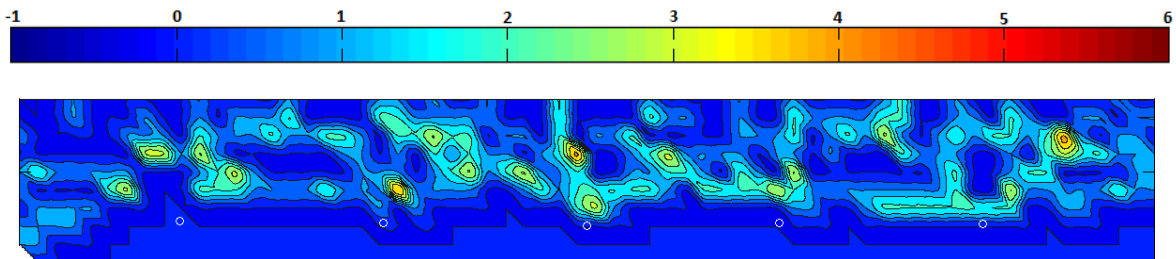


Figure 4.22: Grid 1x1 cm. Damage map Slice 2 block CH02B04

- c) *Grid with cells of 4 x 4 cm:* Slice 2 from Block CH02B04 is again represented in figures 4.23 and 4.24 using a grid with a cell size of 4 x 4 cm

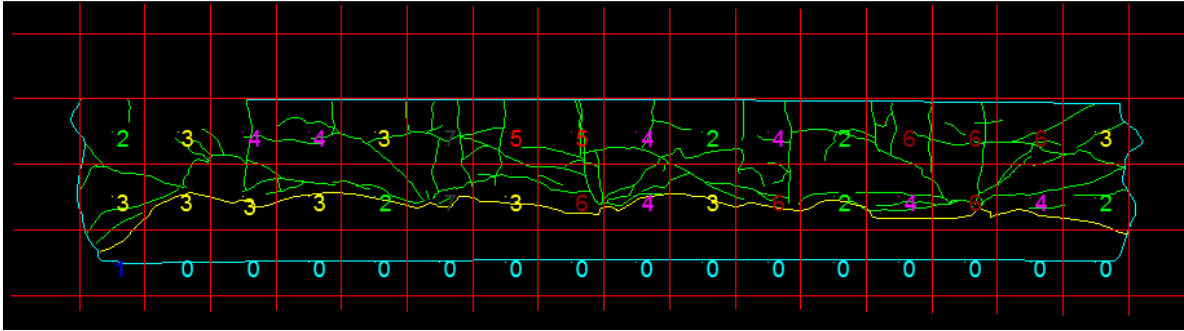


Figure 4.23: Grid 4x4 cm. Slice 2 block CH02B04

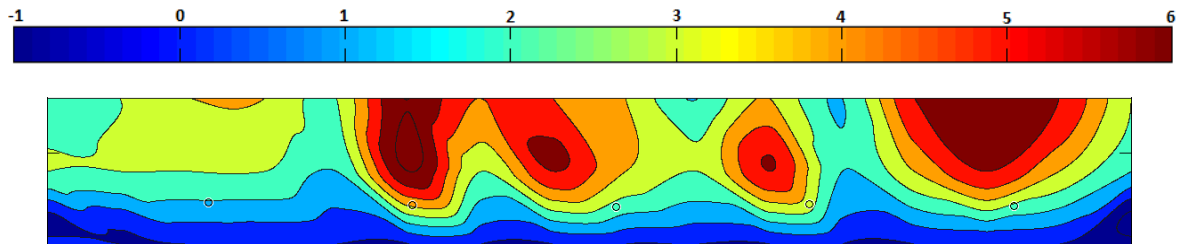


Figure 4.24: Grid 4x4 cm. Damage map Slice 2 block CH02B04

According to the figures presented in this section, it can be seen that the grid with cells of 2 x 2 cm represents the best distribution of crack density. That means: sufficiently large difference between cell crack numbers to identify areas with large damage, like areas around boreholes, and areas with small damage.

Due to the smaller size of the cell in the grid of 1 x 1 cm, a lower number of cracks can be counted in each cell; therefore, a representation of the individual cracks network can be done. However, this makes it harder to identify crack concentration areas, like directly behind a blast hole.

On the other hand, the grid of 4 x 4 cm gives a more general view about crack density. Due to its size, a larger number of cracks is counted in each cell, creating greater crack concentration areas. In this situation, identification with more detail of specific crack concentration areas in the slice can be difficult.

Following the best representation possible, the grid of 2x2 cm cell size was chosen to represent crack density maps.

4.3.5 Classification of slices according to the damage map

Density cracks analysis for all slices are presented in ANNEX V, where density crack maps are shown. Location of where the damage is focused in the slice can be observed. In most of the cases, the crack density is greater around the boreholes.

Variation of the damage according of the location of the slice in a block can be also identified. As can be observed, damage is not constant along the slices of the block. In addition, depending of which block is represented (ANNEX V), the distribution of this damage changes between slices. For this reason, a method to make the damage values comparable must be developed.

This is made according to the number of density points established for each grid. The density range is from 0 to 6, where 0 represents zones without cracks and 6 zones with the maximum crack density. In this way, the mean value for all the numbers that belong to the same slice was calculated (equation 1). The obtained value is a parameter that represents an average measure of crack density in the slice, which is comparable with the damage.

$$\text{Mean Crack Density (MCD) value} = \frac{\sum_{i=1:N} \text{number of cracks in the cell } (i)}{N} \quad (1)$$

where N is the number of cells of the grid.

Mean Crack Density values of the slices are shown in table 4.3:

Block	CH01B01	CH02B01	CH02B02	CH02B03	CH02B04	CH02B05	CH03B04	CH03B05
Delay time (µs)	140-140-140	0-0-0	28-28-28	140-0-0	73-73-73	28-140	28-73-73	28-0-0
Slice 1	0.55	0.77	0.99	0.69	0.99	0.48	0.62	0.65
Slice 2	1.11	0.87	0.86	0.78	1.22	0.52	0.87	0.84
Slice 3	1.50	0.93	0.91	1.00	1.36	0.62	0.79	0.91
Slice 4	1.30	1.22	1.14	1.19	1.83	0.45	0.86	0.80

Table 4.3: Mean Crack Density values

4.3.6 Crack intersection density analysis

Another way to study block damage is assuming that the concentration of crack intersections along the slice is related to the amount of damage created. In this way, the more cracks that intersect in a specific region, the more damage created. The idea is the same as in section 4.3.2 and 4.3.3 but, in this case, the goal is to compare if crack density achieved in section 4.3.2 and 4.3.3 is related with intersection density between cracks. To carry out this analysis, the same grid of 2x2 cm was used.

The same procedure and criteria used in section 4.3.2 and 4.3.3 were followed to create this crack intersection density.

The crack intersection density analysis for all slices is presented in ANNEX VI.

In order to classify the intersection density analysis, the same procedure as in section 4.3.5 has been used. Mean Crack Intersection Density (MCID) values are shown in table 4.4:

Block	CH01B01	CH02B01	CH02B02	CH02B03	CH02B04	CH02B05	CH03B04	CH03B05
Delay time (μ s)	140-140-140	0-0-0	28-28-28	140-0-0	73-73-73	28-140	28-73-73	28-0-0
Slice 1	0.11	0.19	0.19	0.13	0.40	0.09	0.39	0.06
Slice 2	0.45	0.16	0.19	0.17	0.42	0.09	0.25	0.22
Slice 3	0.47	0.40	0.22	0.37	0.48	0.11	0.15	0.25
Slice 4	0.65	0.58	0.37	0.56	0.81	0.07	0.28	0.23

Table 4.4: Mean Crack Intersection Density value.

5 RESULTS

5.1 Data analysis criteria

When the magnetite mortar block has been blasted and the remaining part filled with fast hardening cement, the block is mechanically removed from the yoke by prying on one side. Due to this mechanical action, it is possible to create additional damage on the sides of the specimen.

Several observations on how to analyze the conditions of the specimens before starting to cut them and to draw the 3D model are given. A discussion on removing data is also included:

- a) Not all the blocks are removed by prying from the same side. In addition, there is missing information about on which side of the block the prying was done. Therefore, it is difficult to know on which side of the block additional damage may have been created.
- b) As it is explained in section 2, the block is fixed to the yoke using fast hardening cement. The remaining part of the block, in this case, should have a 5 cm thin layer of this material along the perimeter, back, left and right sides. Since the contour of the specimen is irregular or may be broken, it is possible to mechanically damage the block when removing it.
- c) The crack density in both sides of the block (region between hole 5 and the left hand side and region between hole 1 and the right hand side) are different between slices and between blocks. This situation makes it difficult to know if the cracks in these regions were, in part, created by the mechanical removal (figure 2.3)
- d) The surface created in the 3rd row is irregular and, in some cases, the existence of breakage angle in one of the sides of the blocks can be seen.

Under this light and in order to gather data in constant fashion for all of the blocks, cracks in the edge regions outside holes 1 and 5 should be discarded.

In section 5.3.2.1, a comparison between data using all the cracks information from the slice and that using only cracks between holes 1 and 5 of the slice and excluding the edge regions is presented so as to show the influence of mechanical damage induced when removing blocks from the yoke.

5.2 Crack development comparison using different delay time

As seen in table 2.2, blocks were blasted using different delay times between rows and holes. Three types of comparisons can thus be made:

- a) *Comparison 1: 0-0-0 vs 28-28-28 vs 73-73-73.* Comparison between blocks with different delay time, but the same delay time in all the rows and holes: in this first case, the comparison was done between blocks CH02B01, CH02B02 and CH02B04 (table 2.2). This comparison shows differences in crack development when the block is blasted with a shorter or longer delay time.
- b) *Comparison 2: 0-0-0 vs 28-0-0 vs 140-0-0.* Comparison between blocks changing the delay time in the first row and using simultaneous firing (no delay time) in rows 2 and 3: in this analysis, the comparison was done for the blocks CH02B01, CH03B05 and CH02B03 (table 2.2). Using this comparison, the importance of the delay time on the first row is studied.
- c) *Comparison 3: 28-73-73 vs 73-73-73.* Comparison between blocks changing the delay time of the first row and using a delay time of 73 μ s in rows 2 and 3. The comparison was done between blocks CH03B04 and CH02B04 (table 2.2). This analysis for longer delay time in rows 2 and 3 compares the effect of changing the delay time value in the first row.

Data from the blocks CH01B01 and CH02B05 are not herein used, since block CH01B01 was drilled with seven boreholes and the specific explosive charge was greater than in the others, so data are not comparable with the other blocks. Secondly, only the first row was blasted and in the second, half of the second row of the block CH02B05 the charges didn't detonate, making impossible to compare data with the others blocks. However, such discarded

data may be useful to study the difference of crack development between blasting only the first row and blasting the first and second row.

5.3 Data analysis

To study the effect of the crack development in the block by changing the delay time in the sequence, four different analyses of the data obtained from the 3D model and damage maps of the blocks were performed. The analysis criteria for the three types of comparisons were explained in section 5.2.

5.3.1 Crack family analysis between slices surfaces and blocks.

The first analysis compares the number of cracks created by blasting using different delay times. The analysis is done by studying the number of cracks from each family and from one of each pair of slice surfaces of the block.

The purpose of the analyses is to study whether there are differences between the number of cracks obtained between the slices of the block and between those obtained from the other blocks with which the comparison has been done depending on the delay time.

According to section 5.2, there are three comparison groups; two of them consist of three testing blocks and one of them of two. In this way, twelve comparative analyses for each family were performed between blocks CH02B01, CH02B02 and CH02B04; and CH02B01, CH02B03 and CH03B05 and, finally, other eight comparative analyses for each family between blocks CH02B04 and CH03B04.

Two statistical methods were considered for this study: ANOVA F-test and Kruskal Wallis analysis. See ANNEX IV.

To be able to use the ANOVA F-test, in every comparison, the mean and the variance of the number of cracks for the slices for each block are calculated. The number of data for each calculation is also needed. See ANNEX IV. For Kruskal

Wallis analysis, the number of cracks for the slices of each block is used. These steps must be done for each crack family.

5.3.1.1 Results

The following tables summarize the results of the family analyses between slices and blocks. The three comparison criteria were established using both the ANOVA F-Test and the Kruskal Wallis test methods:

Comparison 1: 0-0-0 vs 28-28-28 vs 73-73-73

Crack Family	F ratio	P-value	F_{critical} (α)	Significant Differences
All families	1.34	0.31	4.26	No
CB 90-80	1.04	0.39	4.26	No
CB 80-30	7.29	0.01	4.26	Yes
CB 30-0	3.55	0.07	4.26	No
CSB	2.79	0.11	4.26	No
Connection	5.33	0.03	4.26	Yes
Parallel	40.06	0.00	4.26	Yes
Dir 90-80	0,05	0.95	4.26	No
Dir 80-30	0.22	0.81	4.26	No
Dir 30-0	0.43	0.66	4.26	No
Shorts	1.43	0.29	4.26	No

Table 5.1: ANOVA F-Test. Comparison 1. $\alpha = 0.05$ and Degrees of freedom (df) = 2

Crack Family	H	P-value	$X^2(\alpha)$	Significant Differences
All families	2.89	0.24	5.99	No
CB 90-80	2.20	0.33	5.99	No
CB 80-30	6.93	0.03	5.99	Yes
CB 30-0	4.68	0.10	5.99	No
CSB	4.57	0.10	5.99	No
Connection	4.88	0.09	5.99	No
Parallel	8.00	0.02	5.99	Yes
Dir 90-80	0.18	0.91	5.99	No
Dir 80-30	0.61	0.74	5.99	No
Dir 30-0	1.74	0.42	5.99	No
Shorts	2.81	0.25	5.99	No

Table 5.2: Kruskal-Wallis H Test. Comparison 1. $\alpha = 0.05$ and $df = 2$

Tables 5.1 and 5.2 show the same result for both tests except for family Connection, where F-test shows significant differences but Kruskal Wallis does not. If P-values for both tests are compared, in general, the ANOVA F test gives higher values when there are not significant differences between data and lower values when there are significant differences than Kruskal Wallis.

F_{ratio} results obtained for families Dir 90-80, Dir 80-30 and Dir 30-0 are strange because, as is explained in Annex VII (page XL), $MSB > MSE$; therefore, $F_{ratio} = \frac{MSB}{MSE} > 1$. However, these values are < 1 .

Comparing crack development by family, in families CB 80-30 and Parallel it is possible to find significant differences between the number of cracks.

In the other families, on the other hand, no significant differences between the number of cracks between slice surfaces are found. In the same way, analysis between all families together shows that there are no differences. This means that if slice surfaces are compared separately, no significant differences related to the number of cracks developed can be found using either longer or shorter delay times for blasting.

Comparison 2: 0-0-0 vs 28-0-0 vs 140-0-0

Crack Family	<i>F</i> ratio	<i>P</i> -value	<i>F</i> _{critical} (α)	Significant Differences
All families	3.30	0.08	4.26	No
CB 90-80	4.33	0.04	4.26	Yes
CB 80-30	0.56	0.59	4.26	No
CB 30-0	2.73	0.12	4.26	No
CSB	1.49	0.276	4.26	No
Connection	4.96	0.4	4.26	Yes
Parallel	14.90	0.00	4.26	Yes
Dir 90-80	1.50	0.274	4.26	No
Dir 80-30	1.95	0.20	4.26	No
Dir 30-0	2.33	0.15	4.26	No
Shorts	1.278	0.325	4.26	No

Table 5.3: ANOVA F-Test. Comparison 2. $\alpha = 0.05$ and $df = 2$

Crack Family	H	<i>P</i> -value	χ^2 (α)	Significant Differences
All families	3.59	0.17	5.99	No
CB 90-80	6.93	0.03	5.99	Yes
CB 80-30	1.19	0.55	5.99	No
CB 30-0	4.45	0.11	5.99	No
CSB	2.92	0.23	5.99	No
Connection	6.07	0.05	5.99	Yes
Parallel	7.63	0.02	5.99	Yes
Dir 90-80	3.13	0.21	5.99	No
Dir 80-30	1.86	0.40	5.99	No
Dir 30-0	2.58	0.28	5.99	No
Shorts	2.58	0.28	5.99	No

Table 5.4: Kruskal-Wallis H Test. Comparison 2. $\alpha = 0.05$ and $df = 2$

Tables 5.3 and 5.4 show the same results for both tests. A strange result, related to the F_{ratio} is found in family CB 80-30, where the value is <1 .

Comparing the crack development by family, in families CB 90-80, Connection and Parallel significant differences in the number of cracks are found.

In the other families, on the other hand, no significant differences in the number of cracks between slice surfaces are found. In the same way, analysis between all families together shows that there are no differences. This means that if slice

surfaces are compared separately, no significant differences related to the number of cracks developed can be found using either longer or shorter delay times in the first row for blasting.

Comparison 3: 28-73-73 vs 73-73-73

<i>Crack Family</i>	<i>F ratio</i>	<i>P-value</i>	<i>F_{critical} (α)</i>	Significant Differences
All families	4.75	0.07	5.99	No
CB 90-80	0.06	0.82	5.99	No
CB 80-30	8.17	0.03	5.99	Yes
CB 30-0	0.11	0.75	5.99	No
CSB	6.40	0.04	5.99	Yes
Connection	0.43	0.54	5.99	No
Parallel	34.94	0.00	5.99	Yes
Dir 90-80	5.99	0.39	5.99	No
Dir 80-30	0.69	0.44	5.99	No
Dir 30-0	0.00	1.00	5.99	No
Shorts	0.00	1.00	5.99	No

Table 5.5: ANOVA F-Test. Comparison 3. α = 0.05 and df = 2

Crack Family	H	<i>P-value</i>	<i>X² (α)</i>	Significant Differences
All families	3.00	0.08	3.84	No
CB 90-80	0.19	0.67	3.84	No
CB 80-30	4.08	0.04	3.84	Yes
CB 30-0	0.19	0.67	3.84	No
CSB	3.00	0.08	3.84	No
Connection	0.33	0.56	3.84	No
Parallel	5.33	0.02	3.84	Yes
Dir 90-80	0.75	0.39	3.84	No
Dir 80-30	0.08	0.77	3.84	No
Dir 30-0	0.33	0.56	3.84	No
Shorts	0.02	0.88	3.84	No

Table 5.6: Kruskal-Wallis H Test. Comparison 3. α = 0.05 and df = 2

Tables 5.5 and 5.6 do not show the same result in both tests calculated for family CSB. The F-test shows significant differences but Kruskal Wallis does not. In

addition, strange results related to the F_{ratio} are found in families CB 90-80, CB 30-0, Connection, Dir 80-30, Dir 30-0 and Shorts, where the values are < 1 .

Comparing crack development by family, in families CB 80-30 and parallel it is possible to find significant differences in the number of cracks. In the remaining families, on the other hand, no significant differences in the number of cracks can be found. In the same way, there are no differences in the analysis for the all families together. This means that the use of a different delay time in the first row has not a high influence in crack development, comparing single slice surfaces, when a longer delay time (73 μ s) is used in the following rows.

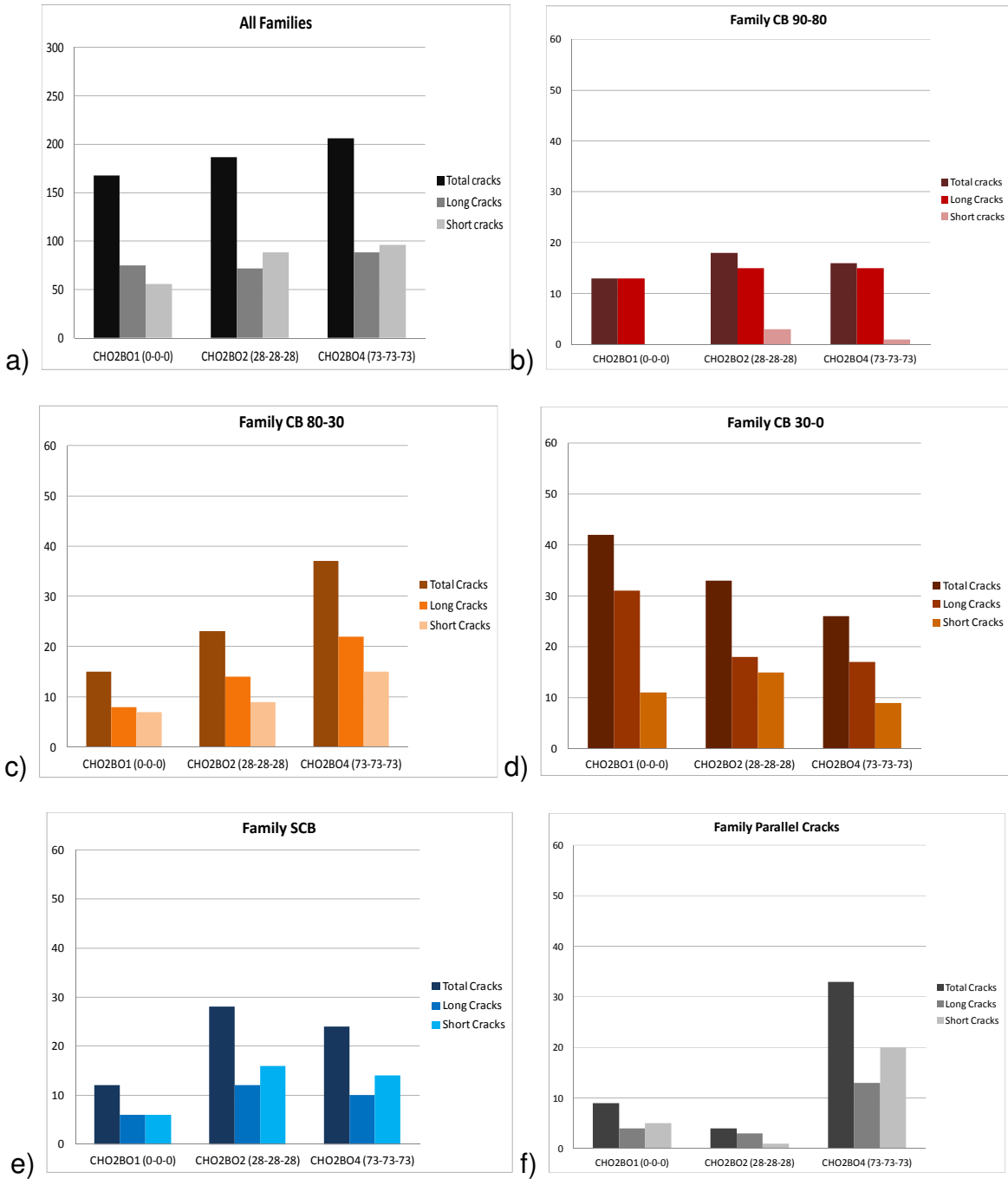
An interesting result is noted for the crack family Parallel: in all three comparisons, significant differences between the number of cracks are found.

5.3.2 Crack family analysis between blocks

In this second analysis a comparison of the number of cracks developed by blasting using different delay times is carried out. The analysis was made by studying the number of cracks from each family; but, in this case, cracks from the four slices were added up, getting this a number of cracks from the all block and comparing those values between blocks blasted with different delay times, according to the criteria established in section 5.2.

Such comparison is depicted in the following graphs, where the number of cracks from each family is shown:

Comparison 1: 0-0-0 vs 28-28-28 vs 73-73-73



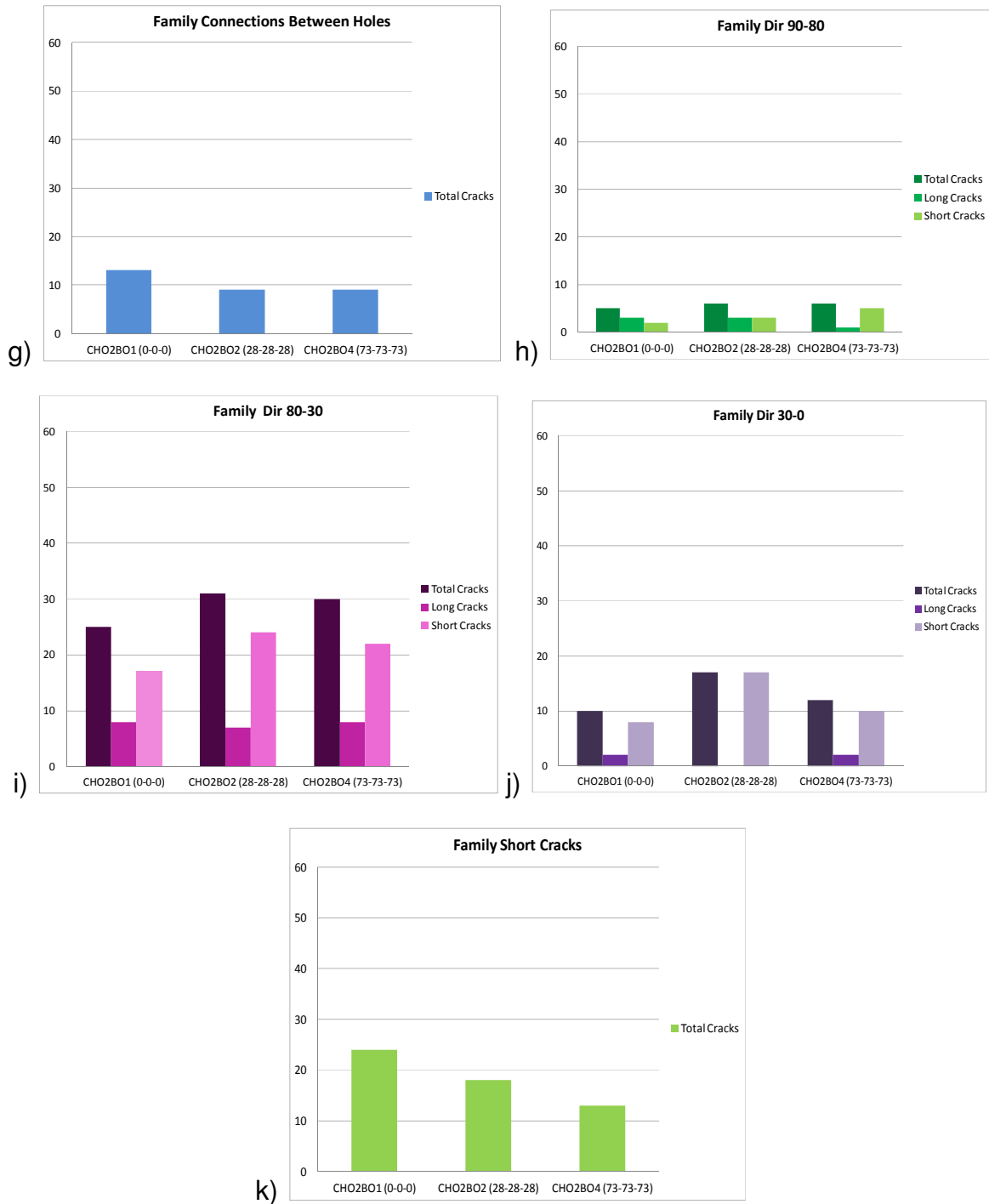


Figure 5.1: Comparison 1:

a) All Families; b) Family CB 90-80; c) Family CB 80-30; d) Family 30-0; e) Family SCB; f) Family Parallel Cracks; g) Family Connection between Holes; h) Family Dir 90-80; i) Family Dir 80-30; j) Family Dir 30-0; k) Family Short Cracks

Graphs from figure 5.1 represent the number of cracks divided by families. In each graph, three columns can be distinguished: the total number of cracks (dark color), long cracks (medium color) and short cracks (light color). Several tendencies can

be identified for the total number of cracks, long and short cracks depending of the delay time:

Figure 5.1. a): All Families: when comparing all families together, a slight increase of number of cracks is found for longer delay times. The longer the delay time the higher the number of cracks.

Figure 5.1. b): Family CB 90-80: The number of cracks developed behind the borehole is similar for the three blocks, which means that independently of the delay time, a crack starting from the borehole limited by a sector between 90° - 80° is developed with the same probability.

Figure 5.1. c): Family CB 80-30: the number of blast induced cracks limited by a sector between 80° - 30° is more than double when the delay time increases from 0 to 73 us. The longer the delay time the higher the number of cracks. In the same way, the longer the delay time, the higher the number of long cracks, in comparison to the short cracks.

Figure 5.1. d): Family CB 30-0: contrary to the previous family, the shorter the delay time, the higher number of cracks in a sector between 30° - 0° and also the higher number of long cracks.

Figure 5.1. e): Family SCB: for this family, the longer the delay time the higher number of cracks, starting from the back side of the block and following a trajectory not directed towards the boreholes.

Figure 5.1. f): For the Parallel crack family, an increase of more than 3 times the number of cracks is achieved by using the longest delay time, see block CH02B04 data.

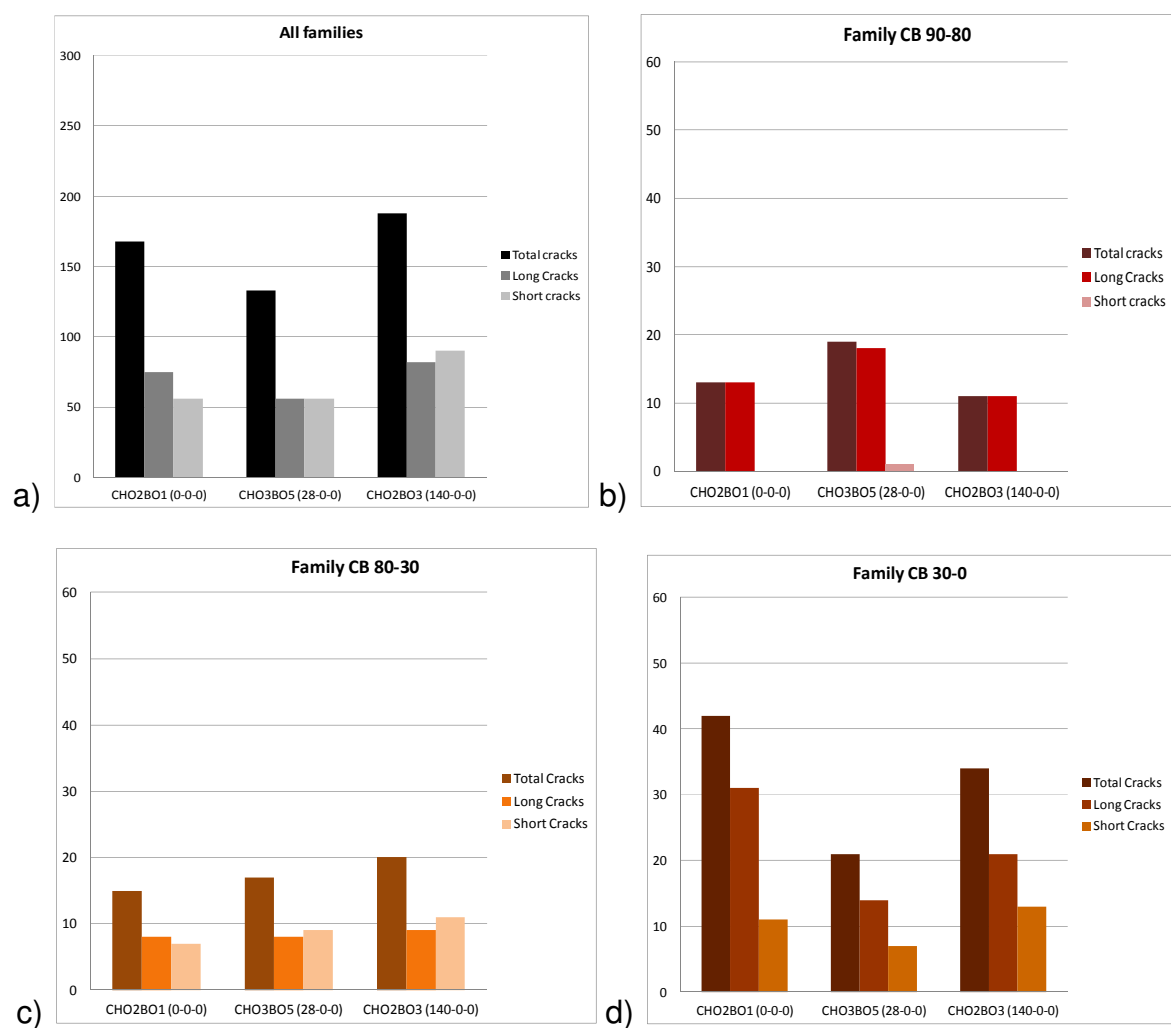
Figure 5.1. g): Family Connection between holes: The number of cracks developed between boreholes is similar for the three blocks; however in block CH02B01, this number is slightly greater. This means that independently of the delay time, connections between boreholes are developed with the same influence.

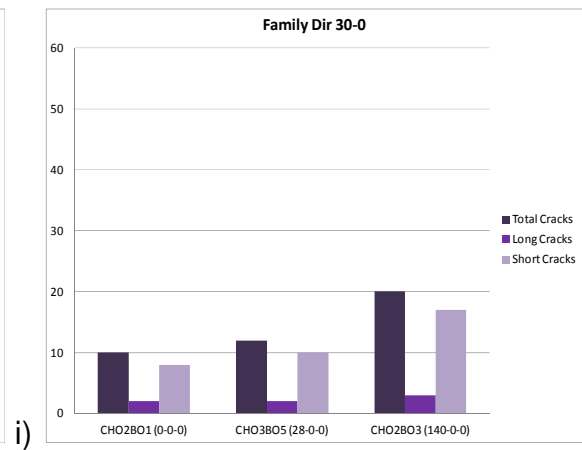
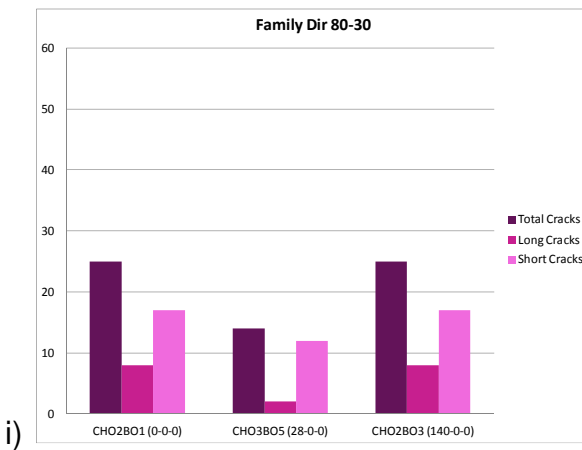
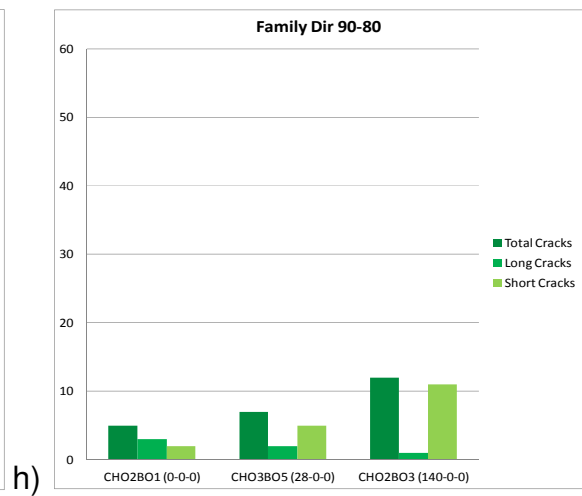
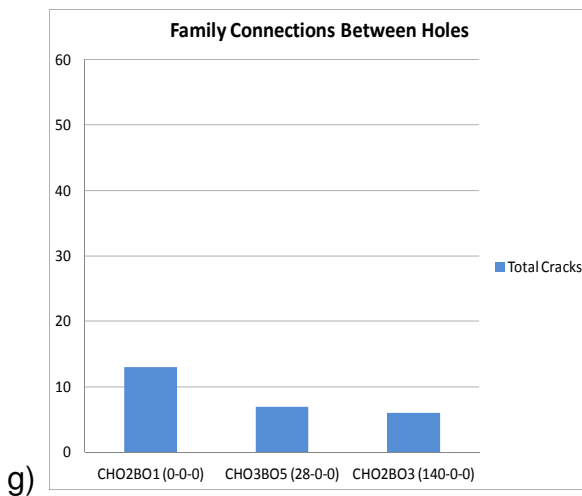
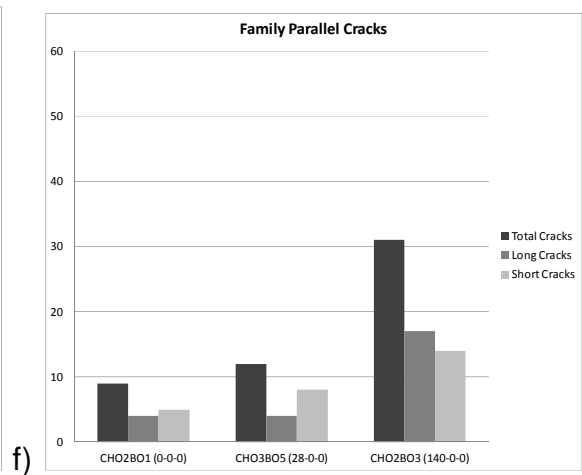
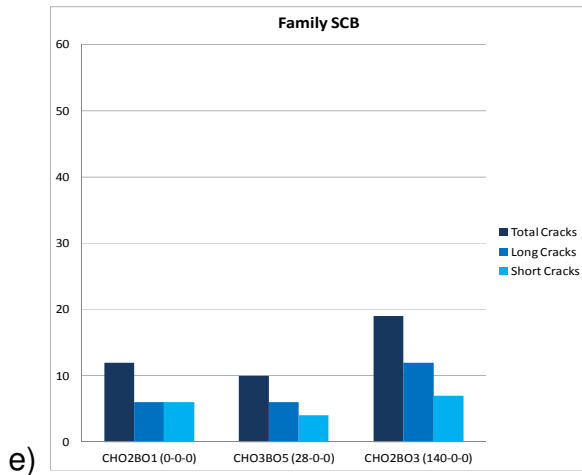
Figure 5.1. h); i); j): Cracks that do not start from the borehole but rather develop a trajectory along a radial direction away from the borehole limited by a sector between 90° - 80° , 80° - 30° or 30° - 0° present similar influence with the use of

different delay times, but with a slight increase in the number of cracks when the delay time is longer than 0-0-0 μ s.

Figure 5.1. k): Family Short cracks: the number of short cracks created around the borehole is slightly influenced by delay times. The shorter the delay time, the higher the number of cracks.

Comparison 2: 0-0-0 vs 28-0-0 vs 140-0-0





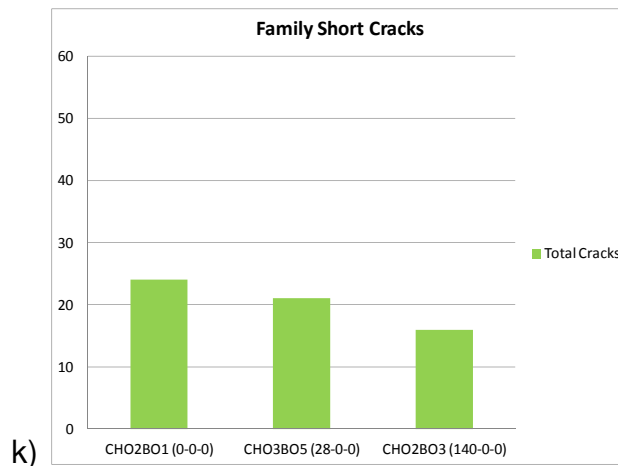


Figure 5.2: Comparison 2:

a) All Families; b) Family CB 90-80; c) Family CB 80-30; d) Family 30-0; e) Family SCB; f) Family Parallel Cracks; g) Family Connection between Holes; h) Family Dir 90-80; i) Family Dir 80-30; j) Family Dir 30-0; k) Family Short Cracks

Graphs from figure 5.2 represent, as explained in comparison 1, the number of cracks per family. Different tendencies can be identified depending on the delay time used in the first row:

Figure 5.2. a): All Families: comparing all families together, a slight increase of number of cracks is found when the largest delay time in the first row is used (140 μ s). However, using a shorter delay time, but longer than 0 μ s (28 μ s), a lower number of cracks is obtained.

Figure 5.2. b): Family CB 90-80: The same effect as in comparison 1 is found. The number of cracks developed behind the borehole is similar for the three blocks, which means that, independently of the delay time, a crack starting from the borehole limited by a sector between 90^o-80^o is developed with the same probability.

Figure 5.2. c): Family CB 80-30: Here the number of cracks limited by a sector between 80^o- 30^o is slightly influenced by the use of different delay times in the first row. Then, a slight increase of the number of cracks is found when increasing the delay time.

Figure 5.2. d): Family CB 30-0: Here the opposite influence than for the previous family is found. Using a shorter delay time in the first row, a higher number of cracks is developed in the sector limited by 30^o- 0^o. A different result is, however,

obtained with the block CH03B05, which presents a lower number of cracks than block CH02B03, blasted with a 140 μs delay time in the first row.

Figure 5.2. e): Family SCB: for this family, the longer the delay time, the higher the number of cracks is found starting from the back side of the block and following a trajectory not directed towards the boreholes.

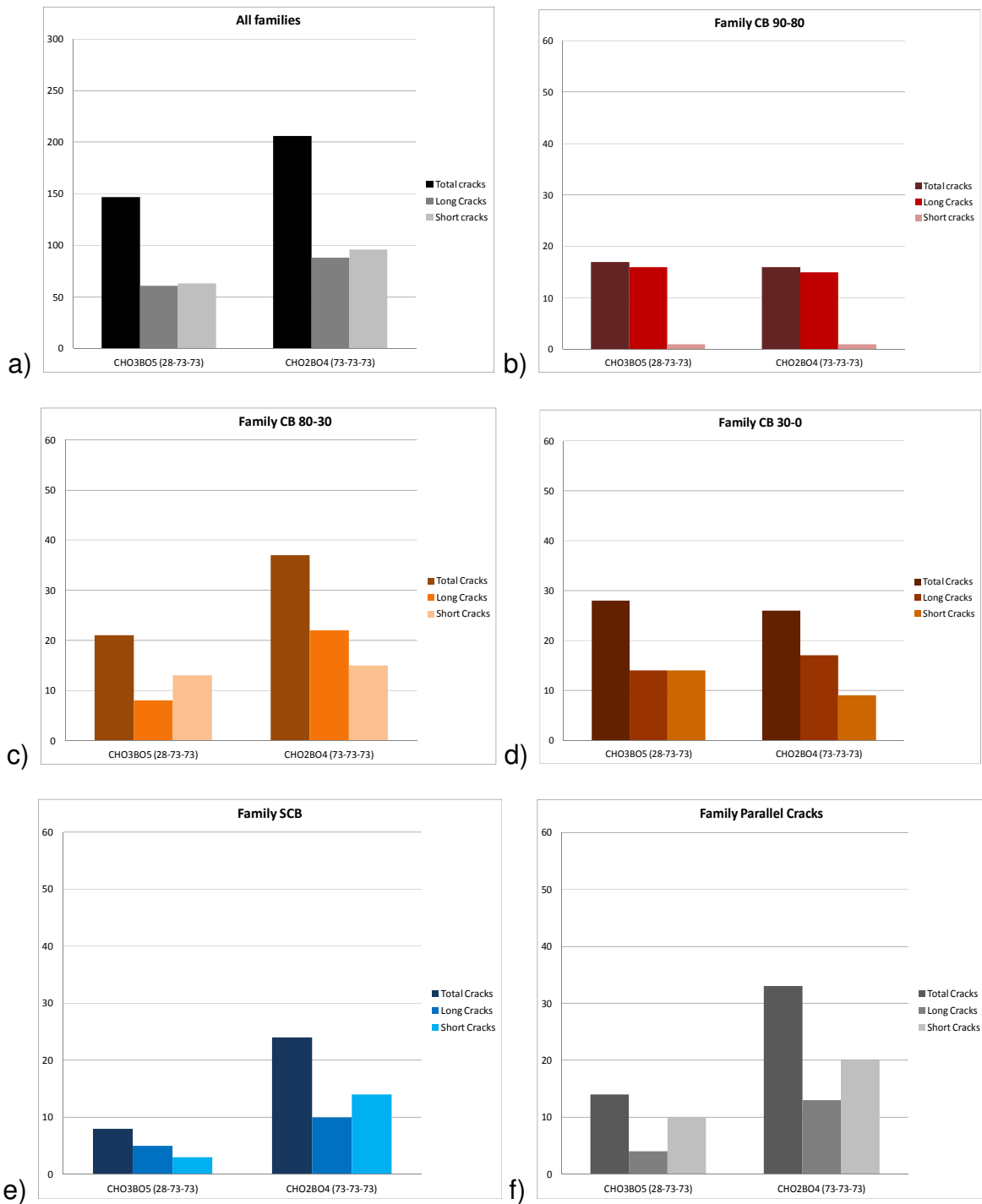
Figure 5.2. f): For the Parallel crack family, a large increase of the number of cracks is found for the 140 μs in the first row, see block CH02B03 data.

Figure 5.2. g): Family Connection between holes: The number of cracks developed between boreholes is similar for the three blocks; however in block CH02B01, this number is slightly greater. This means that independently of the delay time, connections between boreholes are developed with the same probability.

Figure 5.2. h); i); j): Cracks that do not start from the borehole but rather develop a trajectory with a radial direction away from the hole limited by a sector between $90^\circ - 80^\circ$ or $30^\circ - 0^\circ$ show a small influence from the delay time in the first row, showing a slight increase of the number of cracks when the delay time becomes longer. A different result is obtained in sector between $80^\circ - 30^\circ$. In this case, for delay times in the first row of 0 and 140 μs , the number of cracks is approximately the same. However, using a delay time of 28 μs in the first row, a lower number of cracks was found.

Figure 5.2. k): Family short cracks: the number of short cracks created around the borehole is slightly influenced by delay times. The shorter the delay time, the higher the number of cracks becomes.

Comparison 3: 28-73-73 vs 73-73-73



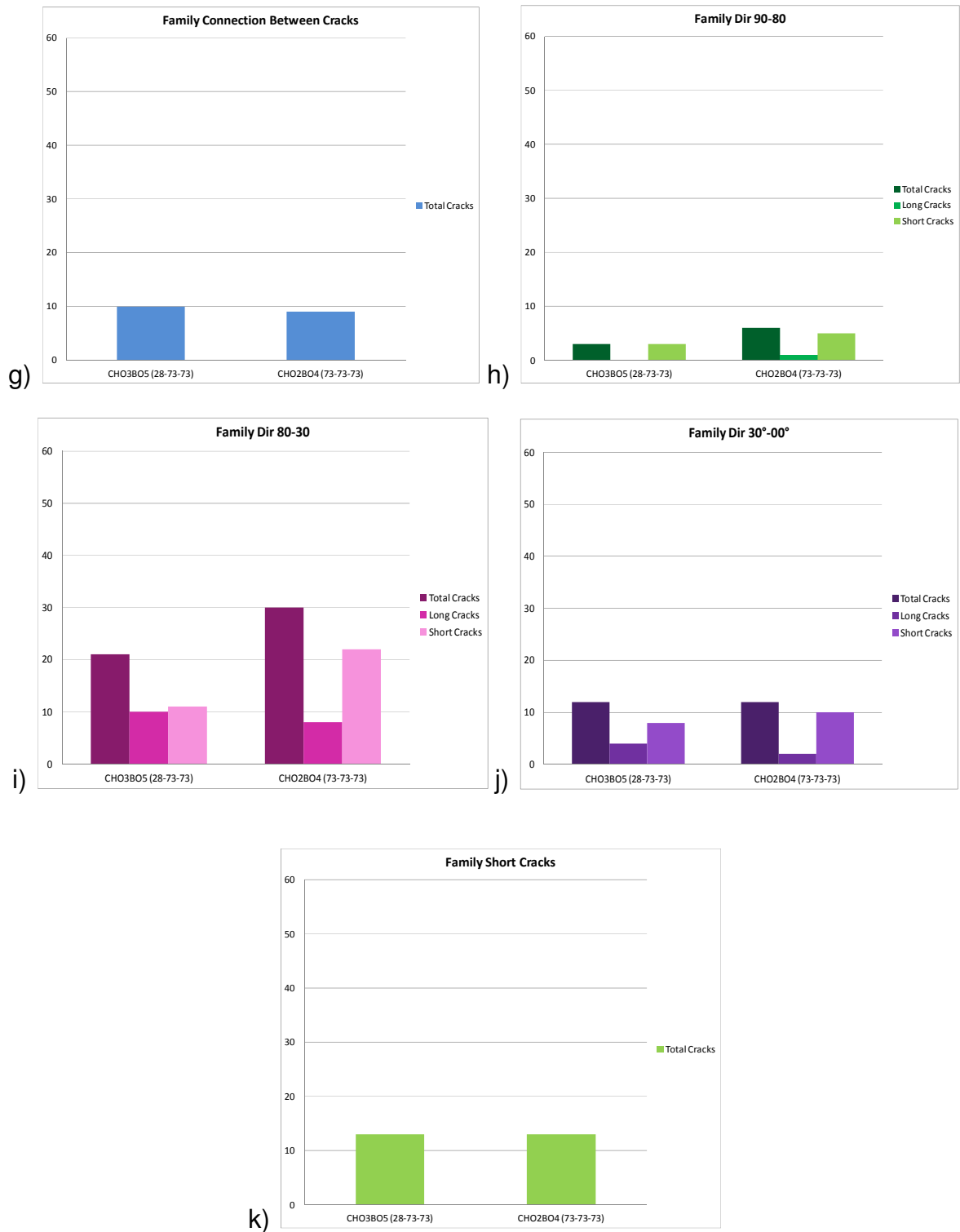


Figure 5.3: Comparison 3:

a) All Families; b) Family CB 90-80; c) Family CB 80-30; d) Family 30-0; e) Family SCB; f) Family Parallel Cracks; g) Family Connection between Holes; h) Family Dir 90-80; i) Family Dir 80-30; j) Family Dir 30-0; k) Family Short Cracks

Graphs from figure 5.3 represent the number of cracks grouped by families. Different tendencies can be identified depending of the delay time used in the first row:

Figure 5.3. a): All Families: comparing all families together, a large increase of number of cracks is found when the longest delay time in the first row is used.

Figure 5.3. b): Family CB 90-80: The number of cracks developed behind the borehole is similar for the two blocks, which means that, independently of the delay time, a crack starting from the borehole limited by a sector between 90° - 80° is developed with the same probability.

Figure 5.3. c): Family CB 80-30: According to the graph, the number of cracks limited by a sector between 80° - 30° is almost the double when the delay time increases in the first row from 28 to 73 us. In this way, the longer delay time, the higher number of cracks.

Figure 5.3. d): Family CB 30-0: a different influence than in the previous family is found in the number of cracks limited by a sector between 30° - 0° : the influence is similar using shorter or longer delay times in the first row.

Figure 5.3. e): Family SCB: for this family, the longer the delay time, the higher number of cracks, starting from the back side of the block and following a trajectory not directed towards the boreholes.

Figure 5.3. f): For the Parallel crack family, a large increase of three times the number of cracks is observed as it was in comparisons 1 and 2 by the longer delay time in the first row, see block CH02B04 data.

Figure 5.3. g): Family Connection between holes: The number of cracks developed between boreholes is similar for the three blocks; however in block CH02B01, this number is slightly greater. This means that independently of the delay time, connections between boreholes are developed with the same influence.

Figure 5.3. h); i); j): Cracks that do not start from the borehole but rather develop a trajectory with a radial direction away from the hole limited by a sector between 90° - 80° or 30° - 0° are not influenced by the delay time in the first row. The number of cracks is approximately the same for the two cases. On the other hand,

in sector between 80° - 30° , a slight increment of the number of cracks is observed when the delay time in the first row is longer.

Figure 5.3. k): Family short cracks: The number of short cracks developed around the borehole is similar for the three blocks, which means that independently of the delay time, connections between boreholes are developed with the same influence.

5.3.2.1 Effect of also using crack data from the side parts of the slices.

Graphs from ANNEX V compare data using all the cracks information from the whole slice rather than using only data between the holes 1 and 5 of the slice. Those values are comparative between blocks blasted with different delay times, according to the criteria established in section 5.2.

Differences in the number of crack can be seen but tendencies between different blocks, plotted according to the three comparisons, remain the same. The only exception in all three comparisons concerns family Dir 30° - 0° . In this case, the number of cracks and tendencies between blocks is different. That situation may mean that the mechanical removal of the block has created additional damage in the sides of the blocks, in the sector limited by 30° - 0° .

5.3.3 Radial crack distribution

The following analysis concerns the distribution of radial cracks for families that start from the borehole (Families CB 90-80, CB 80-30, CB 30-0) and for families that do not start from the borehole but rather develop a trajectory with a radial direction away the hole (Families Dir 90-80, Dir 80-30, Dir 30-0). The development of radial cracks is not always the same around the borehole. As presented in section 5.3.2, different delay times for blasting blocks influences the number of cracks generated. The number of radial cracks distribution around the borehole is also influenced.

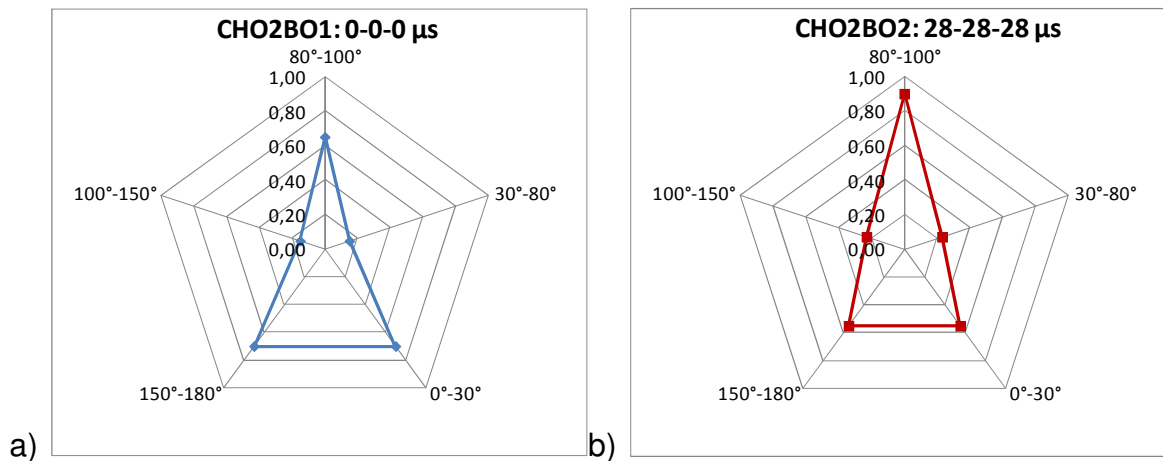
Since the sectors that limit the radial families do not have the same range of degrees, a calculation must be done in advance to obtain a comparable value of the number of cracks for all three sectors. The number of cracks calculated includes the sum of cracks that belong to sectors from both sides of the 90° line. The number of cracks from both sectors is added and divided by two times the degrees of one sector (equation 2).

$$\text{Angular Crack Density (ACD)} = \frac{\text{Number of cracks in sectors}}{2 \times \text{Number of degrees in sector}} \quad (2)$$

This averages of the ACD in the sectors on both sides of the 90° line. This makes the ACD symmetric to the 90° line. Then the same ACD is assigned to both sectors. The results of those calculations are depicted in radial graphs.

Comparison 1: 0-0-0 vs 28-28-28 vs 73-73-73

- a) *Radial crack distribution starting from the borehole (CB 90-80; CB 80-30; CB 30-0).*



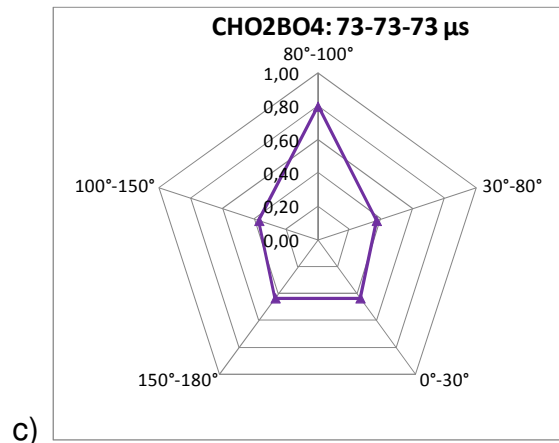


Figure 5.4 a), b), c): Comparison 1. Radial Crack Distribution. Cracks starting from the borehole.

Radial cracks limited in sectors are presented in figure 5.4. To get a symmetric distribution, the sector 90°-80° is rescaled to 100°-80°. The values used in the graph were obtained from the previous calculation using equation 2.

According to the different delay times, a variation in crack distribution can be seen. Blocks blasted with a short (28-28-28) or no delay time (0-0-0) in all the rows have a distribution where a larger ACD are present in the sectors between 30°- 0° and 180°-150° (figures 5.4.a and 5.4.b), resulting then in a triangular shape. Differences between non delay time and short delay times are also seen, obtaining, in the latter, a slight increase of ACD in sectors 80°- 30° and 100°-150° and a slight reduction of ACD in sector 30°- 0° and 180°-150°.

On the other hand, the block blasted with 73 μs delay time (CH02B04; figure 5.4.c) shows a more homogeneous distribution of the radial cracks. The ACD curve is almost pentagonal. As a comparison, the values from block CH02B04 are almost halved in the sector limited by 30°- 0° and 180°- 150° compared with block CH02B01 and are almost doubled in the sector limited by 80°-30° and 150°- 100° compared with blocks CH02B01 and CH02B02.

The ACD value in the sector limited by 100°- 80° is almost the same in all three blocks and rather larger than ACD in other sectors.

b) *Radial crack distribution. Cracks which develop a trajectory with a radial direction away from the hole (Dir 90-80; Dir 80-30; Dir 30-0)*

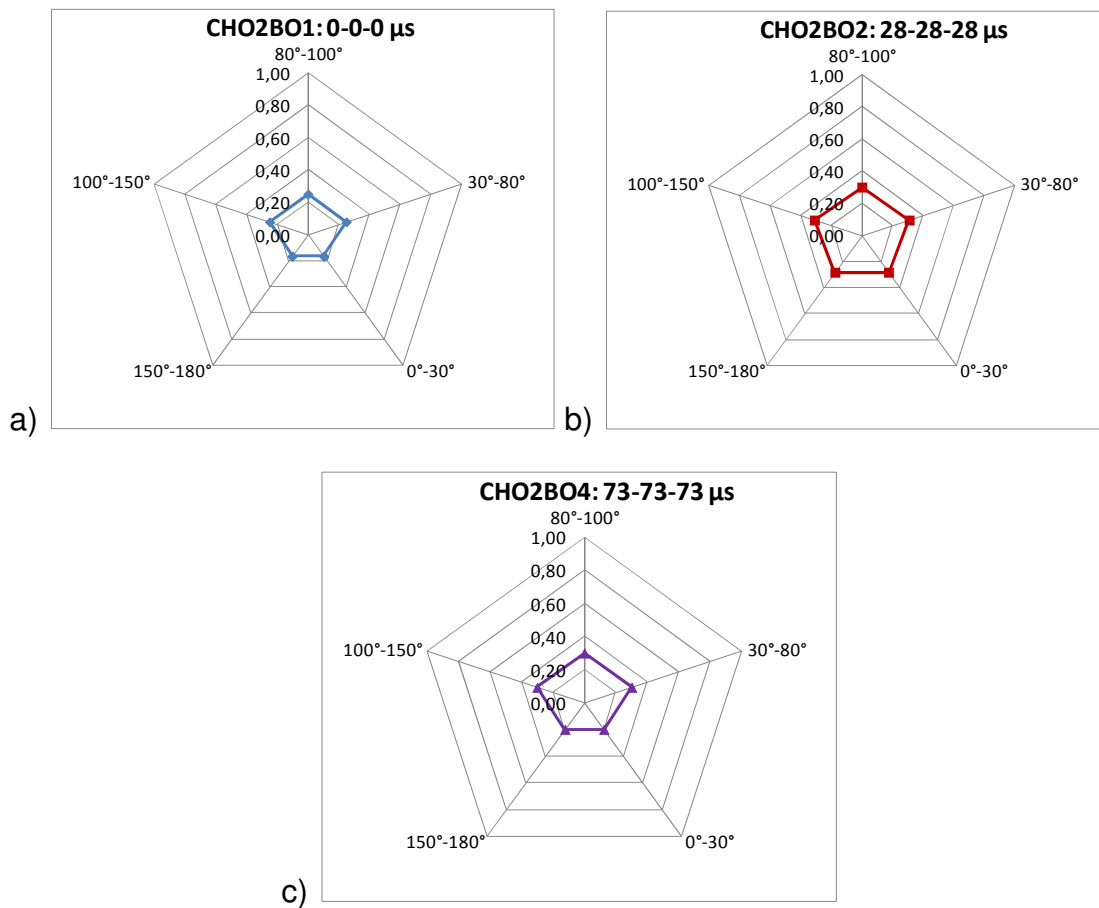


Figure 5.5 a), b), c): Comparison 1. Radial Crack Distribution. Cracks which develop a trajectory with a radial direction away from the hole.

Comparing the radial cracks that develop a trajectory with a radial direction away from the hole (figure 5.5.a, 5.5.b, 5.5.c), similar radial crack distributions are found among blocks CH02B01, CH02B02 and CH02B04. A slight increase in the ACD in all sectors can be seen in block CH02B02 but the shape of the distribution remains unchanged.

In this way, changes in delay time in all the rows have influence on radial cracks starting from the boreholes but not on those that develop a radial trajectory away from the same.

Comparison 2: 0-0-0 vs 28-0-0 vs 140-0-0

a) Radial crack distribution starting from the borehole (CB 90-80; CB 80-30; CB 30-0).

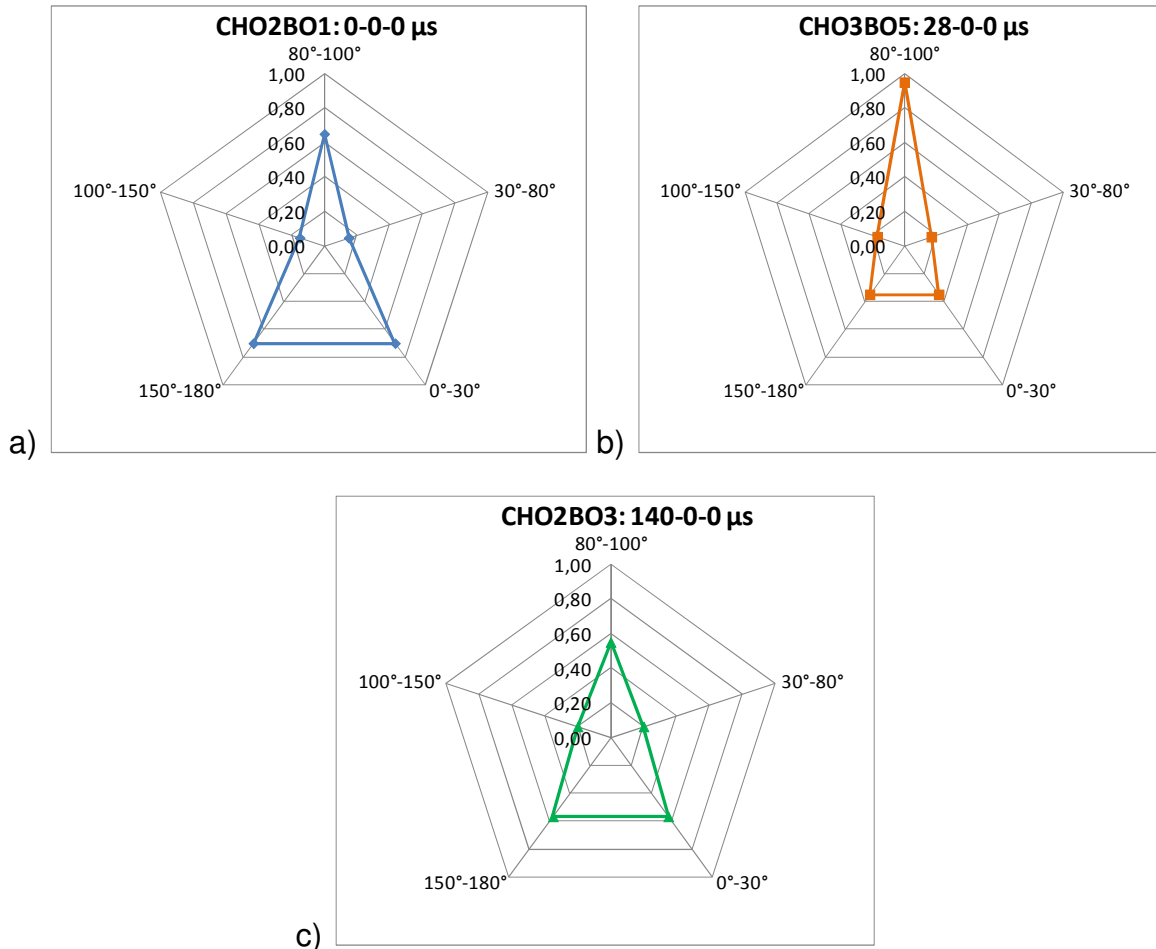


Figure 5.6 a), b), c): Comparison 2. Radial Crack Distribution. Cracks starting from the borehole.

As shown in figure 5.6, radial graphs for blocks CH02B01, CH03B05 and CH02B03 are depicted. Here, the influence on the radial cracks distribution of using different delays in the first row and no delay time in the remaining rows is compared.

Analyzing the three blocks, a triangular shape in all distributions is found. As discussed in section 5.3.2: “comparison 2”, a “strange result” in the crack distribution of block CH03B05 (figure 5.6.b) can be seen: a lower ACD in sectors

30°-0° and 180°-150° and larger ACD in sector 100°-80° is obtained. The values in the sectors 80°-30° and 150°-100° are almost the same.

Accordingly, the highest influence when delay time is changed in the first row, is seen in the sectors limited by 30°-0° and 180°-150°, where a factor of almost 1.5 between values of the blocks is obtained.

b) Radial crack distribution. Cracks with a radial direction away from the hole (Dir 90-80; Dir 80-30; Dir 30-0.

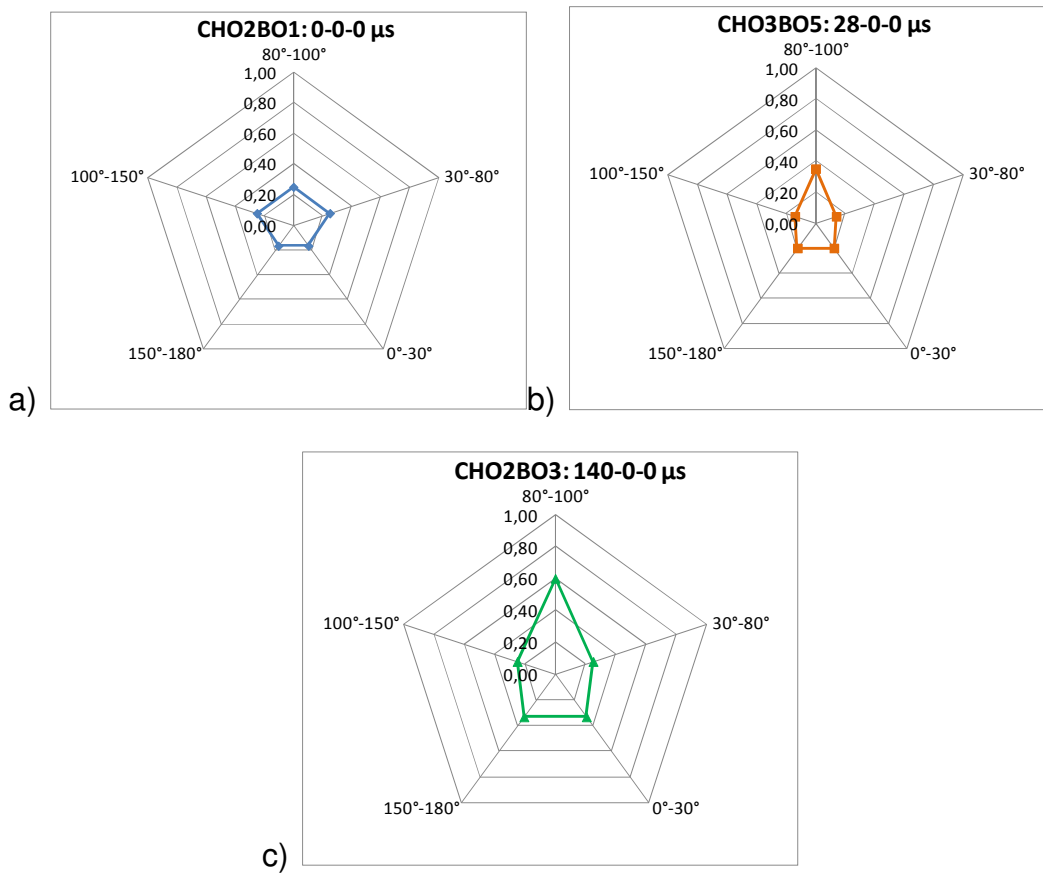


Figure 5.7 a), b), c): Comparison 2. Radial Crack Distribution. Cracks with a radial direction away from the hole.

Comparing radial cracks that develop a trajectory *with* a radial direction away from the hole (figure 5.7.a, 5.7.b, 5.7.c), a similar radial crack distribution can be found between blocks CH02B03 and CH03B05. Such blocks present almost a pentagonal distribution. However, in sector 80°- 30° and 150°-100° the value of cracks is slightly lower and in sector 100°- 80° the ACD value is slightly larger. An increase of the ACD in every sector can be seen in block CH02B03 but the shape

of the distribution remains unchanged. The curve for block CH02B01 presents a more homogenous shape, with similar ACD values to block CH02B03 in all sectors but in sector 100°- 80°, where the value of the second is almost 2 times larger.

Analyzing both radial distributions a) and b), it seems that changes in delay time in the first row, blasting rows 2 and 3 with no delay time, have more influence on radial cracks starting from the borehole than on those that develop a radial trajectory away from the same.

Comparison 3: 28-73-73 vs 73-73-73

a) *Radial crack distribution starting from the borehole (CB 90-80; CB 80-30; CB 30- 0).*

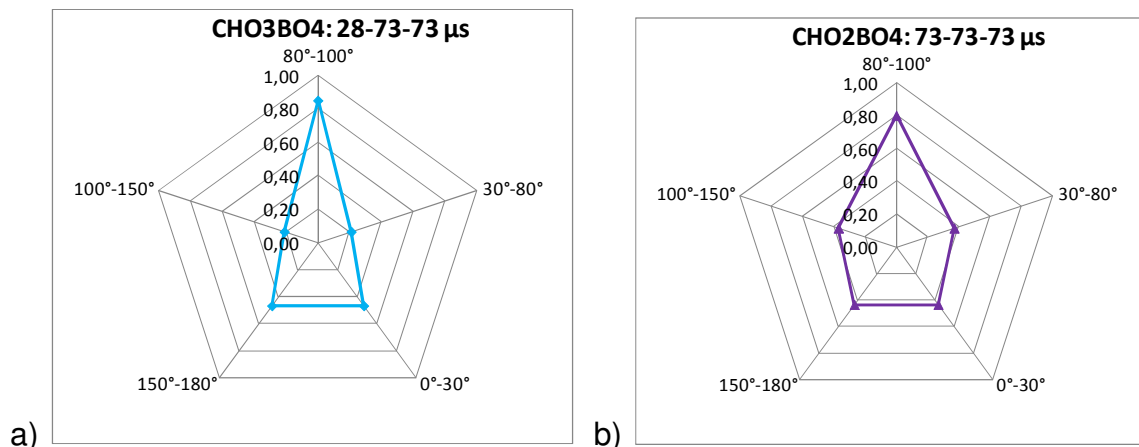


Figure 5.8 a), b): Comparison 3. Radial Crack Distribution. Cracks starting from the borehole.

Density graphs for blocks CH03B04 and CH02B04 are plotted in figure 5.8, where effects of using different delays in the first row and a delay of 73 μs in rows 2 and 3 are compared.

Differences in the shape of ACD distribution are seen: for the block CH02B04 (73-73-73 μs, figure 5.8.a) the shape is nearly pentagonal while for the block CH03B04 (28-73-73 μs, figure 5.8.b) the shape is more triangular. Crack distribution values in sectors 30°- 0°, 180°- 150° and 100°- 80° are almost the same; however, the values in sectors 80°- 30° and 150°- 100° increase by factor 2 using a longer delay time in the first row.

b) *Radial crack distribution. Cracks with a radial direction away from the hole (Dir 90- 80; Dir 80- 30; Dir 30- 0).*

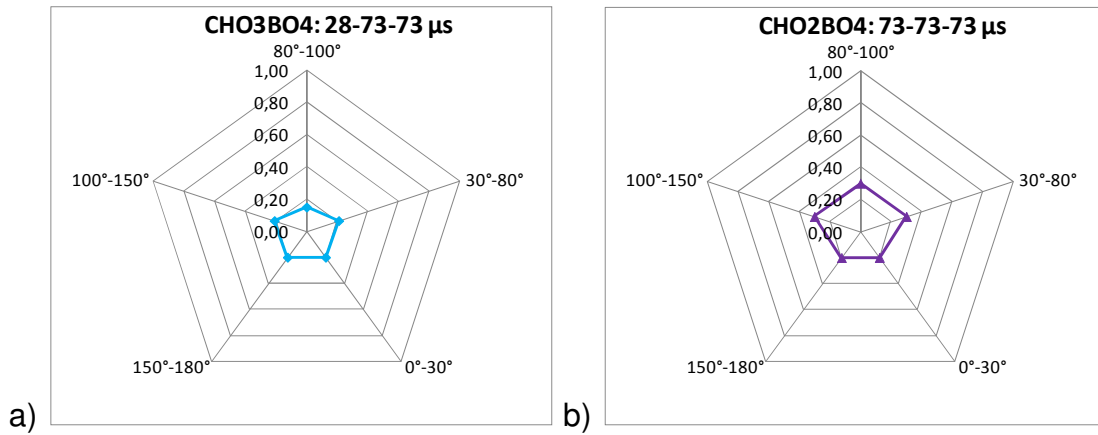


Figure 5.9 a), b): Comparison 3. Radial Crack Distribution. Cracks *with* a radial direction away from the hole.

Comparing radial cracks that develop a trajectory *with* a radial direction away from the hole (figure 5.8.a, 5.8.b), a similar radial crack distribution in sectors 30°-0° and 180°-150° is found. A factor of almost 1.5 between values in sectors 80°-30° and 150°-100° and a factor of 0.5 in sector 100°-80° can be estimated.

5.3.4 Damage map analysis

Here the previous analyses of the number of cracks and crack distribution are correlated with the damage maps calculated in the slices both from crack density and crack intersection density analysis (section 4.3).

As explained in section 4.3, two different calculations were done to represent the damage in each slice surface. The first calculation concerned the crack density. The second one concerned the crack intersection density. Both analyses show an influence of different delay times on the damage created in the slice surface by crack development.

To compare this damage, a representative value from each damage map is calculated as explained in section 4.3.5. The mean from all values of crack density

(MCD. Table 4.3) or crack intersections density (MCID. Table 4.4) associated to the grid (figure 4.18) is calculated. This value represents the mean level of damage in the slice.

Comparisons explained in section 5.2 are used for analyzing how the damage developed in tested blocks is influenced by the different delay times used in the blasting.

Comparison 1: 0-0-0 vs 28-28-28 vs 73-73-73

a) *Analysis of mean crack density*

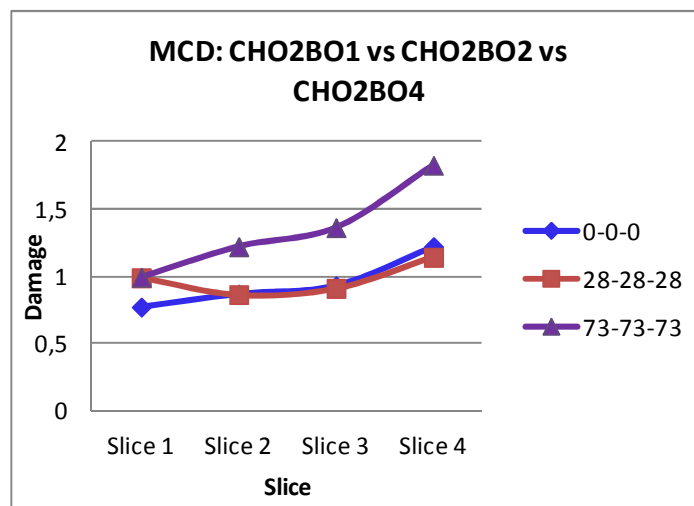


Figure 5.10: Comparison 1. Analysis of mean crack density

Figure 5.10 shows the mean crack density (MCD) values for the four slice surfaces of blocks CH02B01, CH02B02 and CH02B04. Differences in the MCD for each block can be found. Values related to the blocks blasted with delay times of 0-0-0 and 28-28-28 overlap in the graph, which means that there are no substantial differences between the MCD values when using the aforementioned delay times.

On the other hand, the MCD values related to longer delay time (CH02B04: 73-73-73 μ s) are higher for slices 2, 3 and 4; i.e. the longer delay time used for blasting the blocks, the higher the MCD values.

Slice 1, however, has a similar MCD values for the three depicted blocks. Thus, for the block CH02B04, the MCD values increases from top to bottom.

b) Analysis of mean crack intersection density

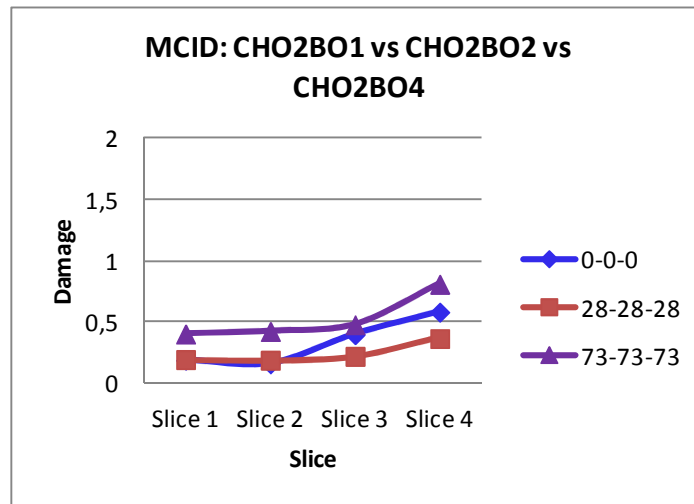


Figure 5.11: Comparison 1. Analysis of mean crack intersection density.

In Figure 5.11, the mean crack intersection density (MCID) values are shown. In this case, a slight increase of values for block CH02B04 is found when comparing them with corresponding values for the blocks blasted with shorter delay time (0-0-0, 28-28-28). The values are almost the same for the three blocks, which means that the influence of using different delay times is not as large in crack intersection density as in crack density.

Comparing the results from both damage analyses, differences of a factor of 2 can be found between MCD and MCID.

Comparison 2: 0-0-0 vs 28-0-0 vs 140-0-0

a) Analysis of mean crack density

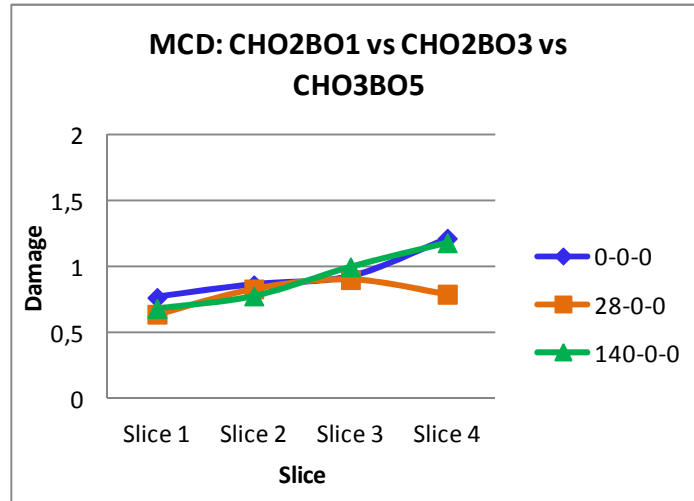


Figure 5.12: Comparison 2. Analysis of mean crack density

Analyzing figure 5.12, MCD values for the four slices surfaces of blocks CH02B01, CO3BO5 and CH02B03 are depicted. In this case, differences in the MCD values developed from each block can be found only in slice 4. According to this graph, no substantial influence in the MCD of the slices is found if different delay times in the first row and no delay time in rows 2 and 3 are used for blasting the blocks.

b) Analysis of mean crack intersection density

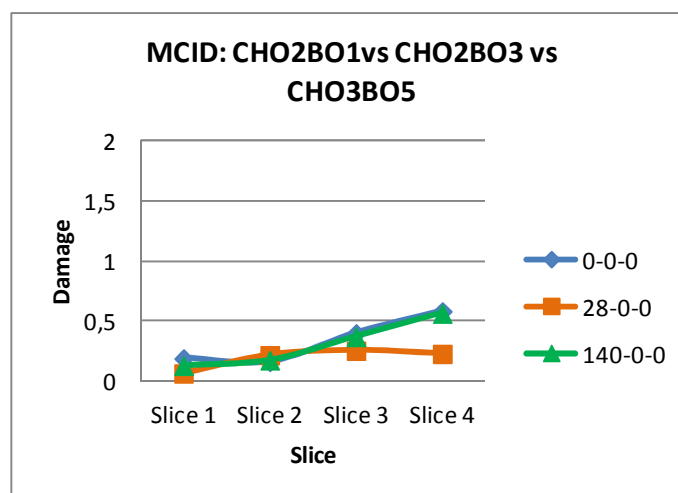


Figure 5.13: Comparison 2. Analysis of mean crack intersection density.

As in figure 5.12, in figure 5.13, no significant differences in the tendency from the MCID values can be observed.

Comparing results from both damage analyses, differences of a factor of 2 can on average be found between mean values of crack density and crack intersection density.

Comparison 3: 28-73-73 vs 73-73-73

a) Analysis of mean crack density

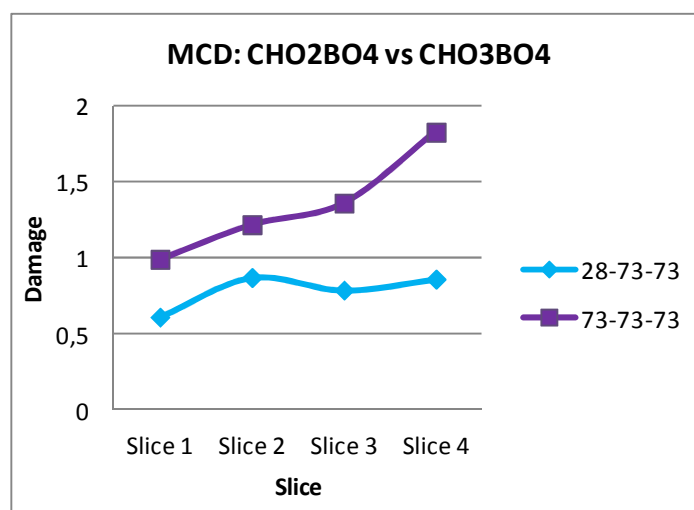


Figure 5.14: Comparison 3. Analysis of mean crack density.

Figure 5.14 represents MCD values from the four slices of blocks CH03B04 and CH02B04. Different influences of slice surfaces for each block can be found. Values related to block blasted with short delay time in the first row (28-73-73) show no influence for the four slices, while block CH02B04 presents a higher influence, which means that the longer delay time in the first row, the higher influence in MCD values.

b) Analysis of mean crack intersection density

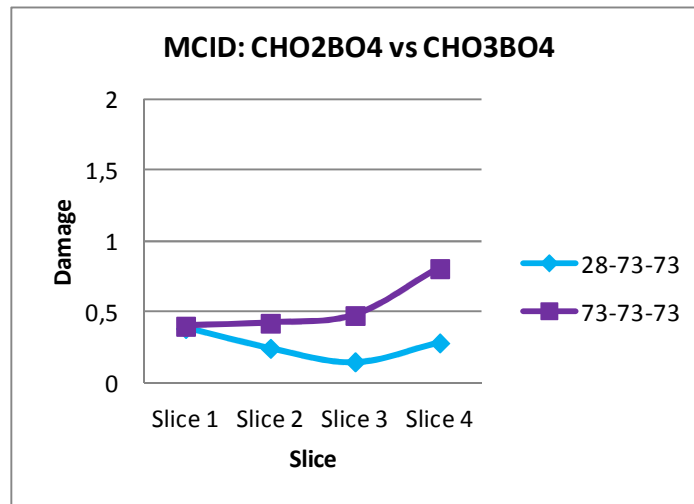


Figure 5.15: Comparison 3. Crack connections mean analysis.

As found for comparisons 1 and 2, differences of factor 2 are found between mean values of crack density and crack intersection density in comparison 3.

Slight differences in the influence for the four slices can be found in figure 5.15, where the longer delay times in the first row, the higher the mean value of crack intersection becomes.

6 CONCLUSIONS

Several techniques for crack detection have been used in order to get a better understanding of how cracks are developed in the rock like mortar by effect of the explosive. The dye penetrant technique was used for emerging crack patterns which were photographed and sketched.

An alternative procedure was used in order to study and compare the damage by crack development created in the remaining (non-blasted) part of the testing blocks blasted at the Chair of Mining Engineering of MUL (Schimek et al.2012) during 2013. In this way, a comparison of crack development caused by different delay times in the sequence for each row (blasting one row at a time) was done.

This alternative procedure is the design of a 3D model of the cracks generated in small scale blasting tests. To obtain the 3D model, the blasted specimen is cut into several slices. Then dye-penetrant is applied to the cut surfaces and the crack trace patterns are photographed. Each slice represents a vertical or horizontal cut through the specimen. These trace patterns are then used to create digital 3D models in AutoCAD

From the AutoCAD models' traces, crack families can be identified based on angles, lengths and origin. These crack families are similar to crack types found in previous crack detection studies done for real blasting specimens. Therefore, similar effects of the explosive, in terms of crack detection, can be found either for theoretical analyses using small scale blasting in ideal rock conditions and analyses in real rock conditions. This correlation has now been made for different types of hard rock (granite in Ouchterlony et al. (1999), gneiss in Ouchterlony et al. (2000) and magnetite mortar for the current MSc Thesis), showing that, in both situations, the same cracks types are developed.

Further analyses could be done in the future for testing blocks made of different types of rock, with the goal of studying if the same crack families have developed.

Four analyses of the data obtained from the 3D model and damage maps of the blocks were performed, comparing the effect of the crack development in the block

and its dependence on the delay time in the blasting sequence. The obtained results are summarized:

- 1) ANOVA F-test and Kruskal Wallis analyses show that if the slice surfaces are compared separately, no significant differences related to the number of cracks developed can be found using either longer or shorter delay times for blasting. An interesting result is obtained for the parallel crack family: significant differences in crack number for this family are found for the three comparisons, which means that the use of longer or shorter delay times may have influence in the probability of developing this type of cracks.
- 2) The second analysis made by studying the four slices together shows different behavior depending of the crack family but similar results can be found for the three comparisons:
 - *All Families*: when comparing all families together, a slight increase of number of cracks is observed for longer delay times. The longer the delay time, the higher the number of cracks.
 - *Family CB 90-80*: The number of cracks developed behind the borehole is similar in every block, which means that independently of the delay time, a crack starting from the borehole limited by a sector between 90° - 80° is developed with the same probability.
 - *Family CB 80-30*: the number of blast induced cracks limited by a sector between 80° - 30° is drastically influenced by the delay time. The longer the delay time, the higher the number of cracks. In the same way, the longer the delay time, the higher the number of long cracks, in comparison to the short cracks.
 - *Family CB 30-0*: contrary to the previous family, the shorter delay time, the higher number of cracks in a sector between 30° - 0° and also the higher number of long cracks. An exception is found in comparison 2 in block CH03B05, which presents a lower number of cracks than block CH02B03, blasted with a $140 \mu\text{s}$ delay time in the first row.
 - *Family SCB*: the longer delay time, the higher the number of cracks, starting from the back side of the block and following a trajectory not directed towards the boreholes.

- *Parallel family*: for the parallel crack family, an increase of more than 3 times the number of cracks is caused by a corresponding longer delay time (see blocks CH02B04 and CHO2BO3 data). Because the number of cracks is similar for the remaining blocks, two different explanations are proposed: the first could be that this high difference between blocks is caused because of the existence of parallel cracks to the surface inside the blocks CH02B04 and CHO2BO3 before blasting. The other explanation may be that these cracks are induced by the returning tensile wave reacting with the compressive wave. In this way, the longer delay time, the higher number of cracks. Further testing blocks analyses should be done to get a better understanding of this finding.
 - *Family Connection between holes*: The number of cracks developed between boreholes is practically the same in every block. This means that independently of the delay time, connections between boreholes are developed with the same probability.
 - Cracks that do not start from the borehole but rather develop a trajectory along a radial direction away from the borehole limited by a sector between $90^\circ - 80^\circ$, $80^\circ - 30^\circ$ or $30^\circ - 0^\circ$ behave in the same way when using different delay times, but with a slight increase in the number of cracks when the delay time is higher than 0-0-0 μs .
 - *Family short cracks*: the number of short cracks created around the borehole is slightly influenced by delay times. The shorter the delay time, the higher the number of cracks.
- 3) The radial crack distribution around the borehole is highly influence by different delay times. As can be seen in comparison 1, when all rows are blasted with the same delay time, the longer the delay time the more regular is the distribution around the borehole. This means that for longer delay times between holes, the more time the cracks have to develop in all direction. When blasting with longer delay times, the ACD in sectors $80^\circ - 30^\circ$ and $150^\circ - 100^\circ$ are double, compared to blasting with shorter delay times. In the same way, the ACD is almost halved in sectors $30^\circ - 0^\circ$ and $180^\circ - 150^\circ$.

On the other hand, the highest influence when delay time is changed only in the first row, is seen in the sectors limited by 30° - 0° and 180° - 150° , where a factor of almost 1.5 between ACD values of the blocks is obtained.

Analyzing radial cracks starting from the borehole and those that develop a radial trajectory away from the same, it seems that changes in delay time have a larger influence in the first case.

- 4) The analyses of mean crack density (MCD) and the analysis of mean crack intersection density (MCID) show that:
 - When the same delay time is used in all the rows, the longer the delay time, the higher the MCD values; and similar changes are found for MCID. Comparing the results from both damage analyses, differences of a factor of 2 can be found between MCD and crack MCDI.
 - When different delay times in the first row and no delay time in rows 2 and 3 is used for blasting the blocks, no substantial influence was found either on the MCD or on the MCID values. Comparing results from both damage analyses, differences of a factor of 2 can be found between MCD and MCID.
 - When different delay times in the first row and delay times of $73 \mu\text{s}$ in rows 2 and 3 is used for blasting the blocks, the longer delay time in the first row, the higher influence on the MCD values; and similar changes are found for MCID. Differences of a factor of 2 can be found between MCD and MCID.

According to the conclusions above, the number of cracks induced by blasting and their distribution in the mortar specimens are significantly influenced by the delay time. Damage in the rock, calculated as crack density and crack connection, i.e. crack intersection density, is also related with the delay time.

The results obtained give a better understanding of how cracks develop in a rock like mortar and how the delay time affects this development.

However, for the credibility of the procedure followed, further analyses, using specimens with the same material properties, with the same delay times and maybe longer are required in order to verify the repeatability of the results of this Thesis.

Further analyses may also be done for blocks with different material properties, with the scope of proving if the conclusions obtained here are also valid for different types of rock.

7 Bibliography

- K Ehrig, J Goebbels, D Meinel, O Paetsch, S Prohaska & V Zobel, 2011. Comparison of crack Detection Methods for Analyzing Damage Processes in Concrete with Computed Tomography. International Symposium on Digital Industrial Radiology and Computed Tomography – Poster 2.
- Y Fujita & Y Hamamoto, 2011. A robust crack detection method from noisy concrete surfaces. *Machine Vision and Applications* vol 22: 245-254. DOI 10.1007/s00138-009-0244-5. Springer-Verlag.
- D Johansson & F Ouchterlony, 2013. Shock Wave Interactions in Rock Blasting: the Use of Short Delays to Improve Fragmentation in Model-Scale. Luleå University of Technology. *Rock Mechanics and Rock Engineering* vol 46(1): 1-18. DOI:10.1007/s00603-012-0249-7. Springer-Verlag.
- S Kim, S Shin, J Park & M Chor, 2011. Calibration of Detection System of Crack in Concrete Structure by Using Image Processing Technology. *Journal of the Korean Society for Nondestructive Testing*. vol 31(6).
- M H B Nasser, R P Young, F Rezanezhad & S H Cho, 2009. Application of 3D X-ray CT scanning techniques to evaluate fracture damage zone in anisotropic granitic rock. *ROCKENG09: Proc. 3rd CANUS Rock Mechanics Symposium*, Toronto, May 2009 (Ed: M. Diederichs and G. Grasselli). PAPER 4050.
- T Nishikawa, J Yoshida & T Sugiyama, 2012. Concrete Crack Detection by Multiple Sequential Image Filtering. *Computer-Aided Civil and Infrastructure Engineering* vol 27: 29 – 47. DOI: 10.1111/j.1467-8667.2011.00716.x.
- F Ouchterlony, 1997. Prediction of crack lengths in rock after cautious blasting with zero inter-hole delay. *Fragblast – International Journal of Blasting and Fragmentation* vol 1: 417-444. Swedish Rock Engineering Research, SveBeFo, Stockholm, Sweden.
- F Ouchterlony, M Olsson & S O Båvik, 1999. Bench blasting in granite with holes with axial notches and radial bottom slots. *Fragblast 6*. Johannesburg, South African Institute of Mining and Metallurgy.
- F Ouchterlony, M Olsson & S O Båvik, 2000. Perimeter blasting in a 130 m road in gneiss with holes with radial bottom slots. *Explosives & Blasting Technique*, Holmberg (ed.) Balkema, Rotterdam, ISBN 90 5809 168 6.
- F Ouchterlony, M Olsson & Bergqvist, 2001. Towards New Swedish Recommendations for Cautious Perimeter Blasting. *EXPLO 2001*. Hunter Valley, NSW, 28 – 31 October 2001.

- F Ouchterlony & P Moser, 2013. Lessons from single-hole blasting in mortar, concrete and rocks. Dept Min. Res. & Petr. Engng, Montanuniversitaet Leoben, Austria. Rock Fragmentation by Blasting – Singh & Sinha (Eds). Taylor & Francis Group, London, ISBN 978-0-415-62143-4.
- S Park, S Ahmad, C B Yun & Y Roh, 2006. Multiple Crack Detection of Concrete Structures Using Impedance-based Structural Health Monitoring Techniques. *Experimental Mechanics* vol 46: 609 – 618. DOI: 10.1007/s11340-006-8734-0.
- H P Rossmannith, V A Hochholdinger & K U-enishi, 2004. On size and boundary effects in scaled model blast. *Fragblast* 9(3): 193 - 174. DOI: 10.1080/13855140500298339.
- D Saiang, 2008. Blast-Induce damage. A summary of SVEBEFO investigations. Luleå University of Technology. Technical Report. Department of Civil and Environment Engineering Division of Rock Mechanics. ISSN: 1402-1536. ISRN: LTU-TR--08/21—SE.
- P Schimek, F Ouchterlony & P Moser, 2012. Experimental blast fragmentation research in model-scale bench blasts. Chair of Mining Engineering, Montanuniversitaet Leoben, Austria.
- T C Su, 2013. Application of Computer Vision to Crack Detection of Concrete Structure. *LACSIT International Journal of Engineering and Technology*, vol 5(4), August 2013. DOI: 10.7763/IJET.2013.V5.596.
- T Yamaguchi & S Hashimoto, 2009. Practical Image Measurement of Crack Width for Real Concrete Structure. *Electronics and Communications in Japan*. vol 92(10).
- T Yamaguchi & S Hashimoto, 2010. Fast crack detection method for large-size concrete surface images using percolation-based image processing. *Machine Vision and Applications* vol 21: 797-809. DOI 10.1007/s00138.009.0189-8.
- D.M. Lane. One-Factor ANOVA.
http://onlinestatbook.com/2/analysis_of_variance/one-way.html
- Graham Hole Research. Skills Kruskal-Wallis handout, version 1.0.
<http://www.sussex.ac.uk/Users/grahamh/RM1web/Kruskal-Wallis%20Handoout2011.pdf>
- NanoXCT. www.nanoxct.eu

8 List of figures

Figure 2.1: Yoke within the walls of the blasting	2
Figure 2.2: Sample blocks formwork (Schimek, 2012).....	3
Figure 2.3: Design of the block for 5 blastholes.....	4
Figure 2.4: Design of the block for 7 blastholes.....	5
Figure 2.5: Initiation from top	5
Figure 2.6: Front view after blasting of: a) 1 st row; b) 2 nd row; c) 3 rd row.....	5
Figure 2.7: Testing block filled with fast hardening cement in front.....	7
Figure 3.1: Explanation 3D X-ray Tomography method.....	8
Figure 3.2.a: Induced Cracks (1) in testing blocks. 3D Tomography method.....	8
Figure 3.2.b: Induced Cracks (2) in testing blocks. 3D Tomography method.....	8
Figure 3.3: Crack detection in horizontal cut. Ouchterlony et al (2000).	12
Figure 3.4: Crack detection in vertical cut. Ouchterlony, Olsson and Båvik (2000)	13
Figure 3.5: Surface cracks detection. Back side block CH01B01	15
Figure 3.6: Dye penetrant application. Back side block CH01B01	15
Figure 3.7: Dye penetrant application. Bottom side block CH01B01	16
Figure 3.8: Distance between slices to cut the testing block.....	16
Figure 3.9: Clarification about the faces of the slices.....	17
Figure 3.10: Photo of the slice after using cleaner. Slice 3 block CH02B04	17
Figure 3.11: Photo of the slice after using developer. Slice 3 block CH02B04....	18
Figure 3.12: Photos by zoom adjusting. Slice 3 block CH02B04.....	18
Figure 3.13: Distance vertical cut. Slice 3 block CH01B01	18
Figure 3.14: Vertical slice after use developer. Slice 3 block CH01B01	18
Figure 3.15: Back side testing block drawing using AutoCAD. Block CH01B01 .	19

Figure 3.16: Drawing of crack traces horizontal slice. Slice 3 Block CH01B01....	20
Figure 3.17: Drawing of crack traces vertical slice. Slice 3 Block CH01B01	20
Figure 3.18: Contour 3D model. Block CH03B05	21
Figure 3.19: 3D model with horizontal Slices. Block CH03B05	22
Figure 3.20.a: 3D model with connections between levels. Block CH03B05.....	23
Figure 3.20.b: Zoom 3D model with connections between levels. Block CH03B05.	23
Figure 4.1: Cracks from borehole in sectors between 90° - 80°	26
Figure 4.2: Cracks from borehole in sectors between 80° - 30°	26
Figure 4.3: Cracks from borehole in sectors between 30° - 0°	27
Figure 4.4: Straight cracks from back side.....	27
Figure 4.5: Connections between boreholes.....	28
Figure 4.6: Parallel cracks to the surface.....	28
Figure 4.7: Cracks with direction to the boreholes in sectors between 90° - 80°	29
Figure 4.8: Cracks with direction to the boreholes in sectors between 80° - 30°	29
Figure 4.9: Cracks with direction to the boreholes in sectors between 30° - 0° ...	30
Figure 4.10: Short cracks from borehole	30
Figure 4.11: Cracks following a direction with angle between 90° - 80°	33
Figure 4.12: Cracks following a direction with angle between 80° - 30°	33
Figure 4.13: Cracks following a direction with angle between 30° - 0°	34
Figure 4.14: Parallel crack to the surface	34
Figure 4.15: Connections between slices	35
Figure 4.16: Grid 2x2 cm	35
Figure 4.17: Grid 2x2 cm. Slice 2 block CH02B04.....	36

Figure 4.18: Imaginary lines (white color) which limit when a crack (green line) is valid or nor	37
Figure 4.19: Connections between cracks separated by the grid	37
Figure 4.20: Damage map Slice 2 block CH02B04	38
Figure 4.21: Grid 1x1 cm. Slice 2 block CH02B04.....	39
Figure 4.22: Grid 1x1 cm. Damage map Slice 2 block CH02B04	39
Figure 4.23: Grid 4x4 cm. Slice 2 block CH02B04.....	40
Figure 4.24: Grid 4x4 cm. Damage map Slice 2 block CH02B04	40
Figure 5.1.a: Comparison 1. All Families.....	52
Figure 5.1.b: Comparison 1. Family CB 90-80.....	52
Figure 5.1.c: Comparison 1. Family CB 80-30.....	52
Figure 5.1.d: Comparison 1. Family CB 30-0.....	52
Figure 5.1.e: Comparison 1. Family SCB	52
Figure 5.1.f: Comparison 1. Family Parallel Cracks.....	52
Figure 5.1.g: Comparison 1. Family Connection between Holes.....	52
Figure 5.1.h: Comparison 1. Family Dir 90-80	52
Figure 5.1.i: Comparison 1. Family Dir 80-30	52
Figure 5.1.j: Comparison 1. Family Dir 30-0	52
Figure 5.1.k: Comparison 1. Family Short Cracks	52
Figure 5.2.a: Comparison 2. All Families.....	56
Figure 5.2.b: Comparison 2. Family CB 90-80.....	56
Figure 5.2.c: Comparison 2. Family CB 80-30.....	56
Figure 5.2.d: Comparison 2. Family CB 30-0.....	56
Figure 5.2.e: Comparison 2. Family SCB	56
Figure 5.2.f: Comparison 2. Family Parallel Cracks.....	56
Figure 5.2.g: Comparison 2. Family Connection between Holes.....	56

Figure 5.2.h: Comparison 2. Family Dir 90-80	56
Figure 5.2.i: Comparison 2. Family Dir 80-30	56
Figure 5.2.j: Comparison 2. Family Dir 30-0	56
Figure 5.2.k: Comparison 2. Family Short Cracks	56
Figure 5.3.a: Comparison 3. All Families	59
Figure 5.3.b: Comparison 3. Family CB 90-80.....	59
Figure 5.3.c: Comparison 3. Family CB 80-30.....	59
Figure 5.3.d: Comparison 3. Family CB 30-0.....	59
Figure 5.3.e: Comparison 3. Family SCB	59
Figure 5.3.f: Comparison 3. Family Parallel Cracks.....	59
Figure 5.3.g: Comparison 3. Family Connection between Holes.....	59
Figure 5.3.h: Comparison 3. Family Dir 90-80	59
Figure 5.3.i: Comparison 3. Family Dir 80-30	59
Figure 5.3.j: Comparison 3. Family Dir 30-0	59
Figure 5.3.k: Comparison 3. Family Short Cracks	59
Figure 5.4: Comparison 1. Radial Crack Distribution. Cracks starting from the borehole	63
Figure 5.5: Comparison 1. Radial Crack Distribution. Cracks <i>which</i> develop a trajectory a radial direction away from the hole	64
Figure 5.6: Comparison 2. Radial Crack Distribution. Cracks starting from the borehole	65
Figure 5.7: Comparison 2. Radial Crack Distribution. Cracks with a radial direction away from the hole	66
Figure 5.8: Comparison 3. Radial Crack Distribution. Cracks starting from the borehole	67
Figure 5.9: Comparison 3. Radial Crack Distribution. Cracks <i>with</i> a radial direction away from the hole	68
Figure 5.10: Comparison 1. Analysis of mean crack density	69

Figure 5.11: Comparison 1. Analysis of mean crack intersection density	70
Figure 5.12: Comparison 2. Analysis of mean crack density	71
Figure 5.13: Comparison 2. Analysis of mean crack intersection density	71
Figure 5.14: Comparison 3. Analysis of mean crack density	72
Figure 5.15: Comparison 3. Analysis of mean crack intersection density	73
Figure I.1: Undisturbed radial cracks behind half cast. Ouchterlony et al. (1999)....	II
Figure I.2: Radial cracks behind half cast disturbed by a existing fracture. Ouchterlony et al. (1999).....	II
Figure I.3: Cracks behind water filled hole. Ouchterlony et al. (1999)	II
Figure I.4: Cracks behind the hole disturbed system. Ouchterlony et al. (1999)...	III
Figure I.5: Conical cracks underneath the slot. Ouchterlony et al. (1999)	III
Figure I.6: Root crack and Bench face crack. Ouchterlony et al. (1999).....	III
Figure I.7: Radial cracks. Saiang (2008)	IV
Figure I.8: Bow-shaped tangential cracks. Saiang (2008).	IV
Figure I.9: Crack patterns observed around $\varnothing 51$ mm blast-holes. Saiang (2008) .	IV
Figure I.10: Crack patterns observed around $\varnothing 24$ mm blast-holes. Saiang (2008)	V
Figure I.11: Pre-existing crack running parallel to the blast-holes. Saiang (2008)	V
Figure I.12: Blast-induced crack propagating along pre-existing crack with a favourable orientation. Saiang (2008)	V
Figure II.1: Slice surface 1 Block CH01B01	VI
Figure II.2: Slice surface 2 Block CH01B01	VI
Figure II.3: Slice surface 3 Block CH01B01	VI
Figure II.4: Slice surface 4 Block CH01B01	VII
Figure II.5: Slice surface 1 Block CH02B01	VII

Figure II.6: Slice surface 2 Block CH02B01	VII
Figure II.7: Slice surface 3 Block CH02B01	VIII
Figure II.8: Slice surface 4 Block CH02B01	VIII
Figure II.9: Slice surface 1 Block CH02B02	IX
Figure II.10: Slice surface 2 Block CH02B02	IX
Figure II.11: Slice surface 3 Block CH02B02	IX
Figure II.12: Slice surface 4 Block CH02B02	IX
Figure II.13: Slice surface 1 Block CH02B03	X
Figure II.14: Slice surface 2 Block CH02B03	X
Figure II.15: Slice surface 3 Block CH02B03	X
Figure II.16: Slice surface 4 Block CH02B03	X
Figure II.17: Slice surface 1 Block CH02B04	XI
Figure II.18: Slice surface 2 Block CH02B04	XI
Figure II.19: Slice surface 3 Block CH02B04	XI
Figure II.20: Slice surface 4 Block CH02B04	XI
Figure II.21: Top Block CH02B05	XII
Figure II.22: Slice surface 1 Block CH02B05	XII
Figure II.23: Slice surface 2 Block CH02B05	XIII
Figure II.24: Slice surface 3 Block CH02B05	XIII
Figure II.25: Bottom Block CH02B05	XIV
Figure II.26: Slice surface 1 Block CH03B04	XV
Figure II.27: Slice surface 2 Block CH03B04	XV
Figure II.28: Slice surface 3 Block CH03B04	XV
Figure II.29: Slice surface 4 Block CH03B04	XV
Figure II.30: Slice surface 1 Block CH03B05	XVI
Figure II.31: Slice surface 2 Block CH03B05	XVI

Figure II.32: Slice surface 3 Block CH03B05.....	XVI
Figure II.33: Slice surface 4 Block CH03B05.....	XVI
Figure III.1: Vertical section Block CH01B01	XVII
Figure III.2: Vertical section Block CH02B01	XVII
Figure III.3: Vertical section Block CH02B02	XVIII
Figure III.4: Vertical section Block CH02B03.....	XVIII
Figure III.5: Vertical section Block CH02B04	XIX
Figure III.6: Vertical section a) Block CH02B05.....	XIX
Figure III.7: Vertical section b) Block CH02B05.....	XIX
Figure III.8: Vertical section c) Block CH02B05	XX
Figure III.9: Vertical section Block CH03B04.....	XX
Figure III.10: Vertical section Block CH03B05.....	XX
Figure IV.1: Crack detection Slice surface 1 Block CH02B01.....	XXI
Figure IV.2: Crack detection Slice surface 2 Block CH02B01.....	XXI
Figure IV.3: Crack detection Slice surface 3 Block CH02B01.....	XXI
Figure IV.4: Crack detection Slice surface 4 Block CH02B01.....	XXI
Figure IV.5: Crack detection Slice surface 1 Block CH02B02.....	XXII
Figure IV.6: Crack detection Slice surface 2 Block CH02B02.....	XXII
Figure IV.7: Crack detection Slice surface 3 Block CH02B02.....	XXII
Figure IV.8: Crack detection Slice surface 4 Block CH02B02.....	XXII
Figure IV.9: Crack detection Slice surface 1 Block CH02B03.....	XXIII
Figure IV.10: Crack detection Slice surface 2 Block CH02B03.....	XXIII
Figure IV.11: Crack detection Slice surface 3 Block CH02B03.....	XXIII
Figure IV.12: Crack detection Slice surface 4 Block CH02B03.....	XXIII
Figure IV.13: Crack detection Slice surface 1 Block CH02B04.....	XXIV
Figure IV.14: Crack detection Slice surface 2 Block CH02B04.....	XXIV

Figure IV.15: Crack detection Slice surface 3 Block CH02B04.....	XXIV
Figure IV.16: Crack detection Slice surface 4 Block CH02B04.....	XXIV
Figure IV.17: Crack detection Slice surface 1 Block CH03B04.....	XXV
Figure IV.18: Crack detection Slice surface 2 Block CH03B04.....	XXV
Figure IV.19: Crack detection Slice surface 3 Block CH03B04.....	XXV
Figure IV.20: Crack detection Slice surface 4 Block CH03B04.....	XXV
Figure IV.21: Crack detection Slice surface 1 Block CH03B05.....	XXVI
Figure IV.22: Crack detection Slice surface 2 Block CH03B05.....	XXVI
Figure IV.23: Crack detection Slice surface 3 Block CH03B05.....	XXVI
Figure IV.24: Crack detection Slice surface 4 Block CH03B05.....	XXVI
Figure V.1: Damage map Slice surface 1 Block CH01B01	XXVII
Figure V.2: Damage map Slice surface 2 Block CH01B01	XXVII
Figure V.3: Damage map Slice surface 3 Block CH01B01	XXVII
Figure V.4: Damage map Slice surface 4 Block CH01B01	XXVII
Figure V.5: Damage map Slice surface 1 Block CH02B01	XXVIII
Figure V.6: Damage map Slice surface 2 Block CH02B01	XXVIII
Figure V.7: Damage map Slice surface 3 Block CH02B01	XXVIII
Figure V.8: Damage map Slice surface 4 Block CH02B01	XXVIII
Figure V.9: Damage map Slice surface 1 Block CH02B02.....	XXIX
Figure V.10: Damage map Slice surface 2 Block CH02B02.....	XXIX
Figure V.11: Damage map Slice surface 3 Block CH02B02.....	XXIX
Figure V.12: Damage map Slice surface 4 Block CH02B02.....	XXIX
Figure V.13: Damage map Slice surface 1 Block CH02B03.....	XXX
Figure V.14: Damage map Slice surface 2 Block CH02B03.....	XXX
Figure V.15: Damage map Slice surface 3 Block CH02B03.....	XXX
Figure V.16: Damage map Slice surface 4 Block CH02B03.....	XXX

Figure V.17: Damage map Slice surface 1 Block CH02B04.....	XXXI
Figure V.18: Damage map Slice surface 2 Block CH02B04.....	XXXI
Figure V.19: Damage map Slice surface 3 Block CH02B04.....	XXXI
Figure V.20: Damage map Slice surface 4 Block CH02B04.....	XXXI
Figure V.21: Damage map Slice surface 1 Block CH02B05.....	XXXII
Figure V.22: Damage map Slice surface 2 Block CH02B05.....	XXXII
Figure V.23: Damage map Slice surface 3 Block CH02B05.....	XXXIII
Figure V.24: Damage map Bottom Block CH02B05.....	XXXIII
Figure V.25: Damage map Slice surface 1 Block CH03B04.....	XXXIV
Figure V.26: Damage map Slice surface 2 Block CH03B04.....	XXXIV
Figure V.27: Damage map Slice surface 3 Block CH03B04.....	XXXIV
Figure V.28: Damage map Slice surface 4 Block CH03B04.....	XXXIV
Figure V.29: Damage map Slice surface 1 Block CH03B05.....	XXXV
Figure V.30: Damage map Slice surface 2 Block CH03B05.....	XXXV
Figure V.31: Damage map Slice surface 3 Block CH03B05.....	XXXV
Figure V.32: Damage map Slice surface 4 Block CH03B05.....	XXXV
Figure VI.1: Intersection damage map Slice surface 1 Block CH01B01	XXXVI
Figure VI.2: Intersection damage map Slice surface 2 Block CH01B01	XXXVI
Figure VI.3: Intersection damage map Slice surface 3 Block CH01B01	XXXVI
Figure VI.4: Intersection damage map Slice surface 4 Block CH01B01	XXXVI
Figure VI.5: Intersection damage map Slice surface 1 Block CH02B01	XXXVII
Figure VI.6: Intersection damage map Slice surface 2 Block CH02B01	XXXVII
Figure VI.7: Intersection damage map Slice surface 3 Block CH02B01	XXXVII
Figure VI.8: Intersection damage map Slice surface 4 Block CH02B01	XXXVII
Figure VI.9: Intersection damage map Slice surface 1 Block CH02B02	XXXVIII
Figure VI.10: Intersection damage map Slice surface 2 Block CH02B02	XXXVIII

Figure VI.11: Intersection damage map Slice surface 3 Block CH02B02	XXXVIII
Figure VI.12: Intersection damage map Slice surface 4 Block CH02B02	XXXVIII
Figure VI.13: Intersection damage map Slice surface 1 Block CH02B03	XXXIX
Figure VI.14: Intersection damage map Slice surface 2 Block CH02B03	XXXIX
Figure VI.15: Intersection damage map Slice surface 3 Block CH02B03	XXXIX
Figure VI.16: Intersection damage map Slice surface 4 Block CH02B03	XXXIX
Figure VI.17: Intersection damage map Slice surface 1 Block CH02B04	XL
Figure VI.18: Intersection damage map Slice surface 2 Block CH02B04	XL
Figure VI.19: Intersection damage map Slice surface 3 Block CH02B04	XL
Figure VI.20: Intersection damage map Slice surface 4 Block CH02B04	XL
Figure VI.21: Intersection damage map Slice surface 1 Block CH02B05	XLI
Figure VI.22: Intersection damage map Slice surface 2 Block CH02B05	XLI
Figure VI.23: Intersection damage map Slice surface 3 Block CH02B05	XLII
Figure VI.24: Intersection damage map Bottom Block CH02B05	XLII
Figure VI.25: Intersection damage map Slice surface 1 Block CH03B04	XLIII
Figure VI.26: Intersection damage map Slice surface 2 Block CH03B04	XLIII
Figure VI.27: Intersection damage map Slice surface 3 Block CH03B04	XLIII
Figure VI.28: Intersection damage map Slice surface 4 Block CH03B04	XLIII
Figure VI.29: Intersection damage map Slice surface 1 Block CH03B05	XLIV
Figure VI.30: Intersection damage map Slice surface 2 Block CH03B05	XLIV
Figure VI.31: Intersection damage map Slice surface 3 Block CH03B05	XLIV
Figure VI.32: Intersection damage map Slice surface 4 Block CH03B05	XLIV
Figure IX.1.a: Comparison 1. All Families	LVIII
Figure IX.1.b: Comparison 1. Family CB 90-80	LVIII
Figure IX.1.c: Comparison 1. Family CB 80-30	LVIII
Figure IX.1.d: Comparison 1. Family CB 30-0	LIX

Figure IX.1.e: Comparison 1. Family SCB.....	LIX
Figure IX.1.h: Comparison 1. Family Dir 90-80.....	LIX
Figure IX.1.i: Comparison 1. Family Dir 80-30.....	LX
Figure IX.1.j: Comparison 1. Family Dir 30-0.....	LX
Figure IX.1.f: Comparison 1. Family Parallel Cracks	LX
Figure IX.2.a: Comparison 2. All Families	LXI
Figure IX.2.b: Comparison 2. Family CB 90-80	LXI
Figure IX.2.c: Comparison 2. Family CB 80-30	LXI
Figure IX.2.d: Comparison 2. Family CB 30-0	LXII
Figure IX.2.e: Comparison 2. Family SCB.....	LXII
Figure IX.2.h: Comparison 2. Family Dir 90-80.....	LXII
Figure IX.2.i: Comparison 2. Family Dir 80-30.....	LXIII
Figure IX.2.j: Comparison 2. Family Dir 30-0.....	LXIII
Figure IX.2.f: Comparison 2. Family Parallel Cracks	LXIII
Figure IX.3.a: Comparison 3. All Families	LXIV
Figure IX.3.b: Comparison 3. Family CB 90-80	LXIV
Figure IX.3.c: Comparison 3. Family CB 80-30	LXIV
Figure IX.3.d: Comparison 3. Family CB 30-0	LXV
Figure IX.3.e: Comparison 3. Family SCB.....	LXV
Figure IX.3.h: Comparison 3. Family Dir 90-80.....	LXV
Figure IX.3.i: Comparison 3. Family Dir 80-30.....	LXVI
Figure IX.3.j: Comparison 3. Family Dir 30-0.....	LXVI
Figure IX.3.f: Comparison 3. Family Parallel Cracks	LXVI

9 List of tables

Table 2.1: Ingredients and proportions of magnetite mortar.....	3
Table 2.2: Information about testing blocks.....	6
Table 4.1: Color coded families of crack traces in horizontal slices.....	25
Table 4.2: Color coded families of crack traces in vertical slices.....	31
Table 4.3: Mean damage value of Crack Density.....	40
Table 4.4: Mean values of damage as measured by crack intersection density..	41
Table 5.1: ANOVA F-Test. Comparison 1	46
Table 5.2: Kruskal-Wallis H Test. Comparison 1	47
Table 5.3: ANOVA F-Test. Comparison 2	48
Table 5.4: Kruskal-Wallis H Test. Comparison 2.....	48
Table 5.5: ANOVA F-Test. Comparison 3	49
Table 5.6: Kruskal-Wallis H Test. Comparison 3.....	49
Table VIII.1: Data crack detection Block CH02B01	LI
Table VIII.2: Data crack detection Block CH02B02	LII
Table VIII.3: Data crack detection Block CH02B03	LIII
Table VIII.4: Data crack detection Block CH02B04	LIV
Table VIII.5: Data crack detection Block CH03B04	LV
Table VIII.6: Data crack detection Block CH03B05	LVI

Annex table of contents

Annex table of contents	I
ANNEX I: Crack patterns pictures.....	II
ANNEX II: Digital picture of horizontal sections of slice surfaces.	VI
ANNEX III: Digital picture of vertical sections of slice surfaces.....	XVII
ANNEX IV: Crack families detection	XXI
ANNEX V: Crack density damage maps.....	XXVII
ANNEX VI: Intersection crack density damage maps.....	XXXVI
ANNEX VII: ANOVA F-Test an Kruskal Wallis methods	XLV
ANNEX VIII: Data crack detection families	LI
ANNEX IX: Comparison between data when using all the crack information from the slice and when using only cracks inside the edges	LVII

ANNEX I: Crack patterns pictures

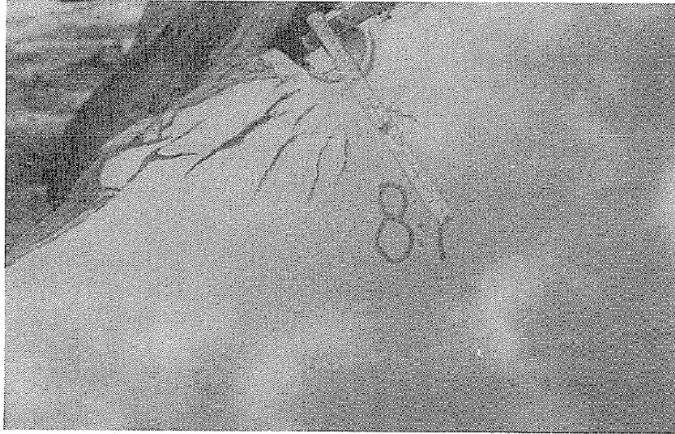


Figure I.1: Undisturbed radial cracks behind half cast. Ouchterlony et al. (1999).

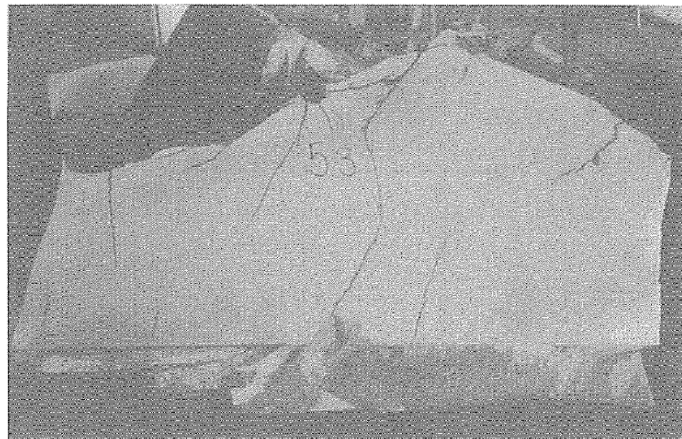


Figure I.2: Radial cracks behind half cast disturbed by an existing fracture. Ouchterlony et al. (1999).

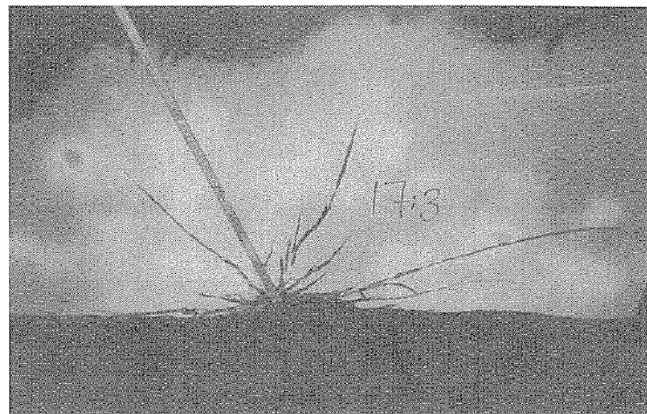


Figure I.3: Cracks behind water filled hole. Ouchterlony et al. (1999).

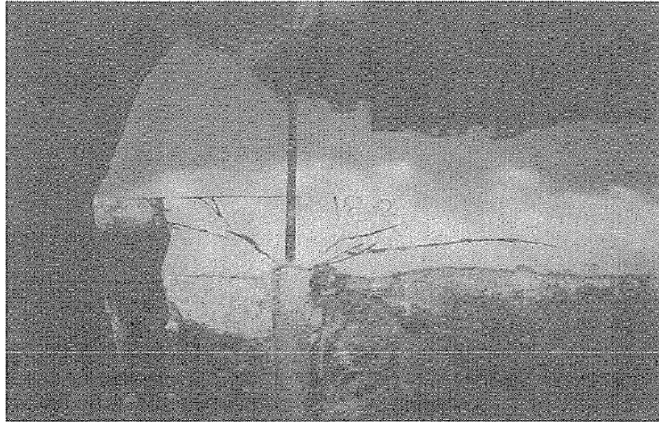


Figure I.4: Cracks behind the hole. Disturbed system. Ouchterlony et al. (1999).

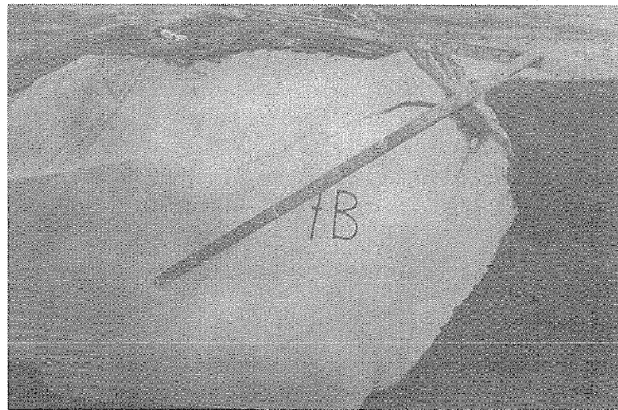


Figure I.5: Conical cracks underneath the slot. Ouchterlony et al. (1999).

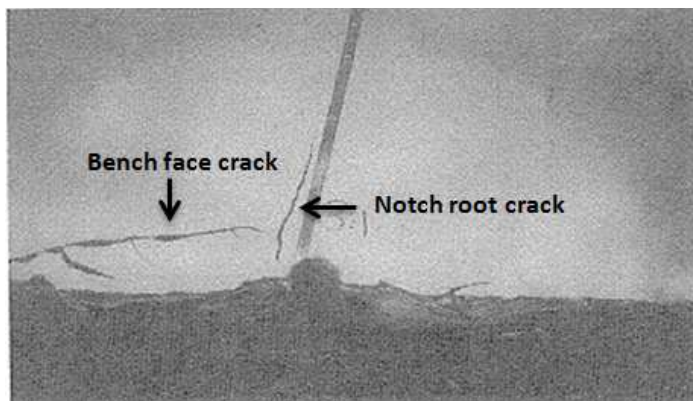


Figure I.6: Notch root crack and Bench face crack. Ouchterlony et al. (1999).



Figure I.7: Radial cracks. Saiang (2008).



Figure I.8: Bow-shaped tangential cracks. Saiang (2008).



Figure I.9: Crack patterns observed around Ø51mm blast-holes. Saiang (2008).



Figure I.10: Crack patterns observed around $\varnothing 24\text{mm}$ blast-holes. Saiang (2008).

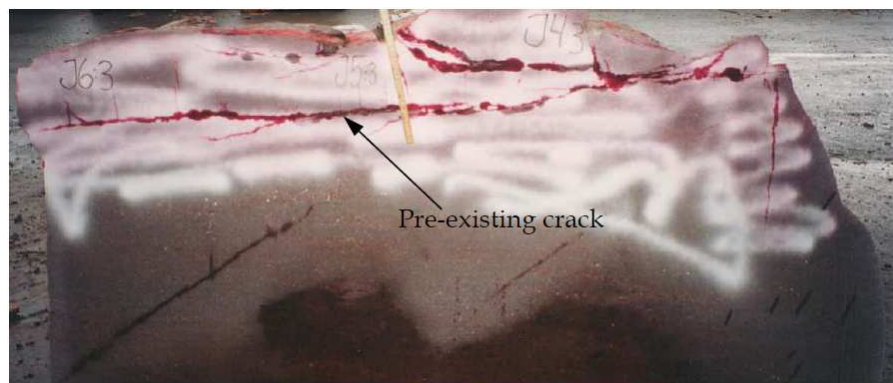


Figure I.11: Pre-existing crack running parallel to the blast-holes. Saiang (2008).

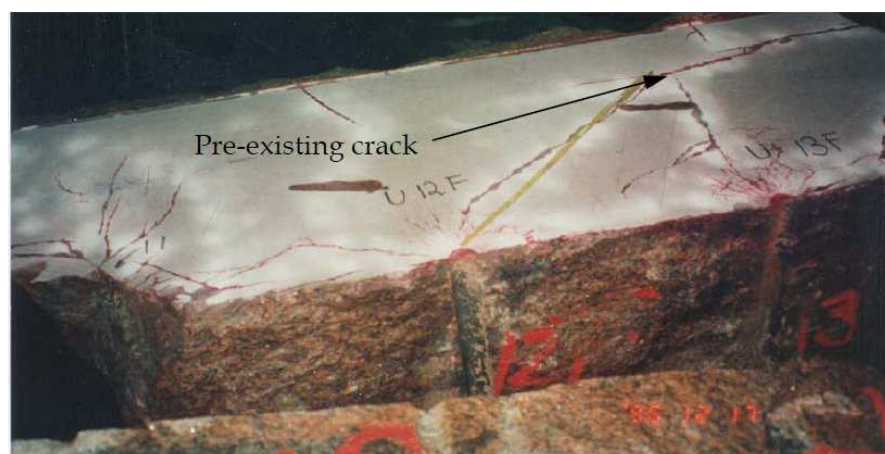


Figure I.12: Blast-induced crack propagating along pre-existing crack with a favorable orientation. Saiang (2008).

ANNEX II: Digital picture of horizontal sections of slice surfaces.

Block CH01B01

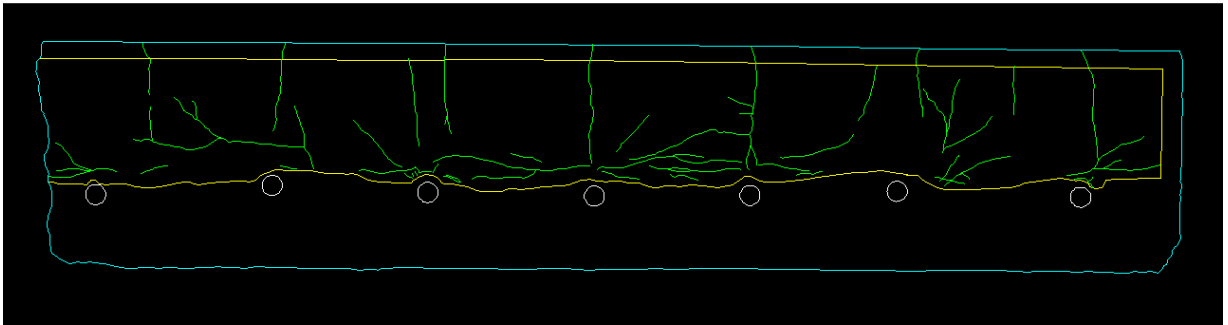


Figure II.1: Slice surface 1. Block CH01B01

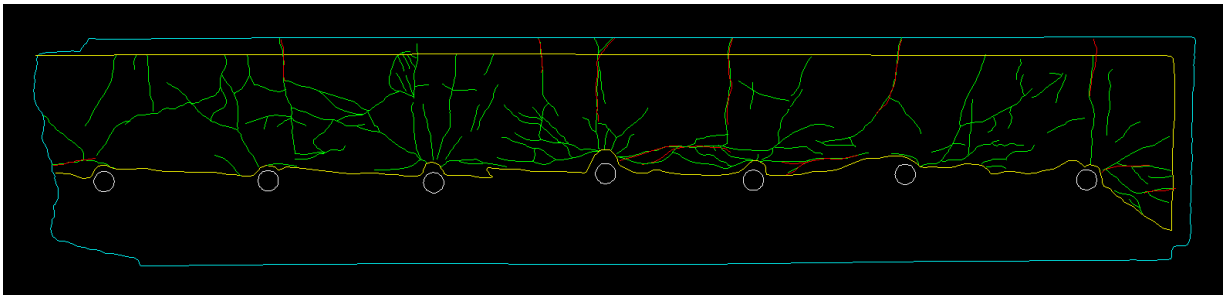


Figure II.2: Slice surface 2. Block CH01B01

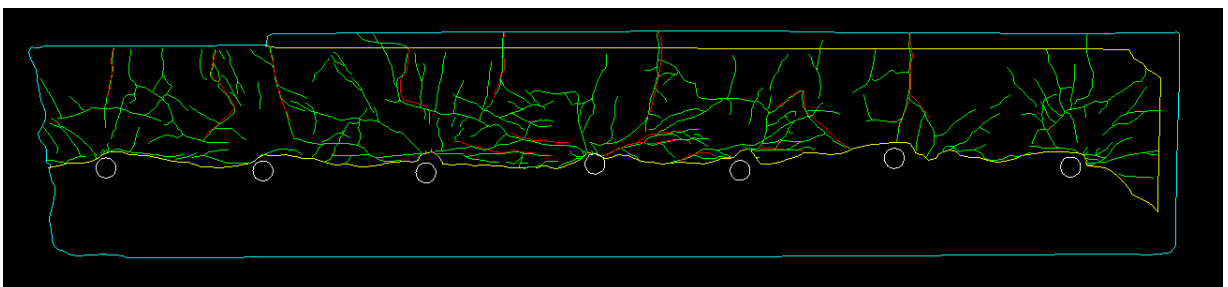


Figure II.3: Slice surface 3. Block CH01B01

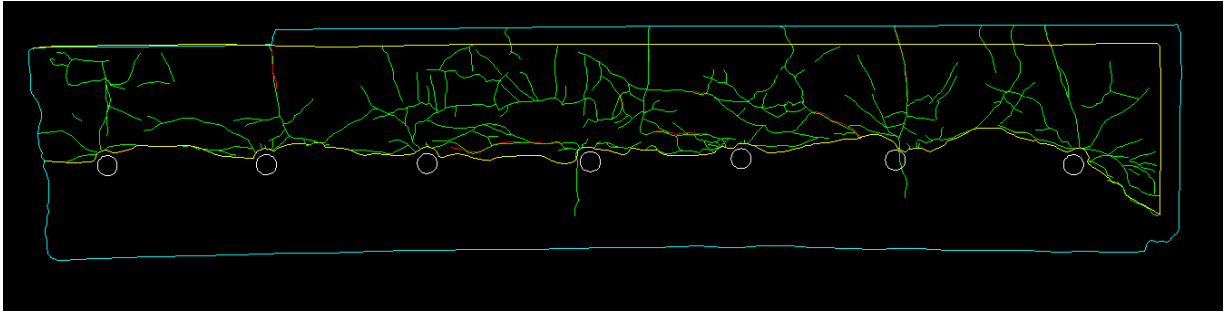


Figure II.4: Slice surface 4. Block CH01B01

Block CH02B01

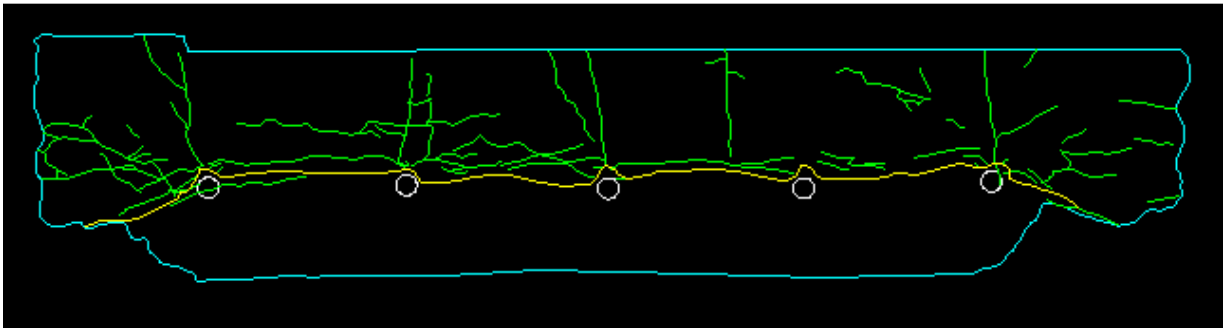


Figure II.5: Slice surface 1. Block CH02B01

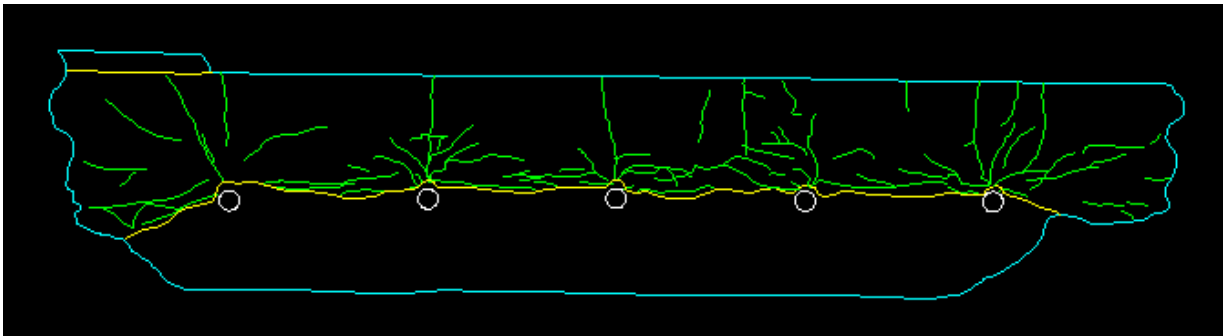


Figure II.6: Slice surface 2. Block CH02B01

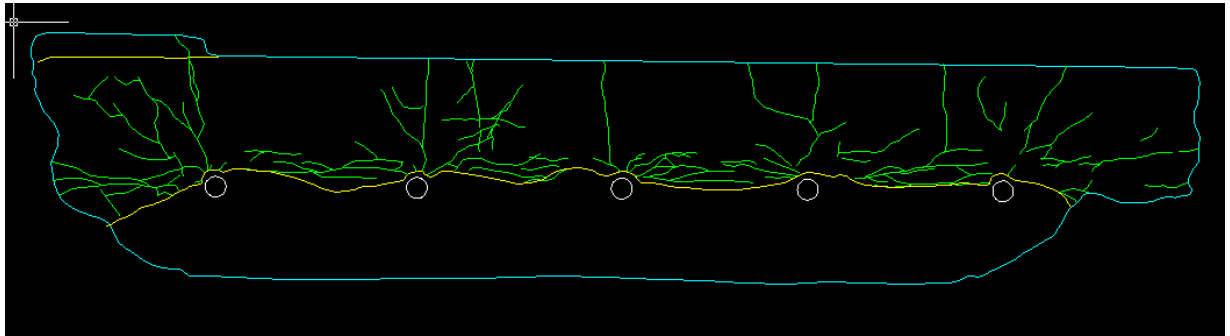


Figure II.7: Slice surface 3. Block CH02B01

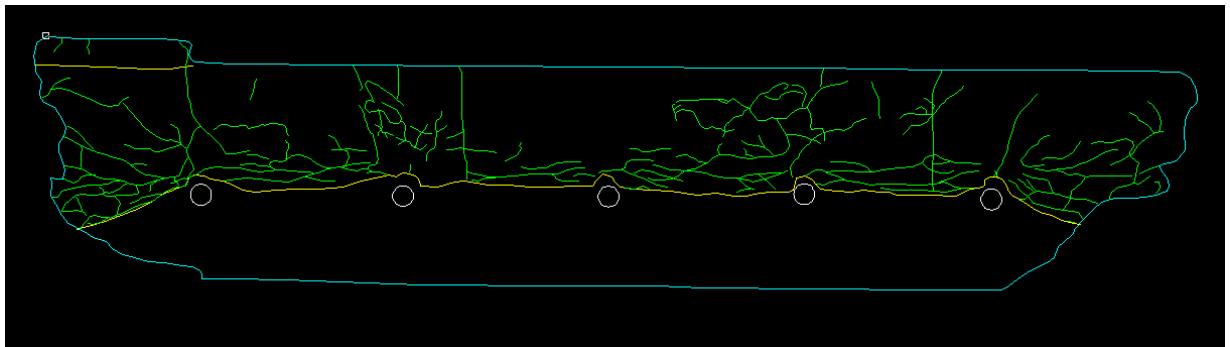


Figure II.8: Slice surface 4. Block CH02B01

Block CH02B02

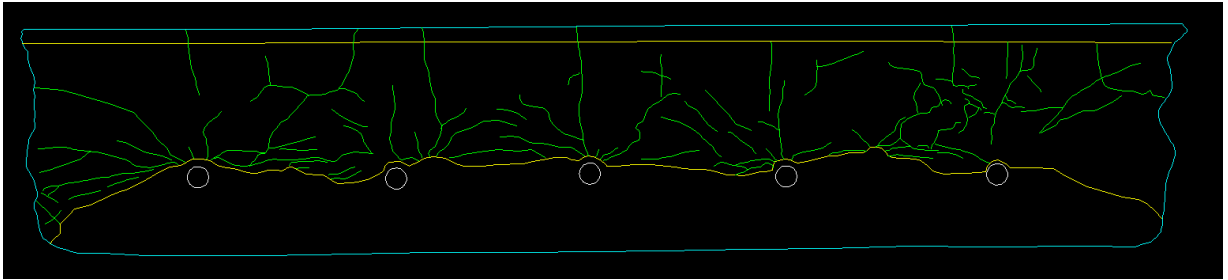


Figure II.9: Slice surface 1. Block CH02B02

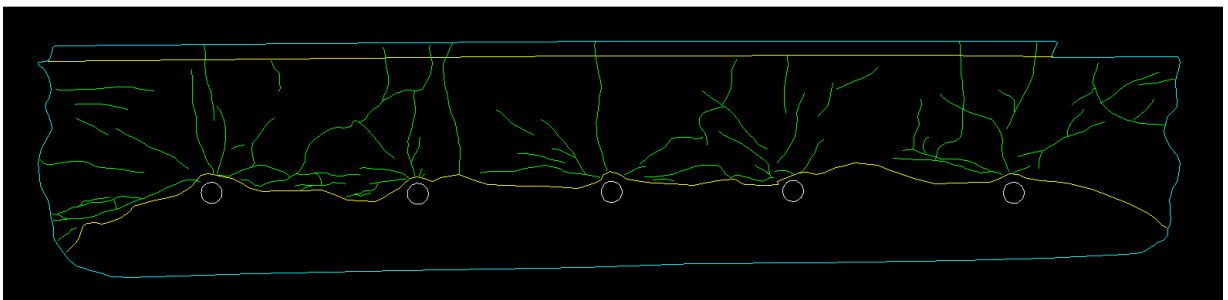


Figure II.10: Slice surface 2. Block CH02B02

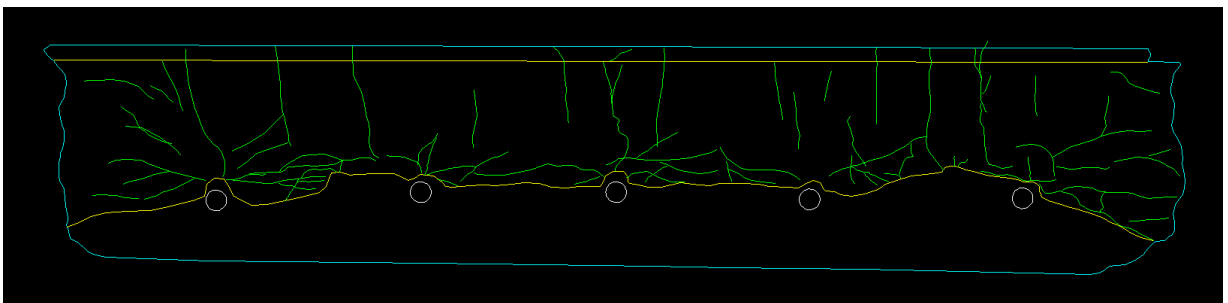


Figure II.11: Slice surface 3. Block CH02B02

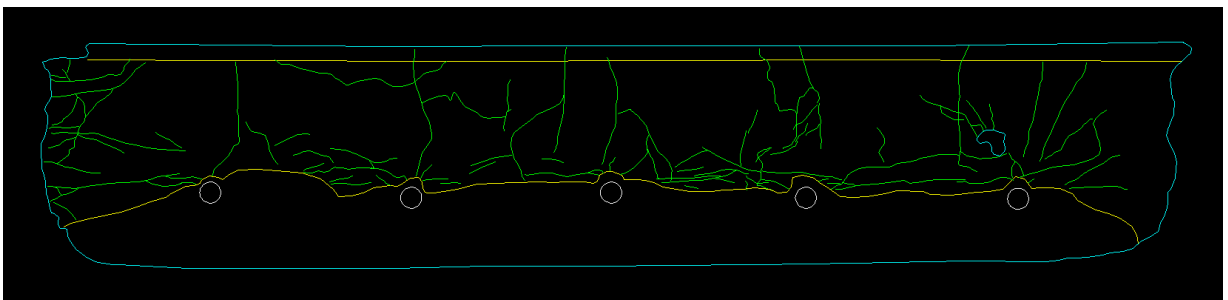


Figure II.12: Slice surface 4. Block CH02B02

Block CH02B03

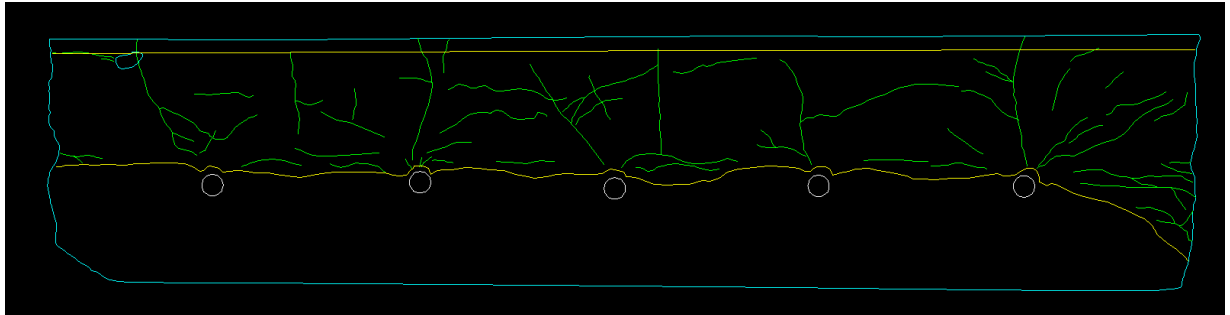


Figure II.13: Slice surface 1. Block CH02B03

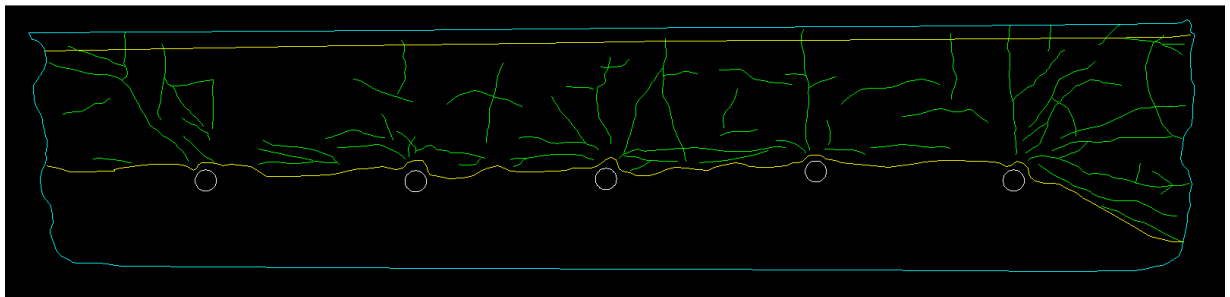


Figure II.14: Slice surface 2. Block CH02B03

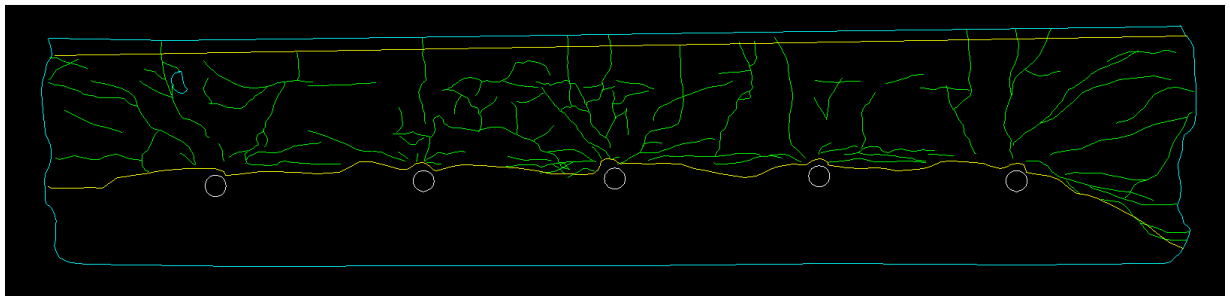


Figure II.15: Slice surface 3. Block CH02B03

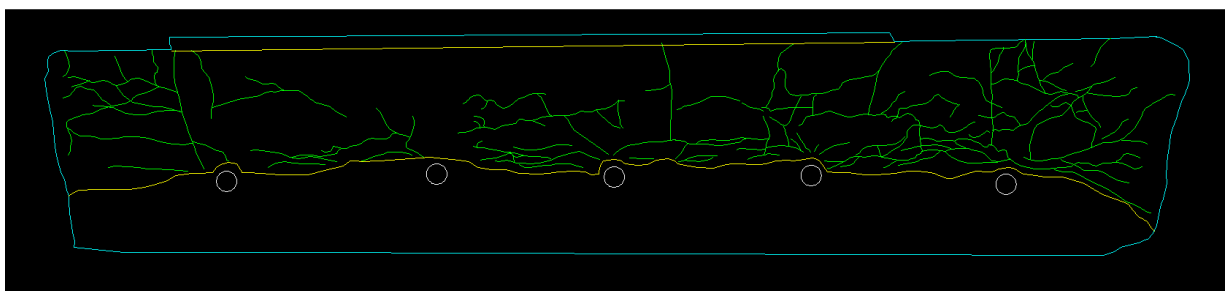


Figure II.16: Slice surface 4. Block CH02B03

Block CH02B04

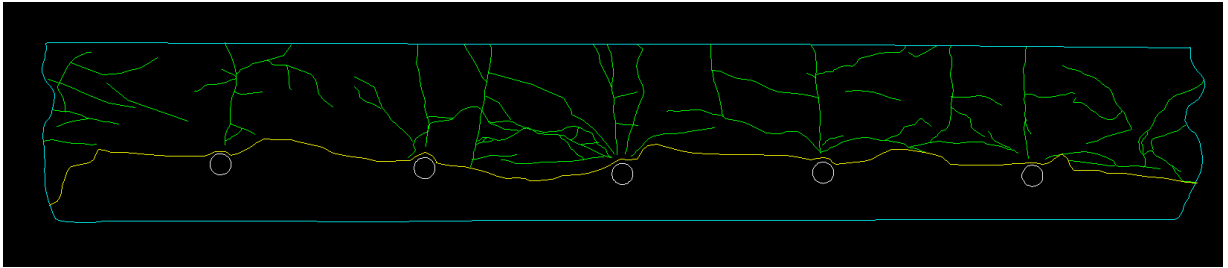


Figure II.17: Slice surface 1. Block CH02B04

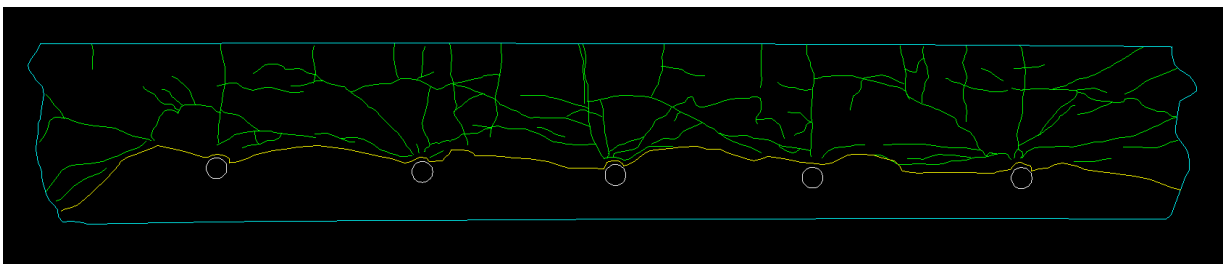


Figure II.18: Slice surface 2. Block CH02B04

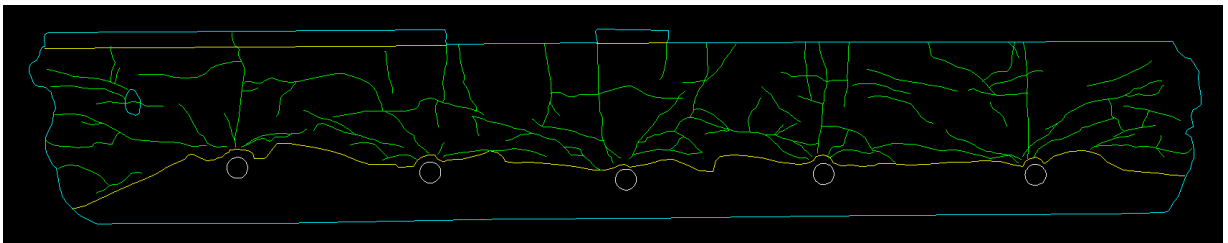


Figure II.19: Slice surface 3. Block CH02B04

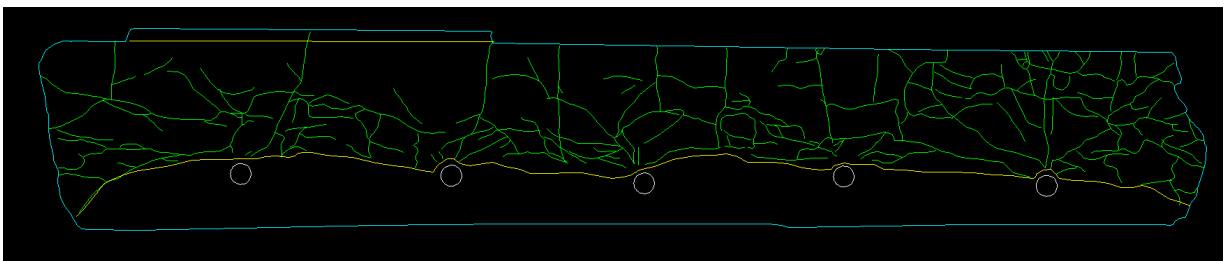


Figure II.20: Slice surface 4. Block CH02B04

Block CH02B05

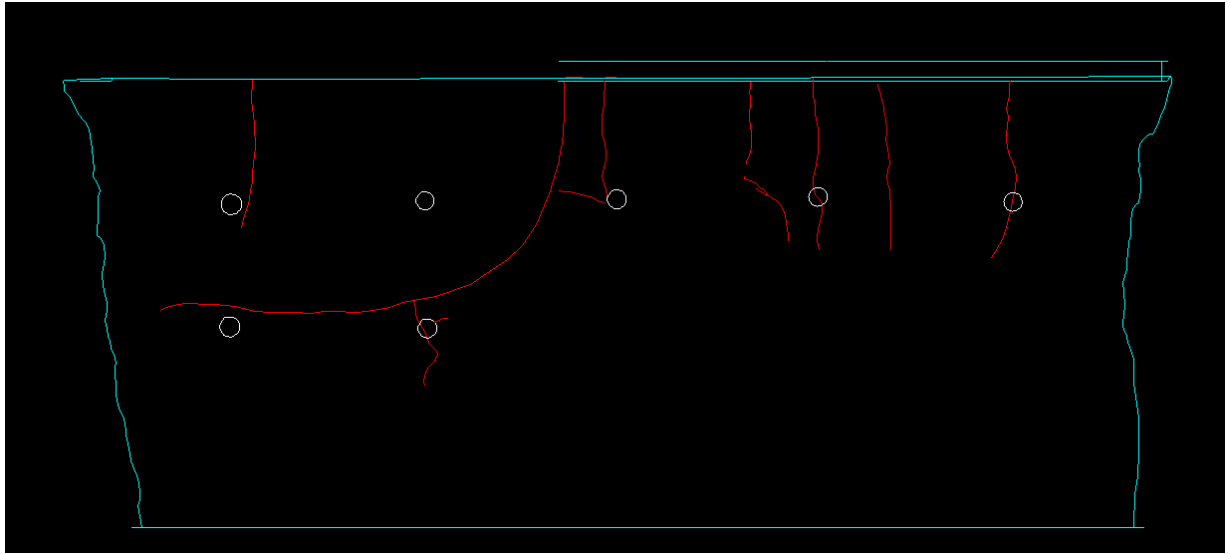


Figure II.21:Top. Block CH02B05

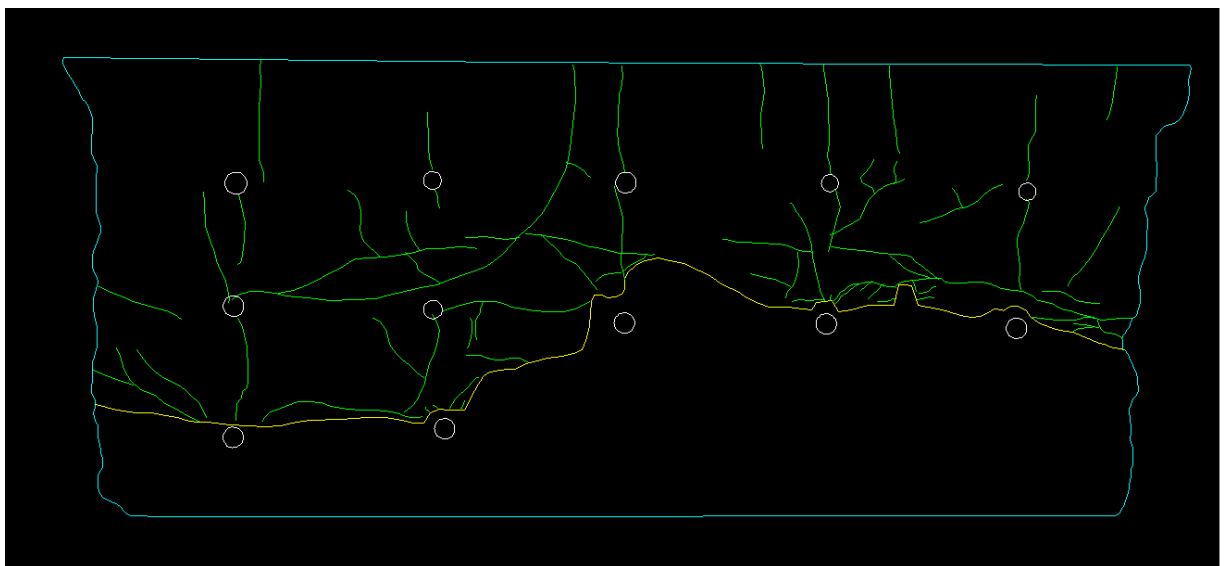


Figure II.22:Slice surface 1. Block CH02B05

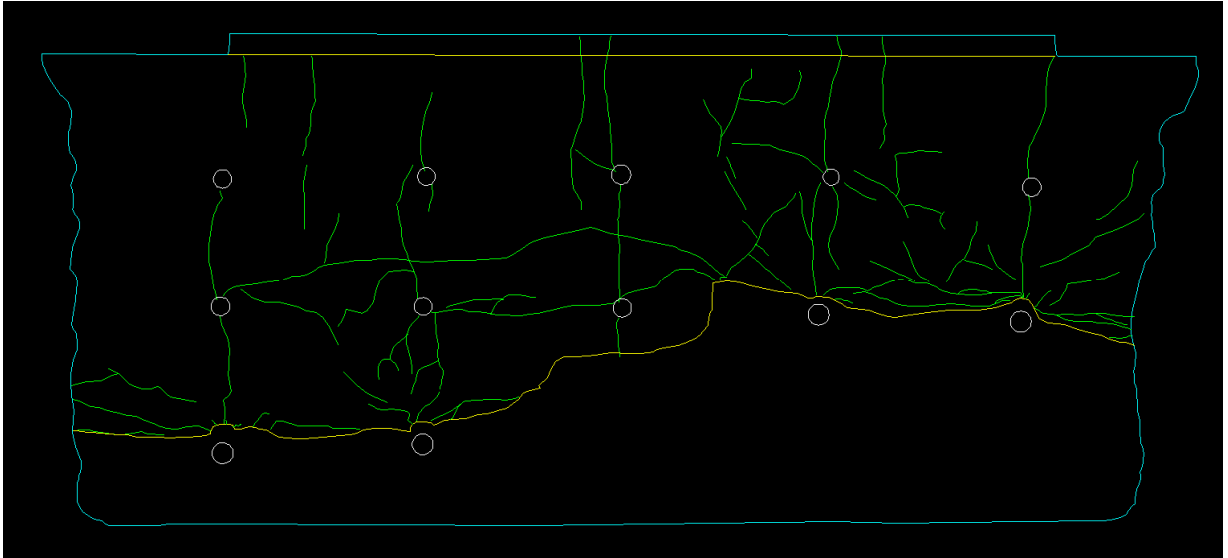


Figure II.23:Slice surface 2. Block CH02B05

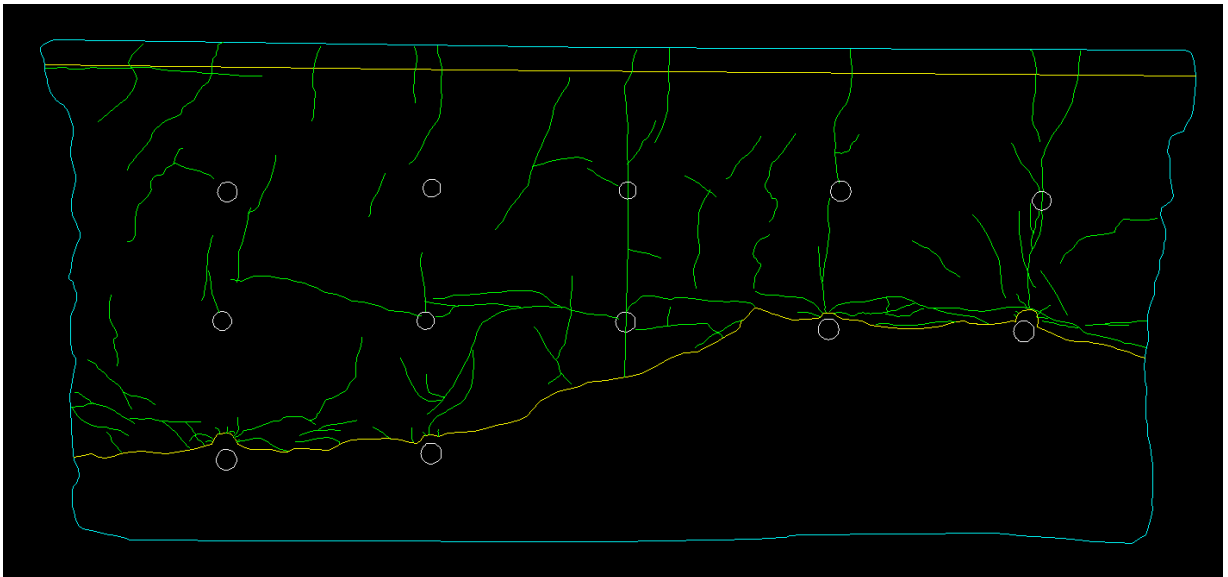


Figure II.24:Slice surface 3. Block CH02B05

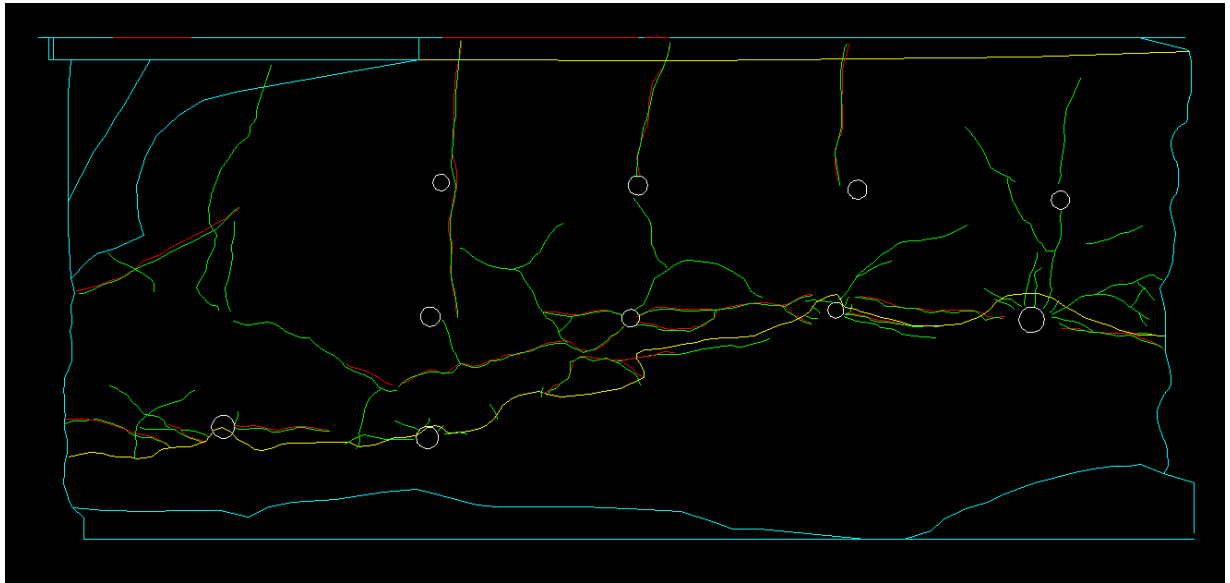


Figure II.25: Bottom. Block CH02B05

Block CH03B04

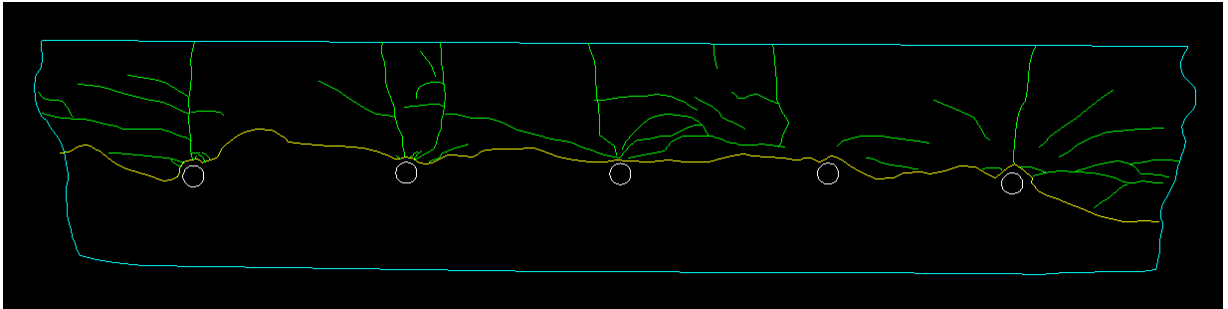


Figure II.26: Slice surface 1. Block CH03B04

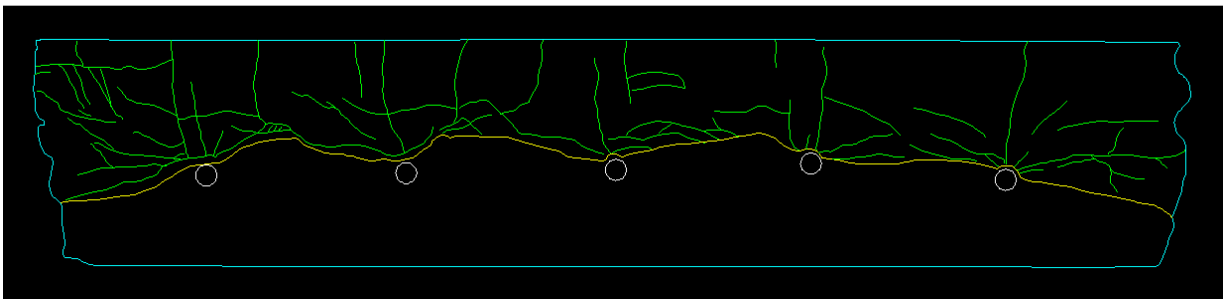


Figure II.27: Slice surface 2. Block CH03B04

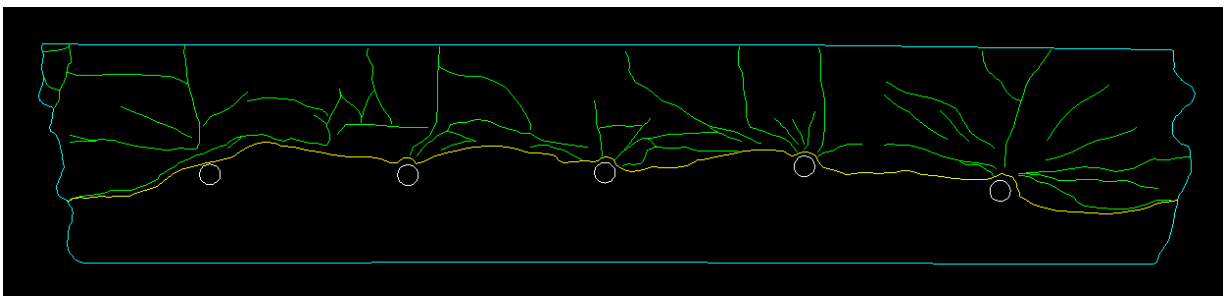


Figure II.28: Slice surface 3. Block CH03B04

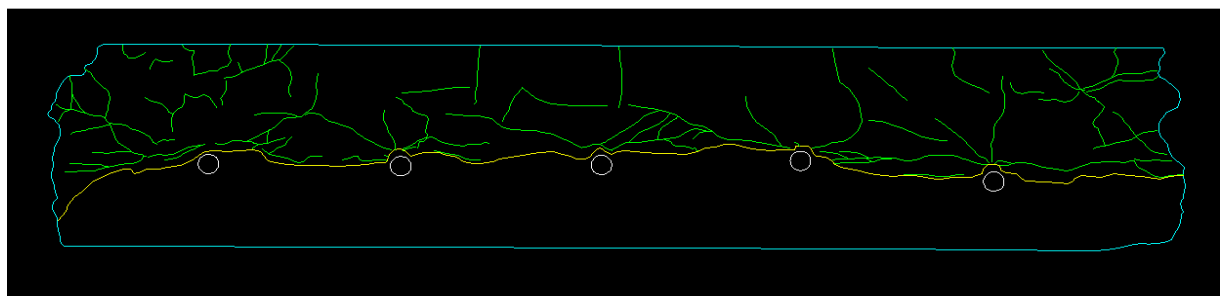


Figure II.29: Slice surface 4. Block CHO3B

Block CH03B05

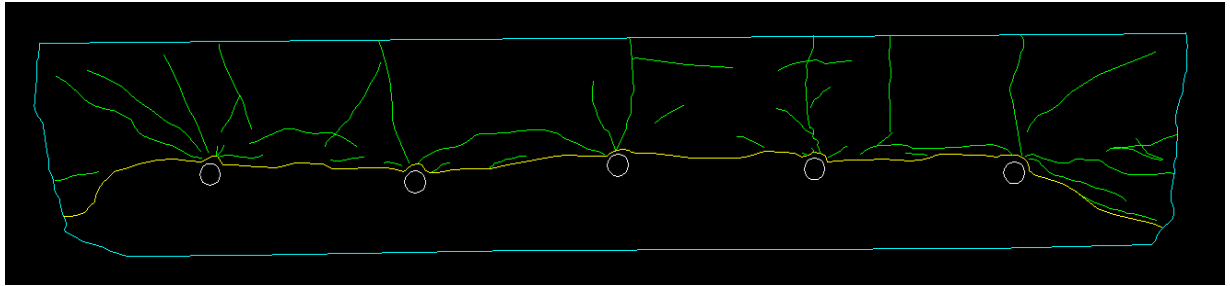


Figure II.30: Slice surface 1. Block CH03B05

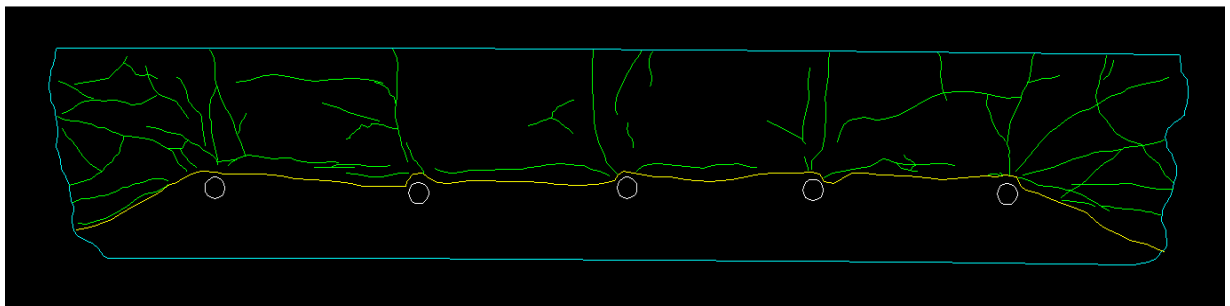


Figure II.31: Slice surface 2. Block CH03B05

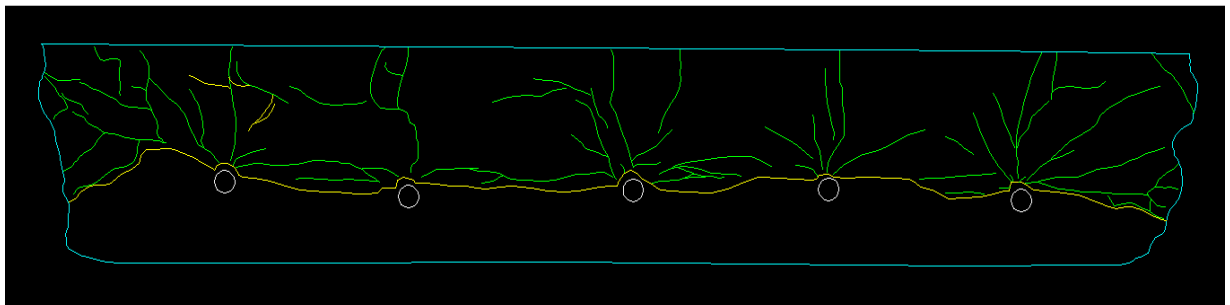


Figure II.32: Slice surface 3. Block CH03B05

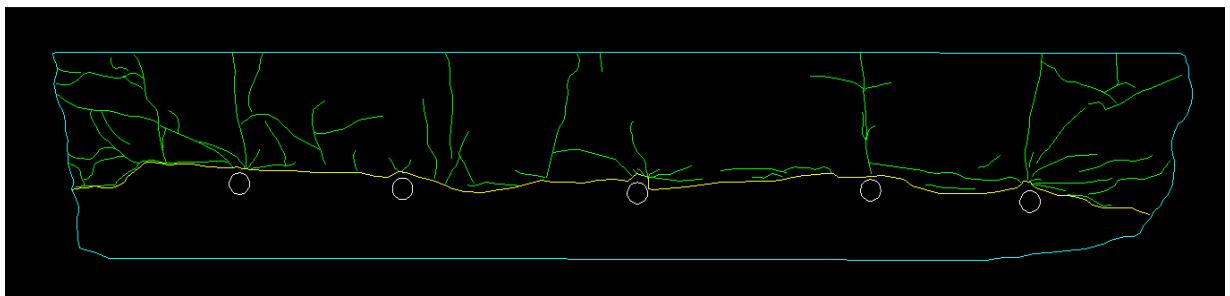


Figure II.33: Slice surface 4. Block CH03B05

ANNEX III: Digital picture of vertical sections of slice surfaces.

Block CH01B01

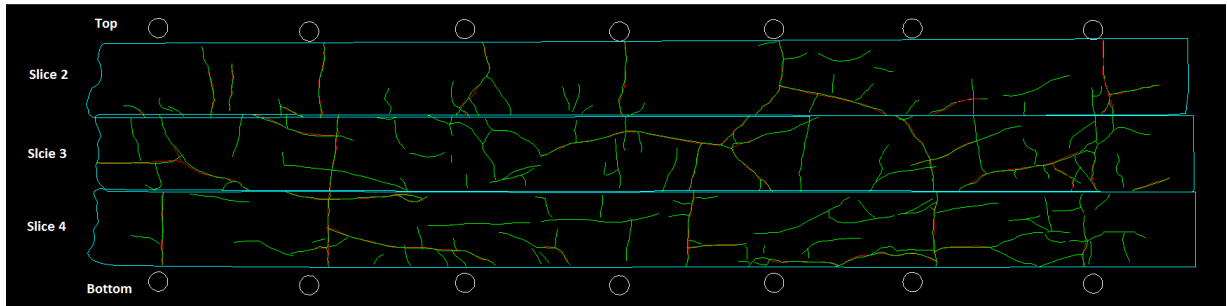


Figure III.1: Vertical section. Block CH01B01

Block CH02B01

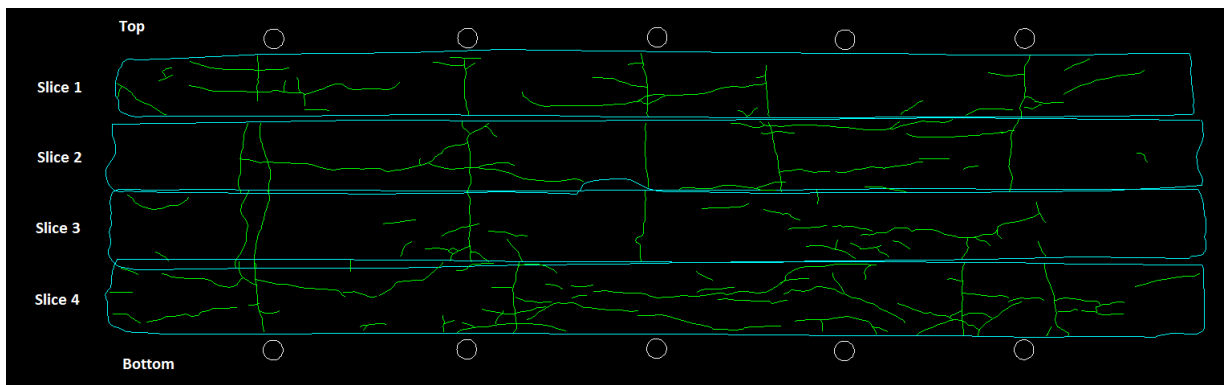


Figure III.2: Vertical section. Block CH02B01

Block CH02B02

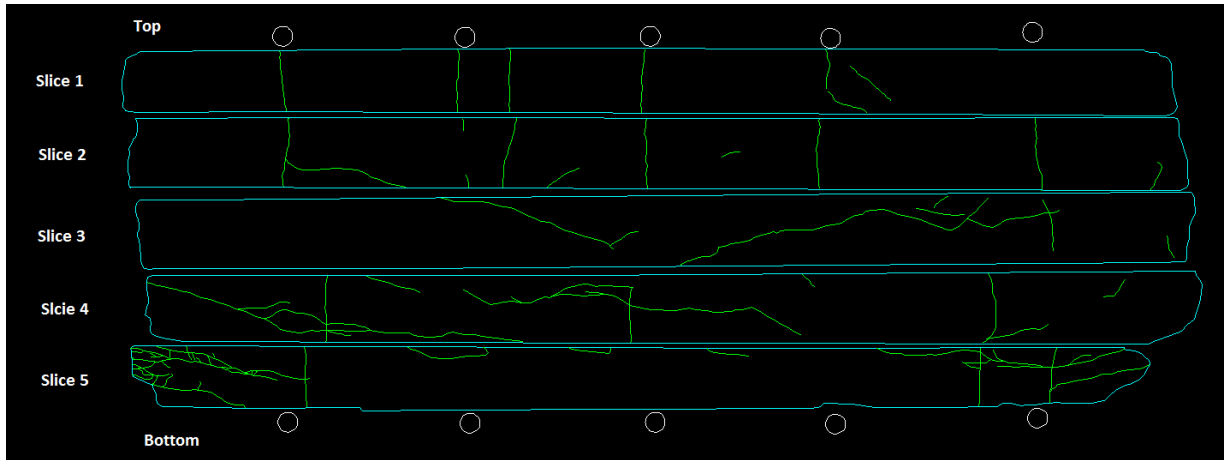


Figure III.3: Vertical section. Block CH02B02

Block CH02B03

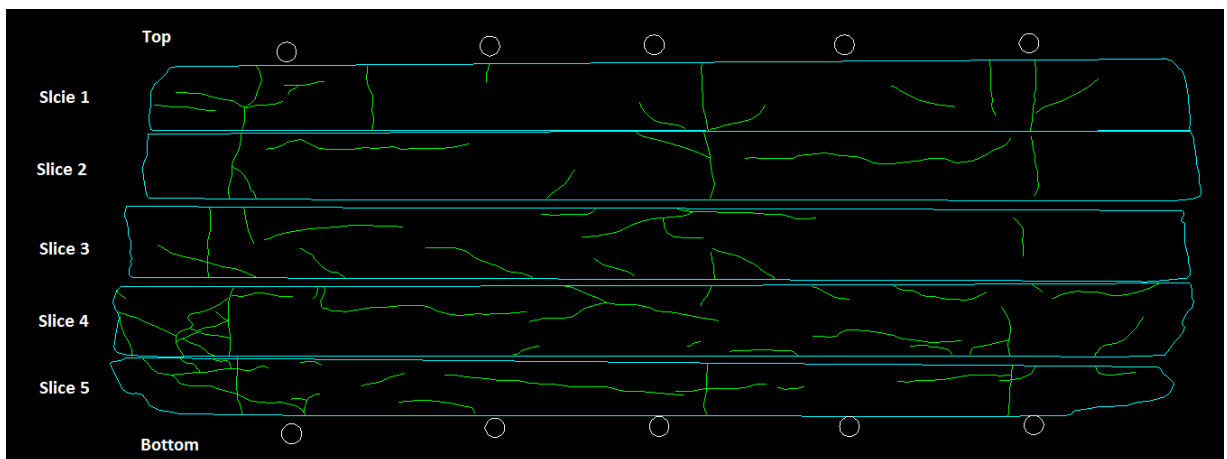


Figure III.4: Vertical section. Block CH02B03

Block CH02B04

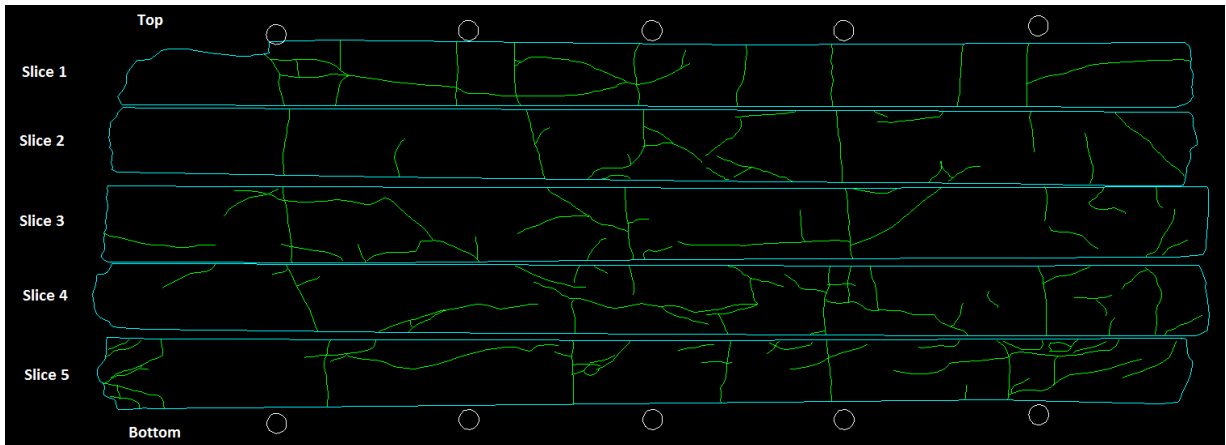


Figure III.5: Vertical section. Block CH02B04

Block CH02B05

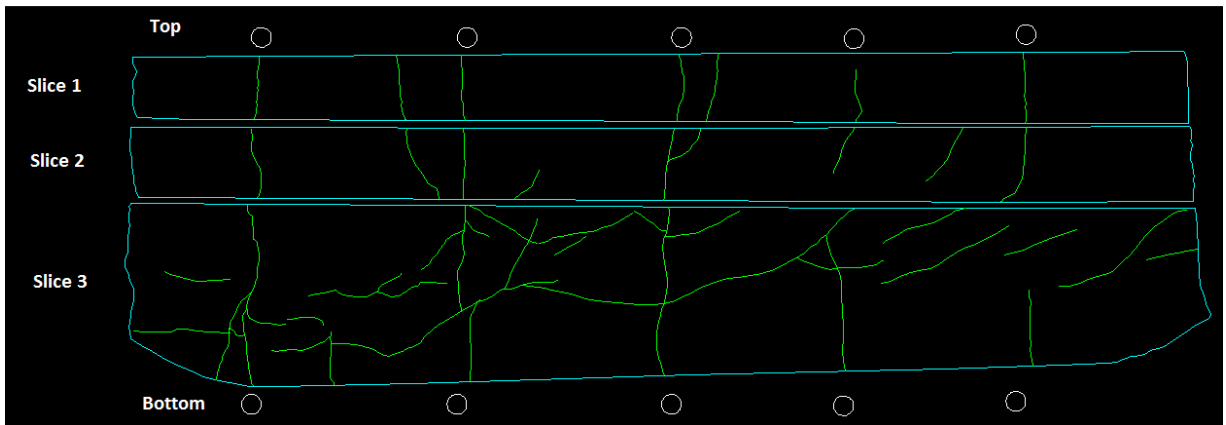


Figure III.6: Vertical section a). Block CH02B05

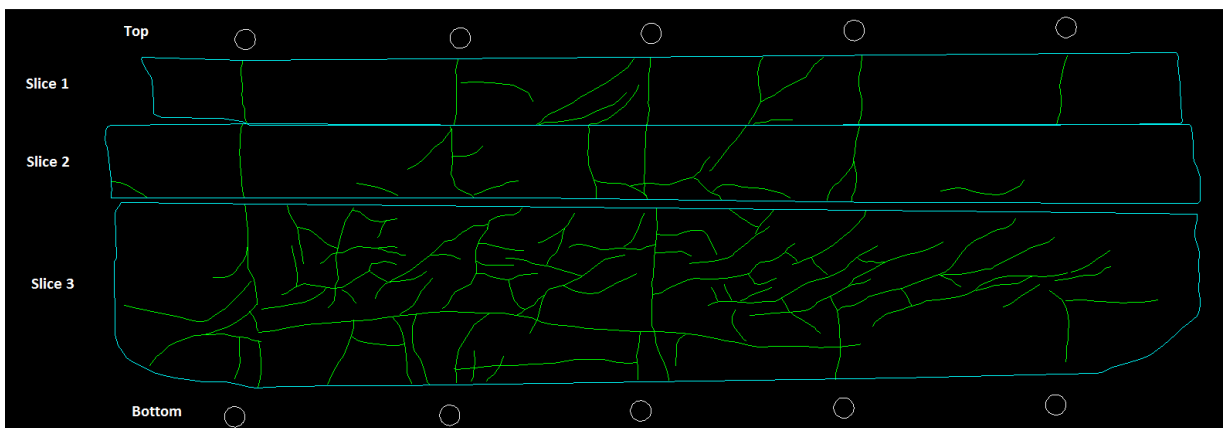


Figure III.7: Vertical section b). Block CH02B05

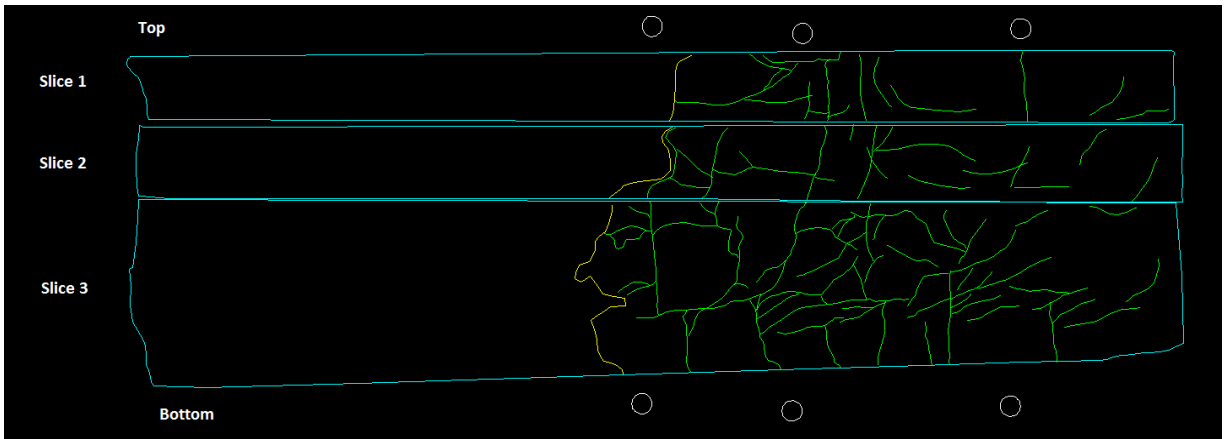


Figure III.8: Vertical section c). Block CH02B05

Block CH03B04

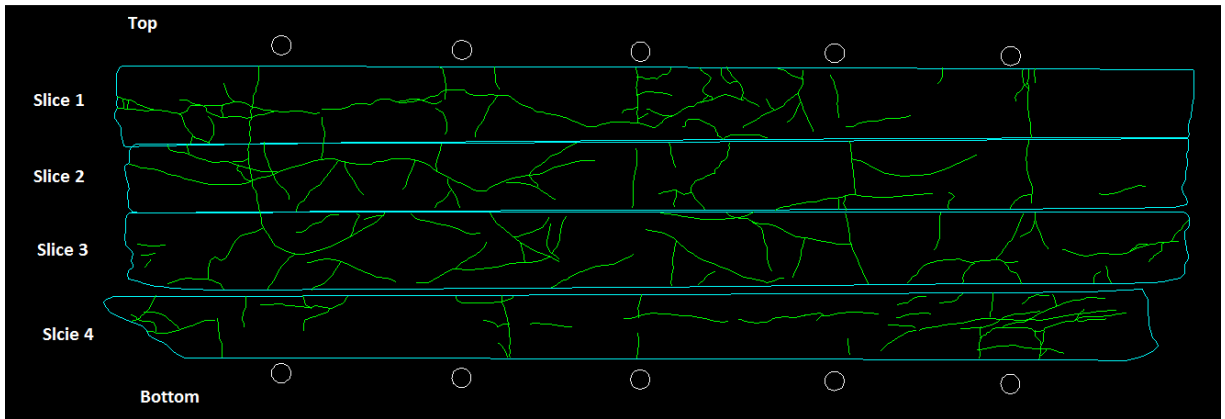


Figure III.9: Vertical section. Block CH03B04

Block CH03B05

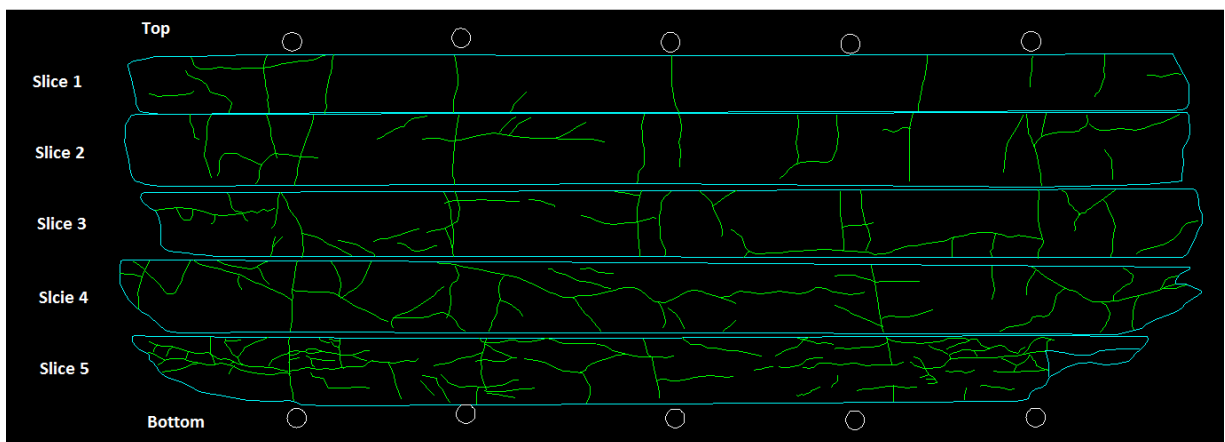


Figure III.10: Vertical section. Block CH03B05

ANNEX IV: Crack families detection

Block CH02B01

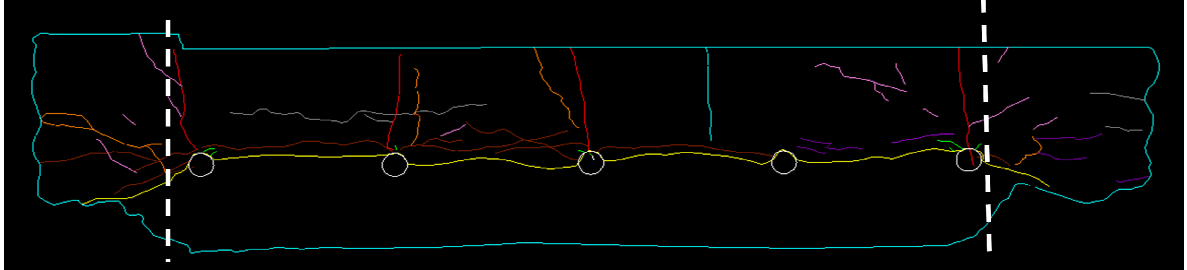


Figure IV.1: Crack detection. Slice surface 1. Block CH02B01

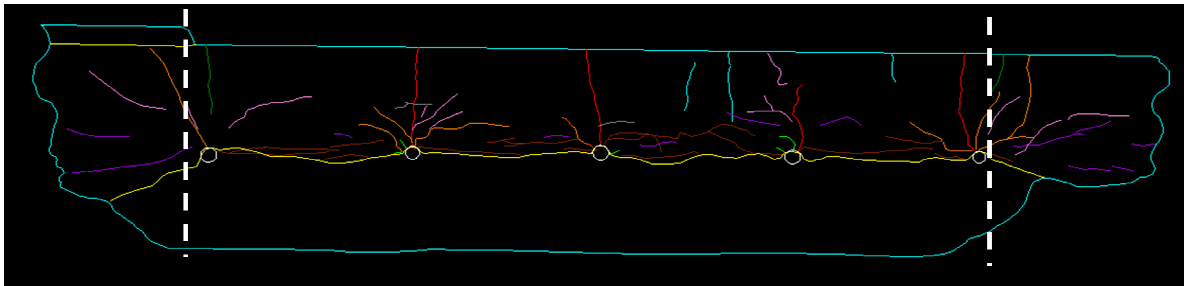


Figure IV.2: Crack detection. Slice surface 2. Block CH02B01

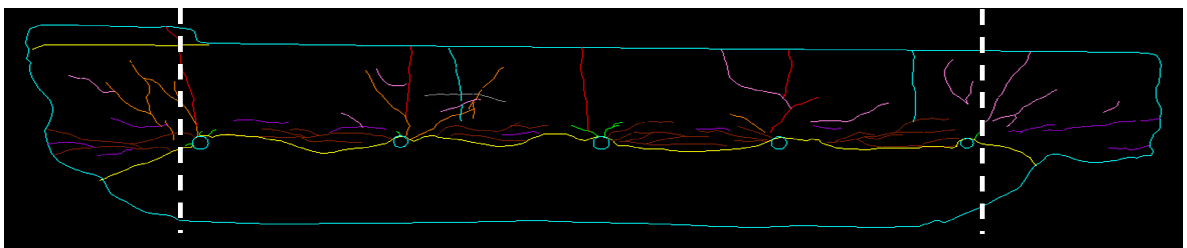


Figure IV.3: Crack detection. Slice surface 3. Block CH02B01

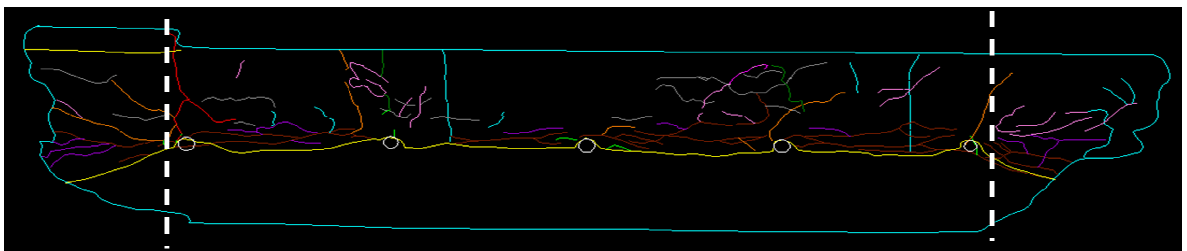


Figure IV.4: Crack detection. Slice surface 4. Block CH02B01

Block CH02B02

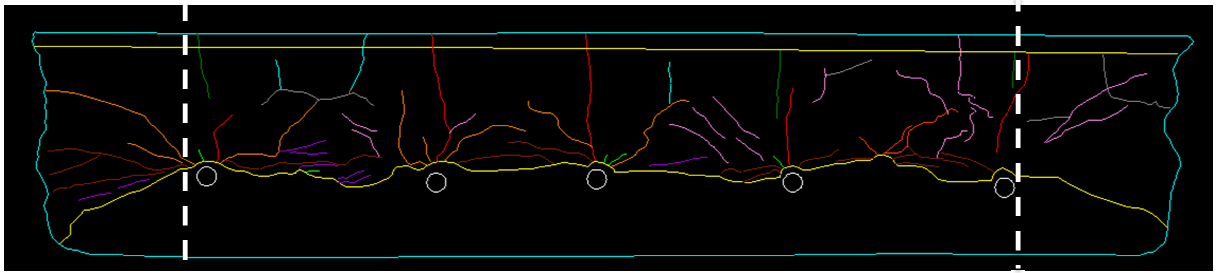


Figure IV.5: Crack detection. Slice surface 1. Block CH02B02

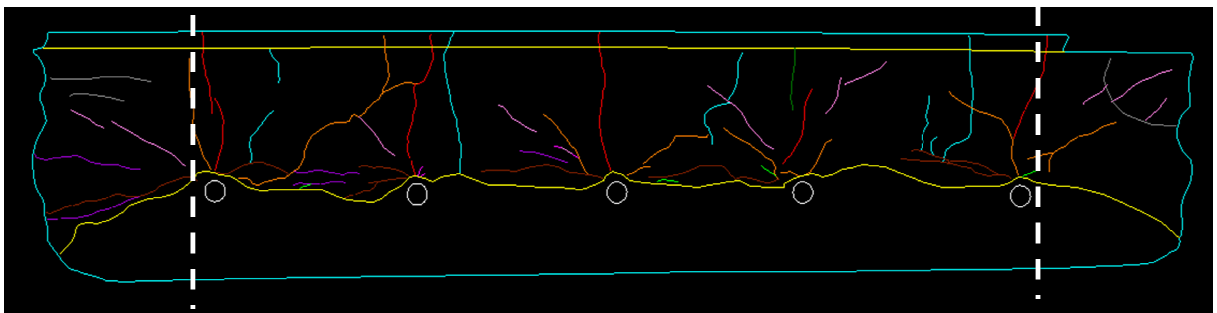


Figure IV.6: Crack detection. Slice surface 2. Block CH02B02

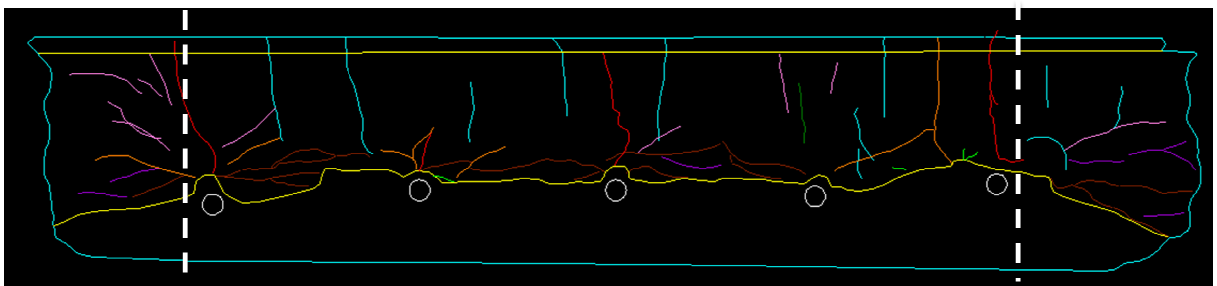


Figure IV.7: Crack detection. Slice surface 3. Block CH02B02

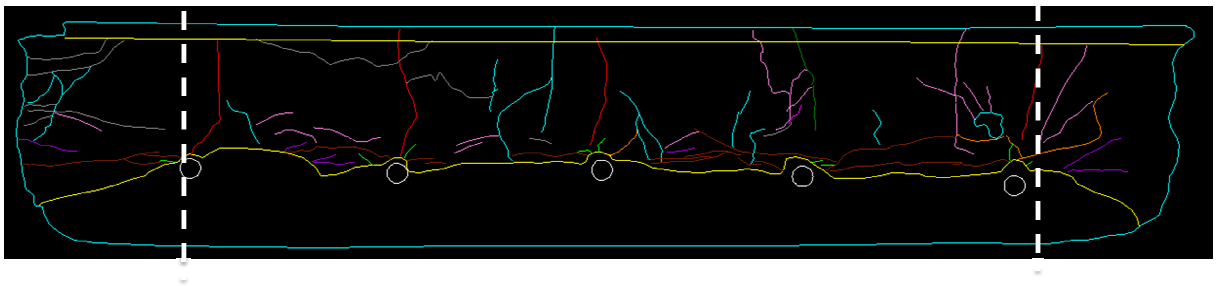


Figure IV.8: Crack detection. Slice surface 4. Block CH02B02

Block CH02B03

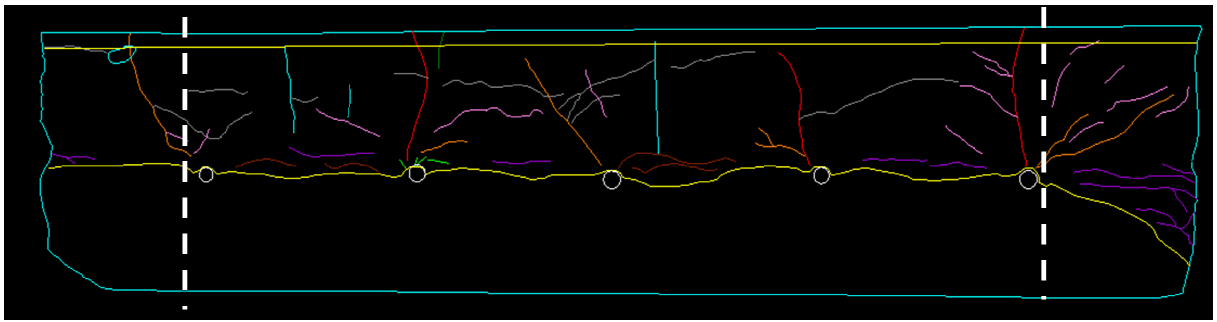


Figure IV.9: Crack detection. Slice surface 1. Block CH02B03

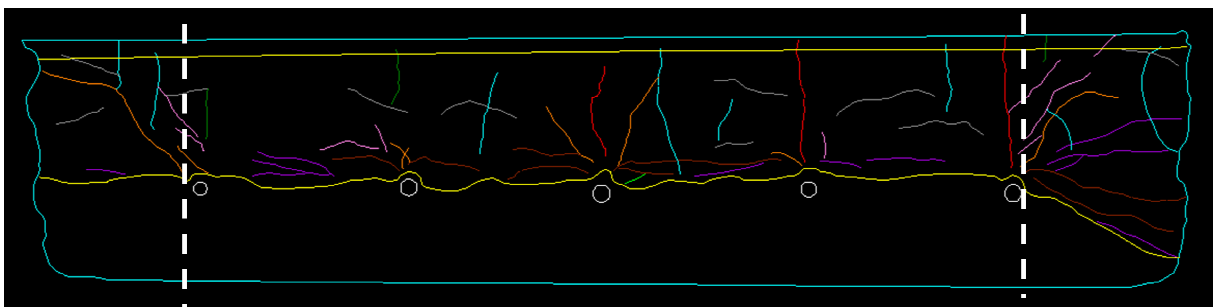


Figure IV.10: Crack detection. Slice surface 2. Block CH02B03

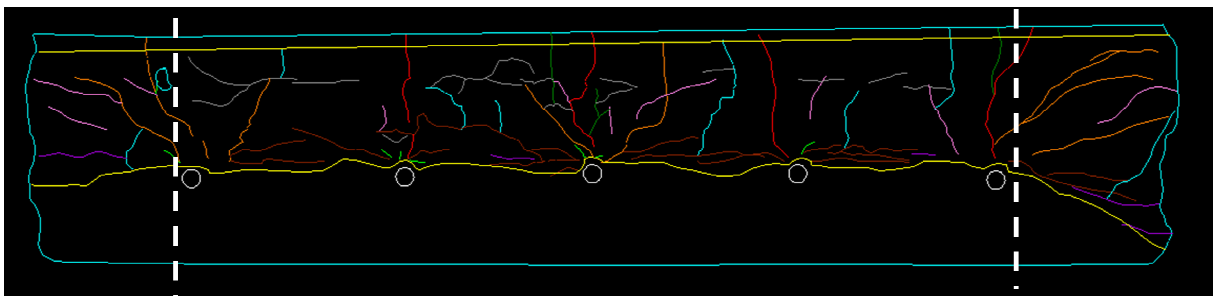


Figure IV.11: Crack detection. Slice surface 3. Block CH02B03

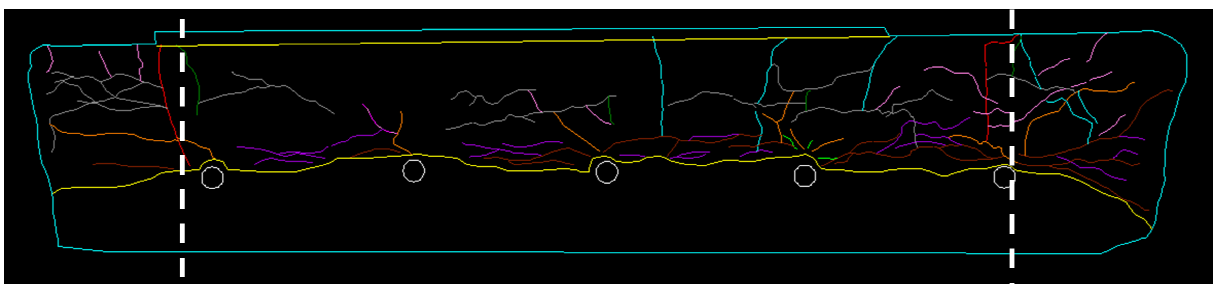


Figure IV.12: Crack detection. Slice surface 4. Block CH02B03

Block CH02B04

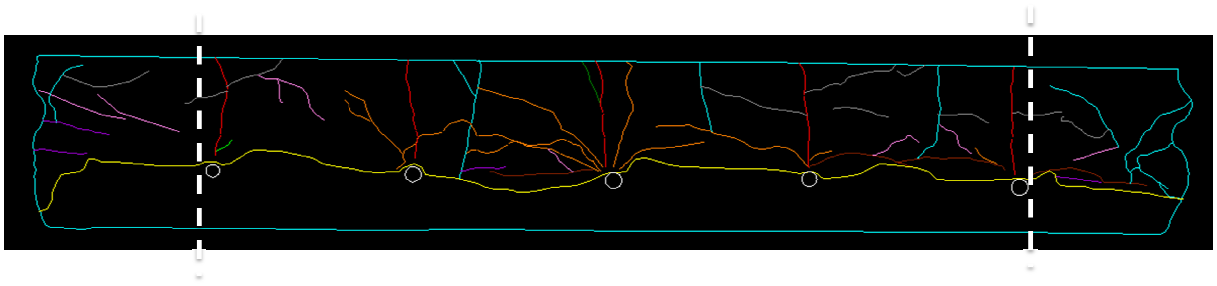


Figure IV.13: Crack detection. Slice surface 1. Block CH02B04

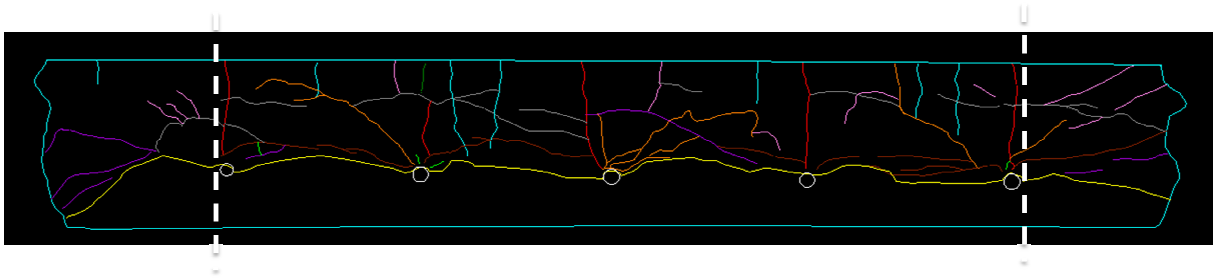


Figure IV.14: Crack detection. Slice surface 2. Block CH02B04

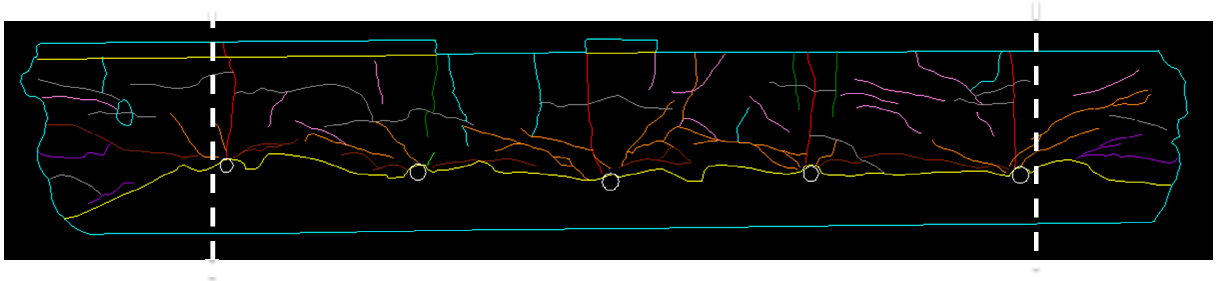


Figure IV.15: Crack detection. Slice surface 3. Block CH02B04

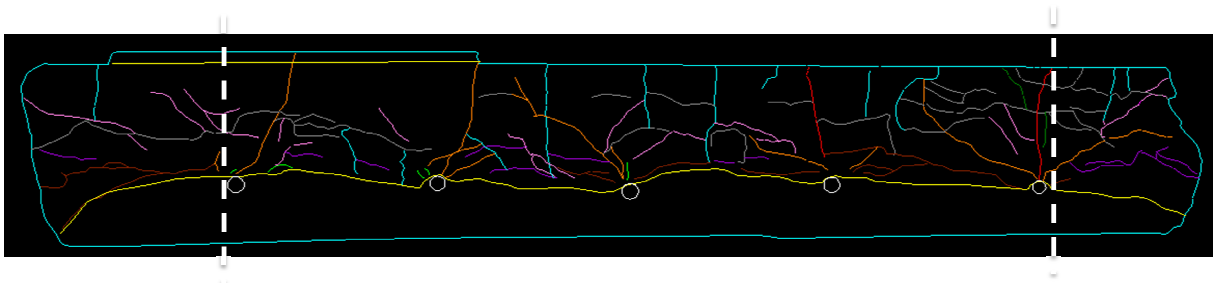


Figure IV.16: Crack detection. Slice surface 4. Block CH02B04

Block CH03B04

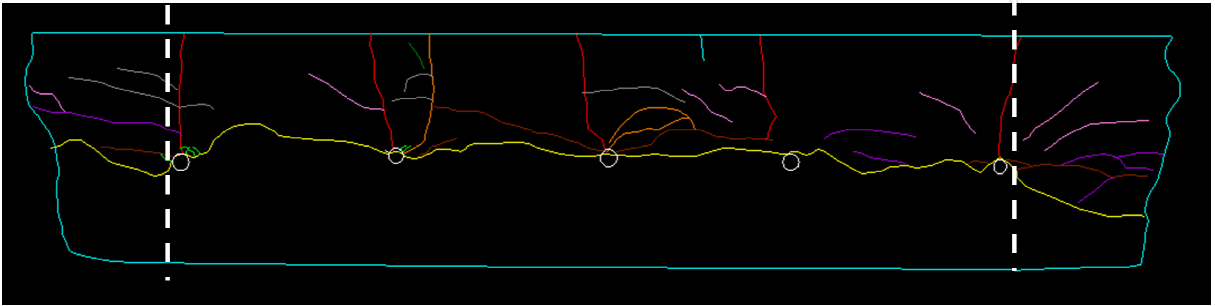


Figure IV.17: Crack detection. Slice surface 1. Block CH03B04

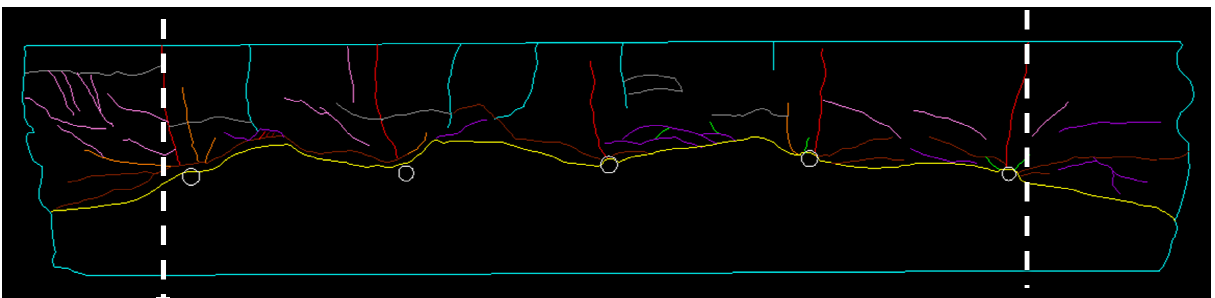


Figure IV.18: Crack detection. Slice surface 2. Block CH03B04

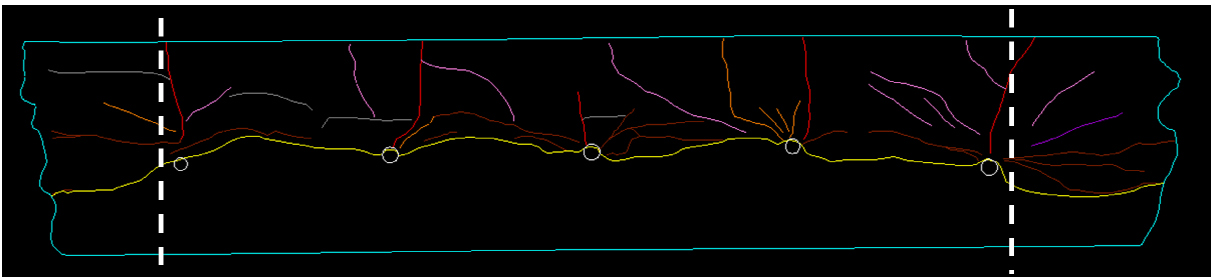


Figure IV.19: Crack detection. Slice surface 3. Block CH03B04

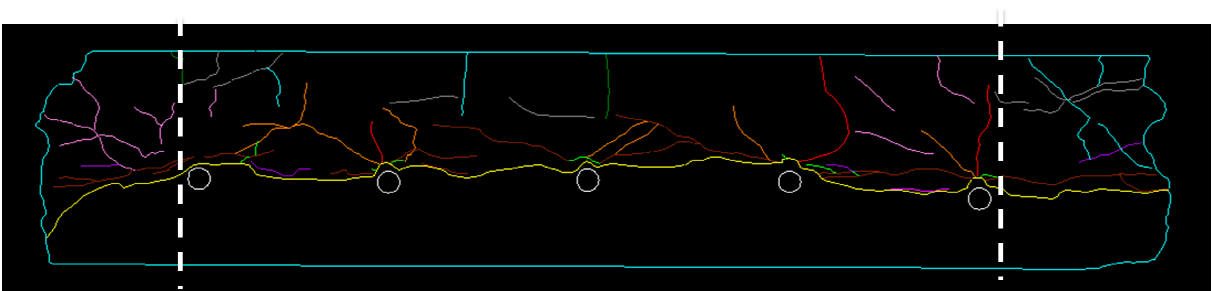


Figure IV.20: Crack detection. Slice surface 4. Block CH03B04

Block CH03B05

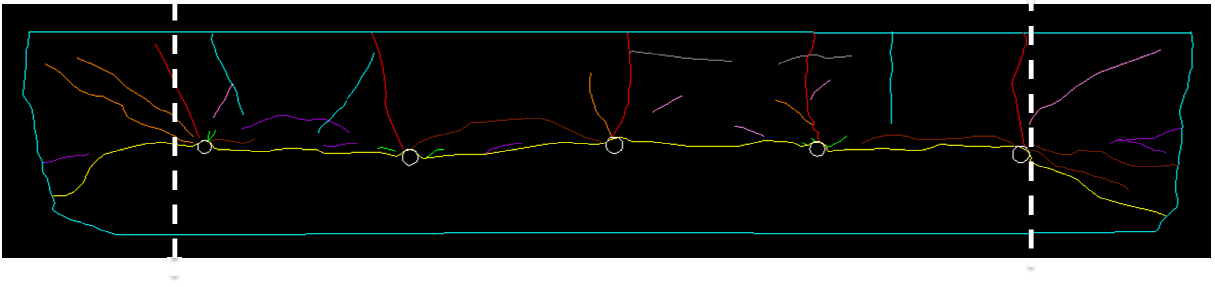


Figure IV.21: Crack detection. Slice surface 1. Block CH03B05

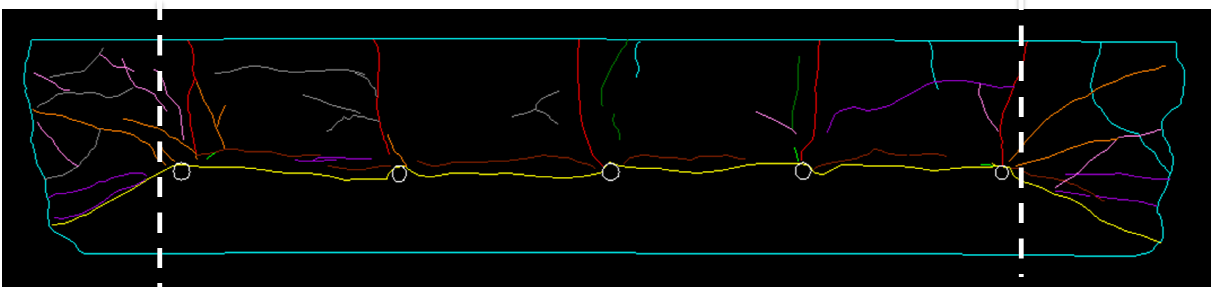


Figure IV.22: Crack detection. Slice surface 2. Block CH03B05

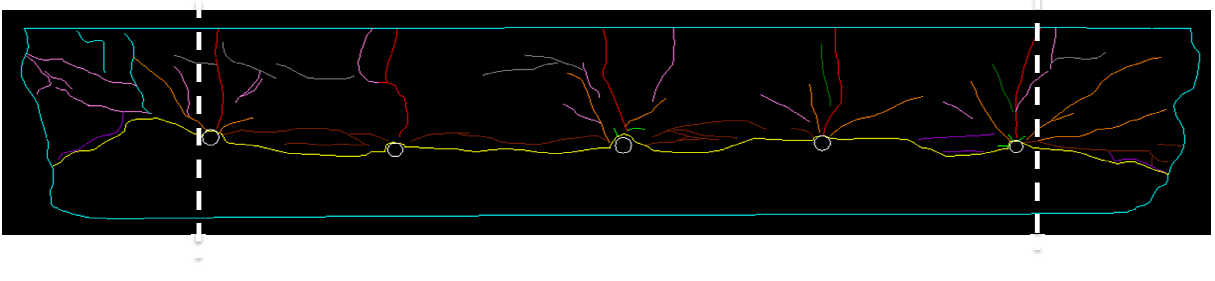


Figure IV.23: Crack detection. Slice surface 3. Block CH03B05

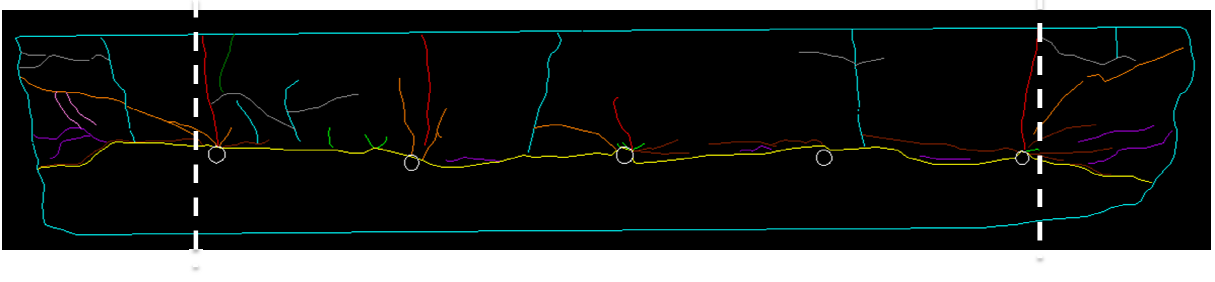


Figure IV.24: Crack detection. Slice surface 4. Block CH03B05

ANNEX V: Crack density damage maps



Block CH01B01

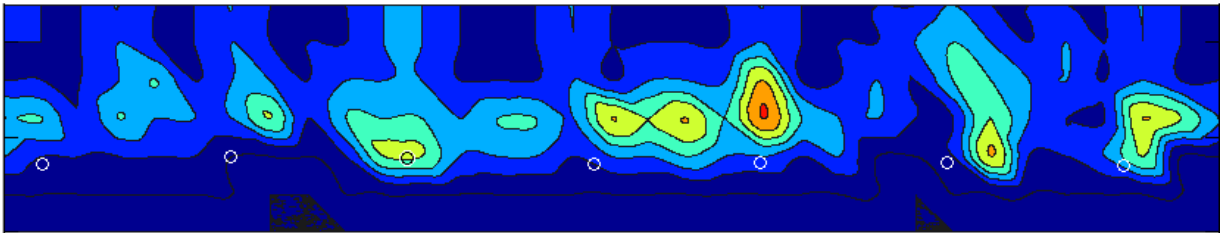


Figure V.1: Damage map. Slice surface 1. Block CH01B01

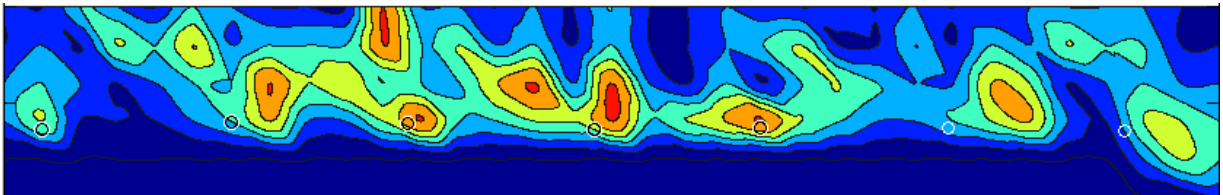


Figure V.2: Damage map. Slice surface 2. Block CH01B01

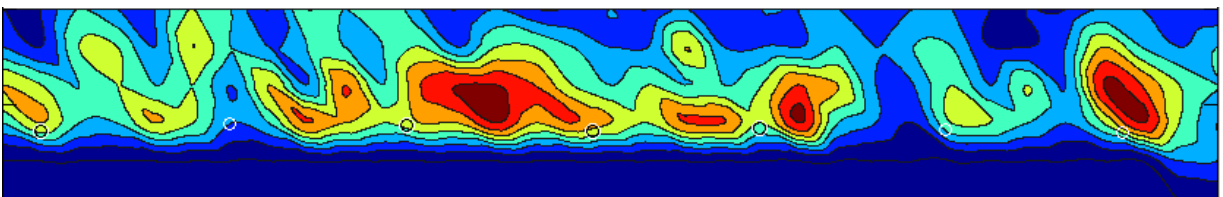


Figure V.3: Damage map. Slice surface 3. Block CH01B01

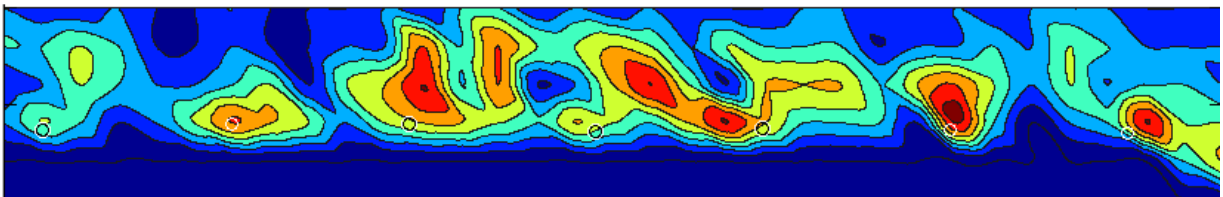


Figure V.4: Damage map. Slice surface 4. Block CH01B01



Block CH02B01

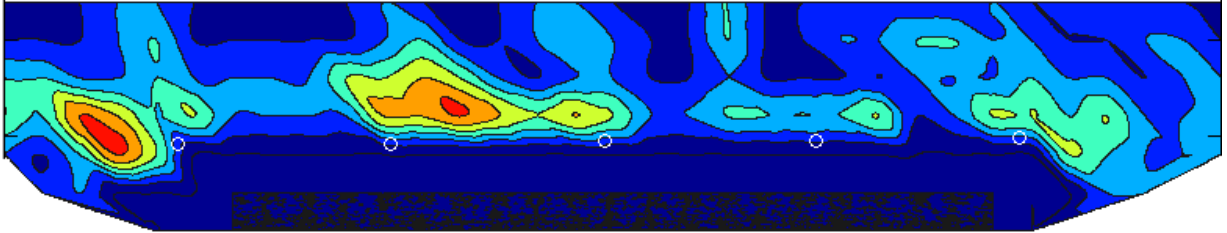


Figure V.5: Damage map. Slice surface 1. Block CH02B01

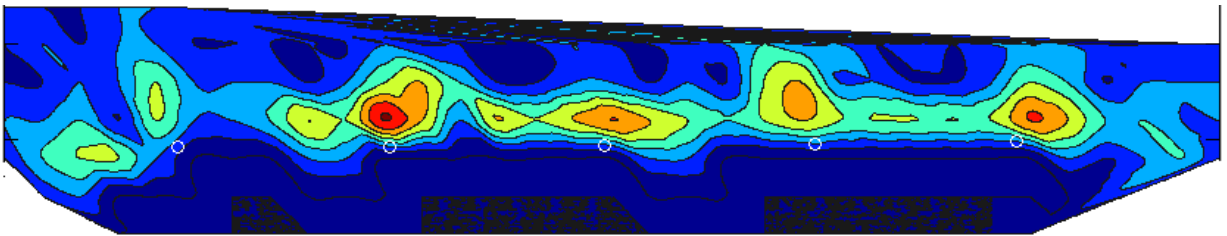


Figure V.6: Damage map. Slice surface 2. Block CH02B01

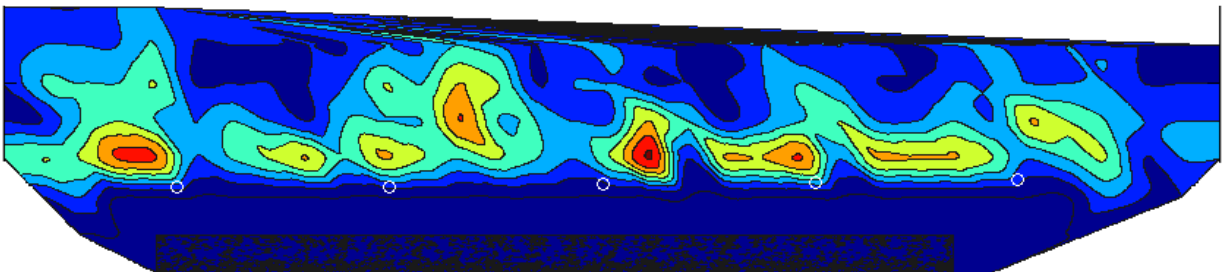


Figure V.7: Damage map. Slice surface 3. Block CH02B01

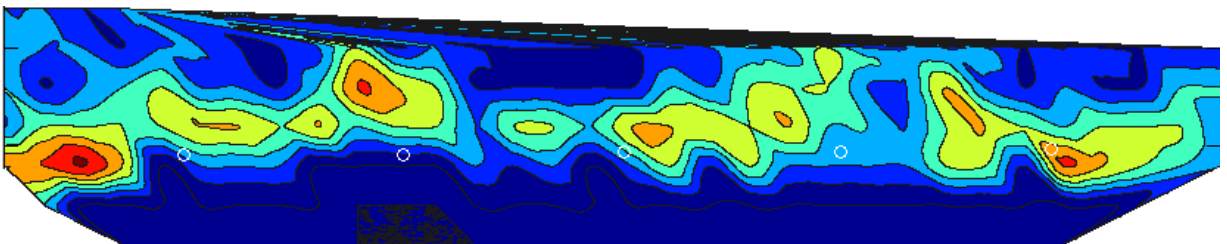


Figure V.8: Damage map. Slice surface 4. Block CH02B01



Block CH02B02

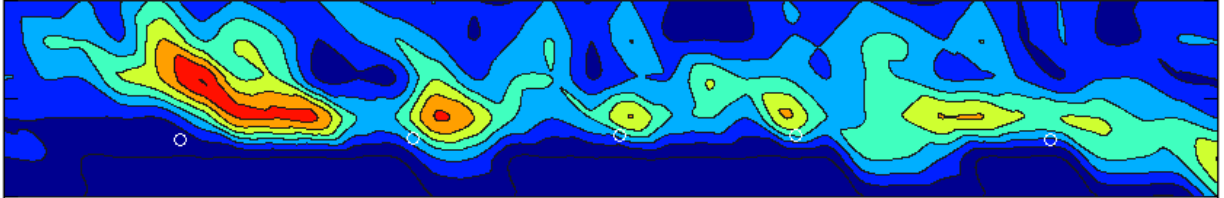


Figure V.9: Damage map. Slice surface 1. Block CH02B02

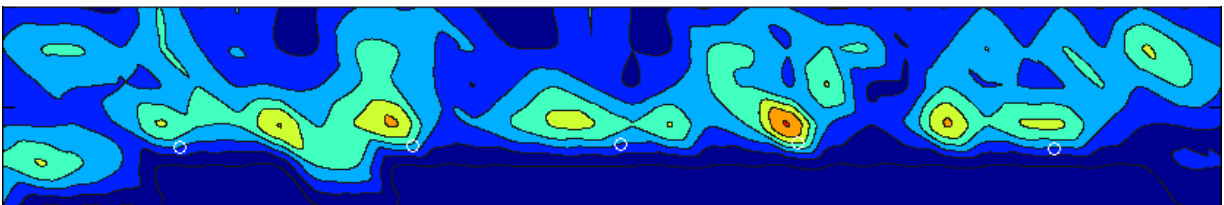


Figure V.10: Damage map. Slice surface 2. Block CH02B02

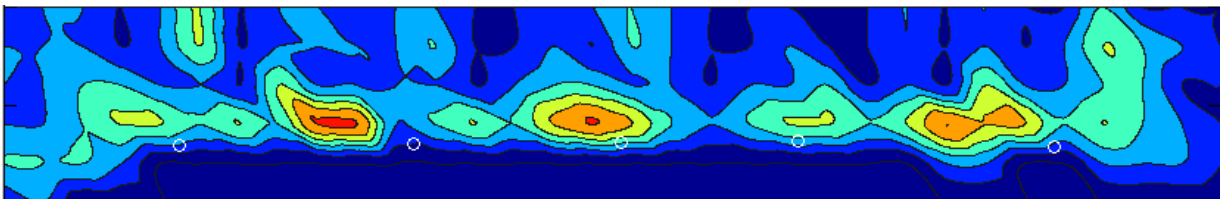


Figure V.11: Damage map. Slice surface 3. Block CH02B02

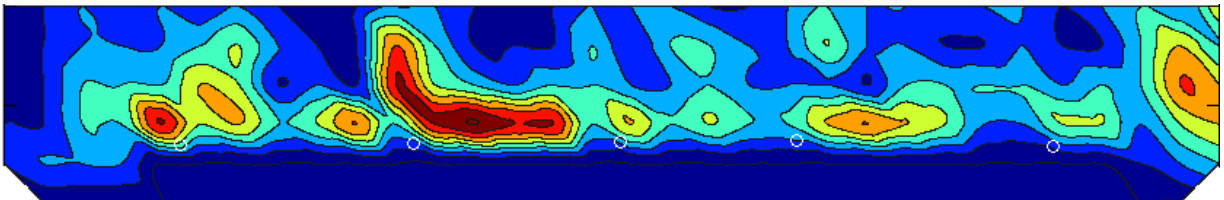


Figure V.12: Damage map. Slice surface 4. Block CH02B02



Block CH02B03

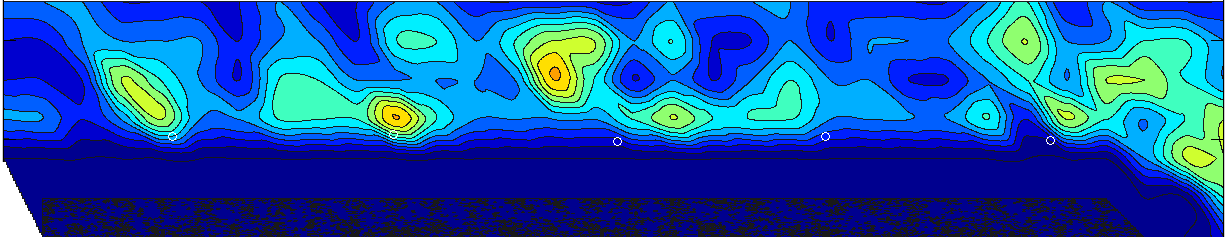


Figure V.13: Damage map. Slice surface 1. Block CH02B03

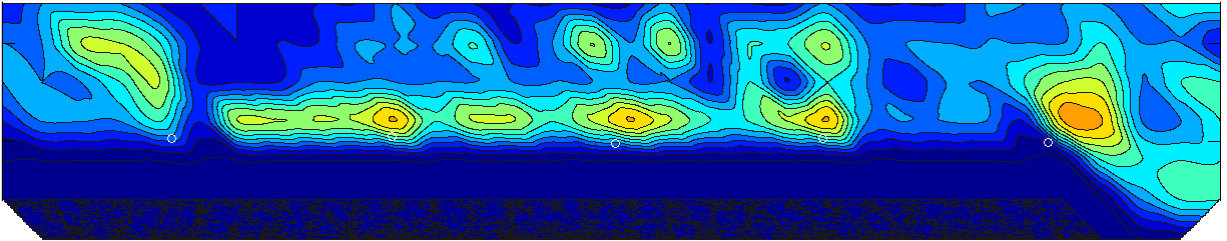


Figure V.14: Damage map. Slice surface 2. Block CH02B03

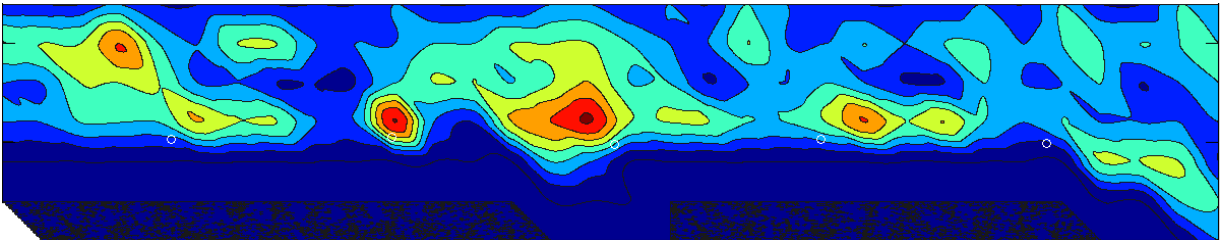


Figure V.15: Damage map. Slice surface 3. Block CH02B03

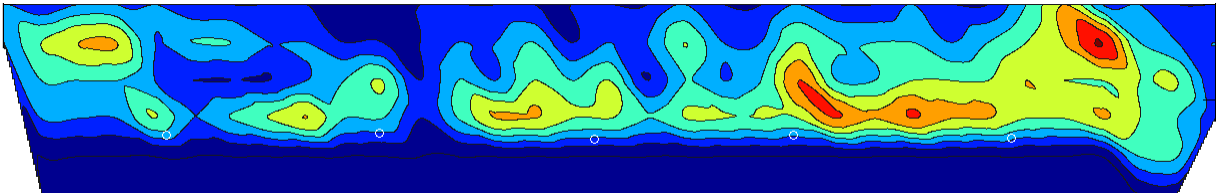


Figure V.16: Damage map. Slice surface 4. Block CH02B03



Block CH02B04

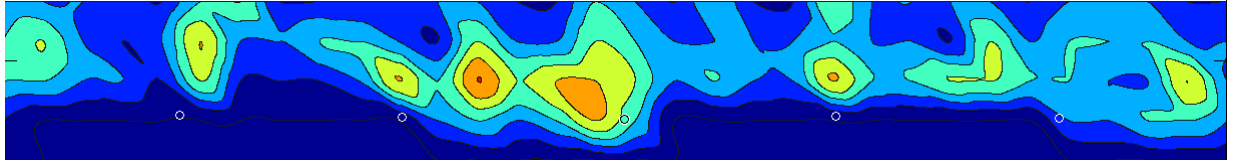


Figure V.17: Damage map. Slice surface 1. Block CH02B04

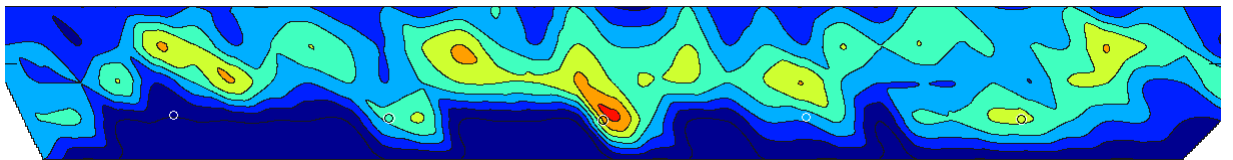


Figure V.18: Damage map. Slice surface 2. Block CH02B04

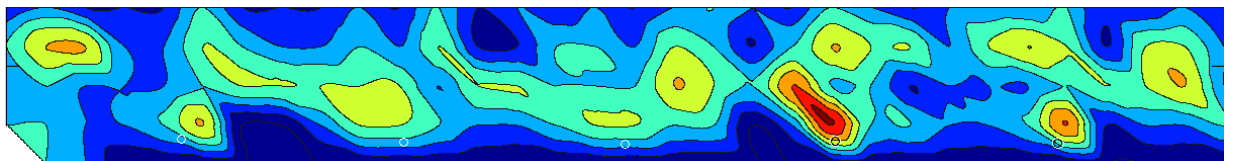


Figure V.19: Damage map. Slice surface 3. Block CH02B04

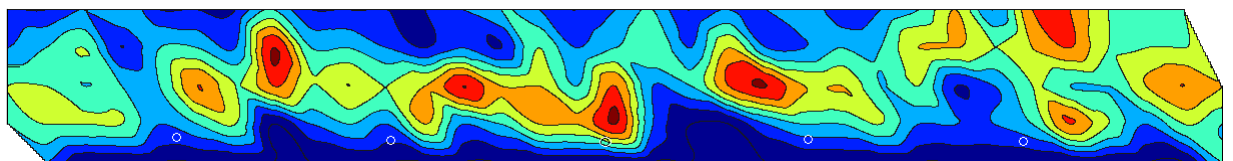


Figure V.20: Damage map. Slice surface 4. Block CH02B04



Block CH02B05

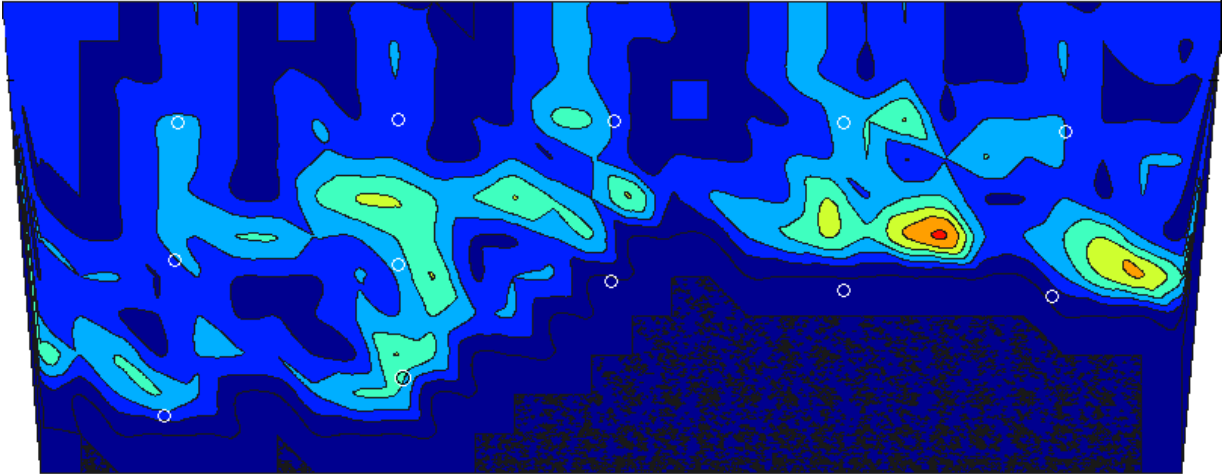


Figure V.21: Damage map. Slice surface 1. Block CH02B05

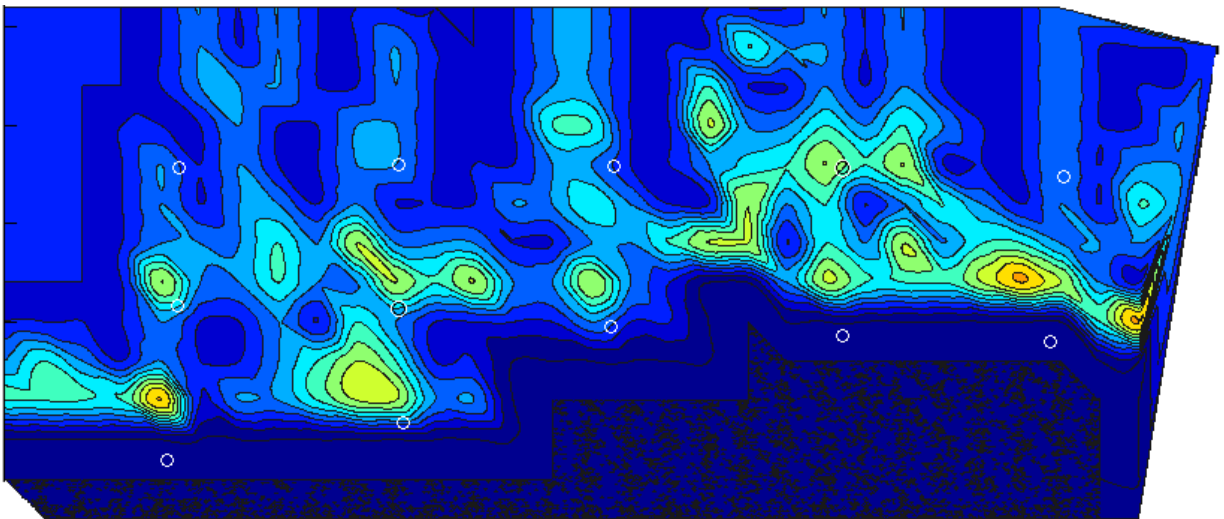


Figure V.22: Damage map. Slice surface 2. Block CH02B05

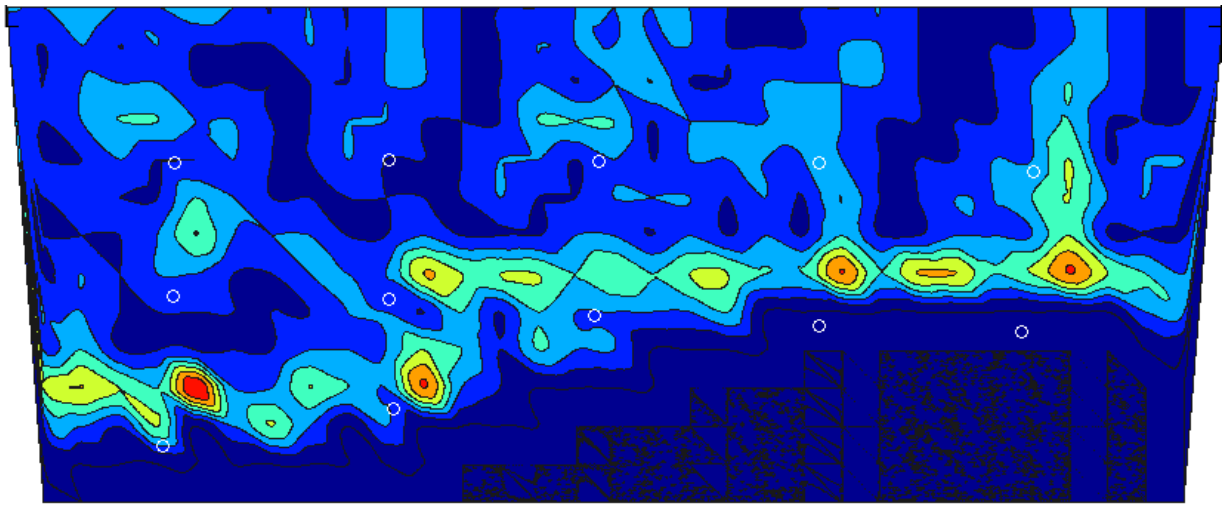


Figure V.23: Damage map. Slice surface 3. Block CH02B05

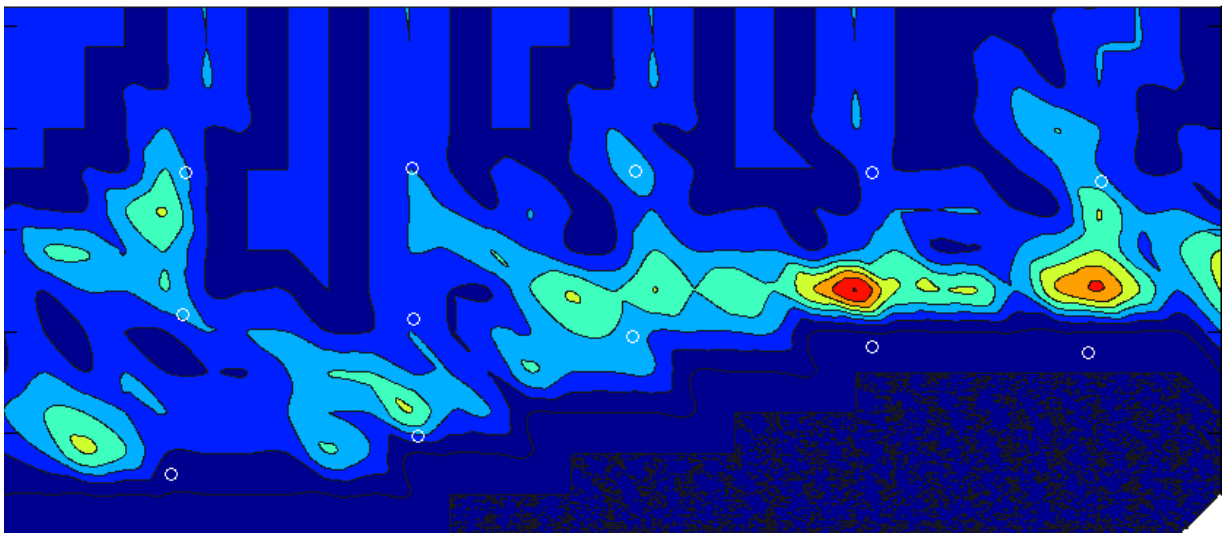


Figure V.24: Damage map. Slice surface 4. Block CH02B05



Block CH03B04

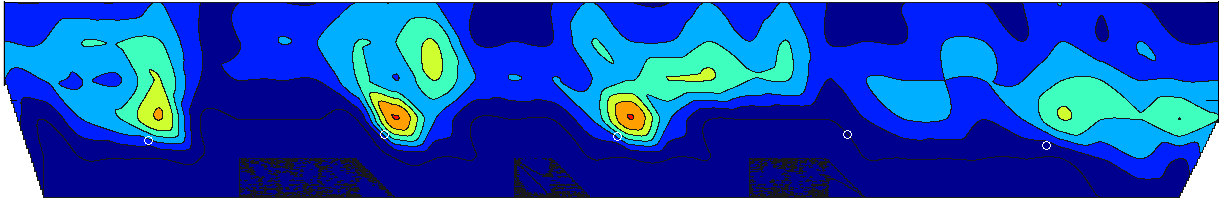


Figure V.25: Damage map. Slice surface 1. Block CH03B04

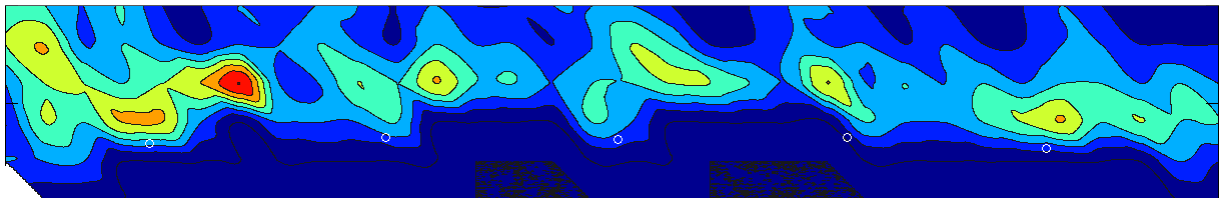


Figure V.26: Damage map. Slice surface 2. Block CH03B04

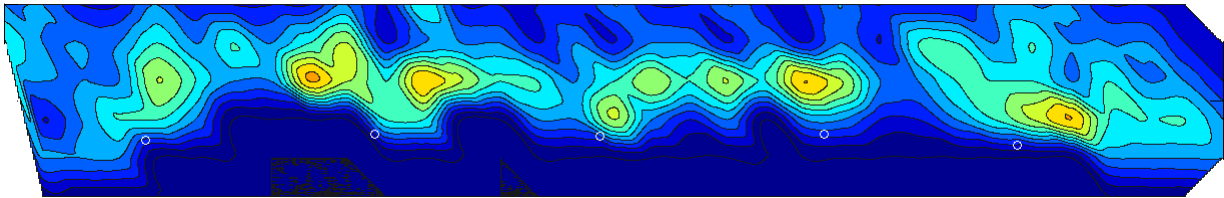


Figure V.27: Damage map. Slice surface 3. Block CH03B04

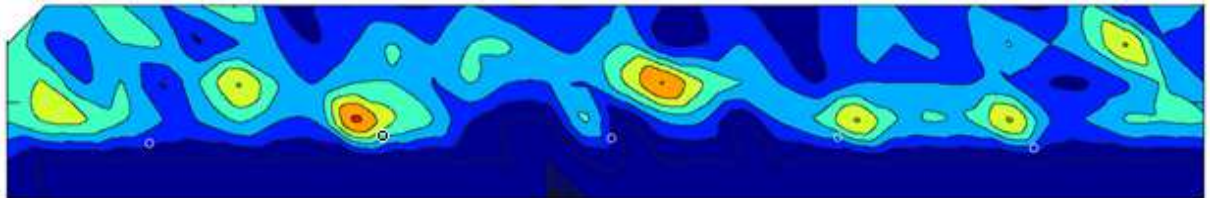


Figure V.28: Damage map. Slice surface 4. Block CHO3B



Block CH03B05

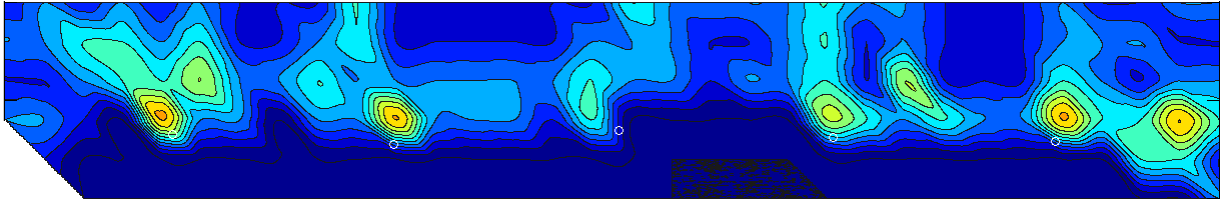


Figure V.29: Damage map. Slice surface 1. Block CH03B05

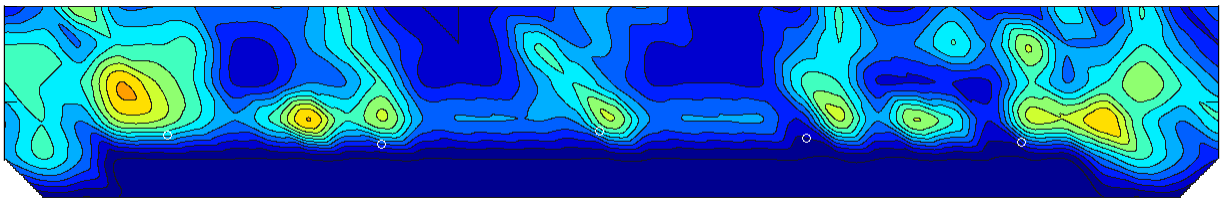


Figure V.30: Damage map. Slice surface 2. Block CH03B05

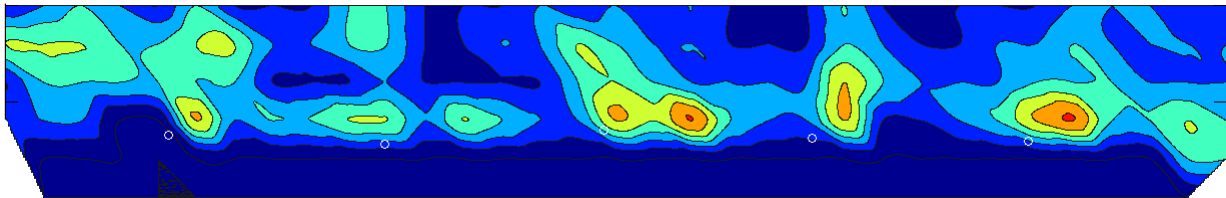


Figure V.31: Damage map. Slice surface 3. Block CH03B05

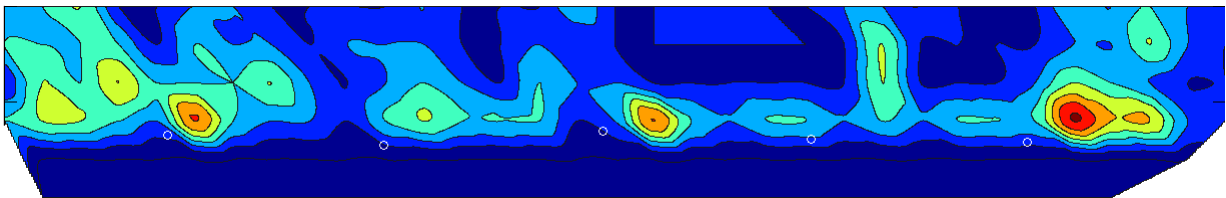


Figure V.32: Damage map. Slice surface 4. Block CH03B05

ANNEX VI: Intersection crack density damage maps



Block CH01B01

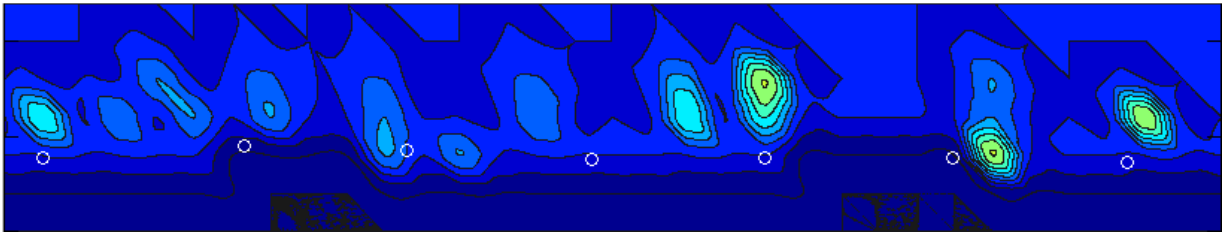


Figure VI.1: Intersection damage map. Slice surface 1. Block CH01B01

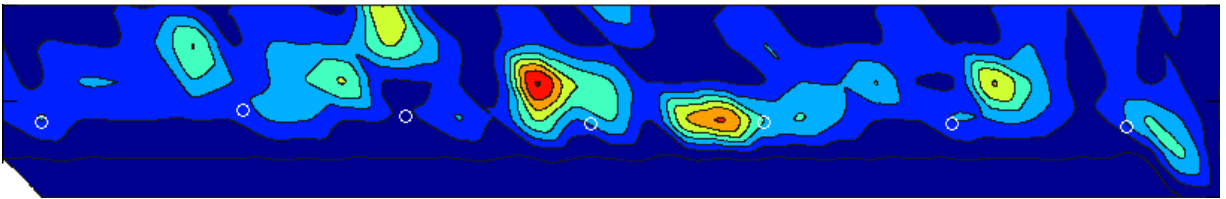


Figure VI.2: Intersection damage map. Slice surface 2. Block CH01B01

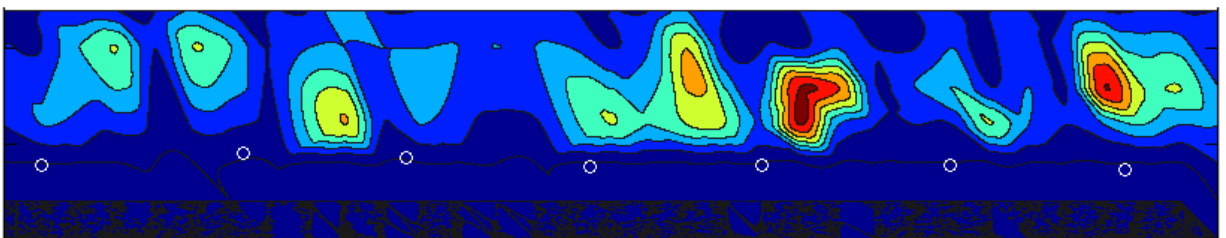


Figure VI.3: Intersection damage map. Slice surface 3. Block CH01B01

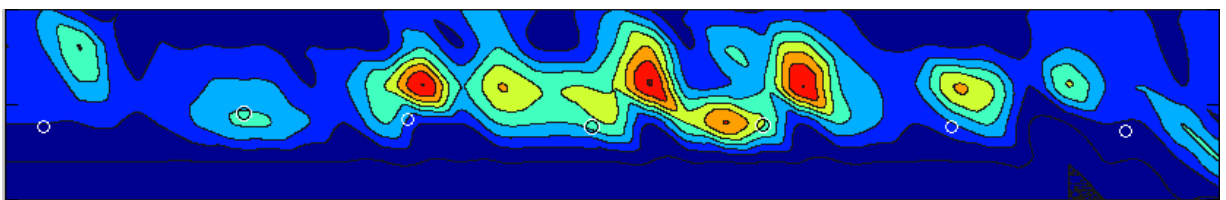


Figure VI.4: Intersection damage map. Slice surface 4. Block CH01B01



Block CH02B01

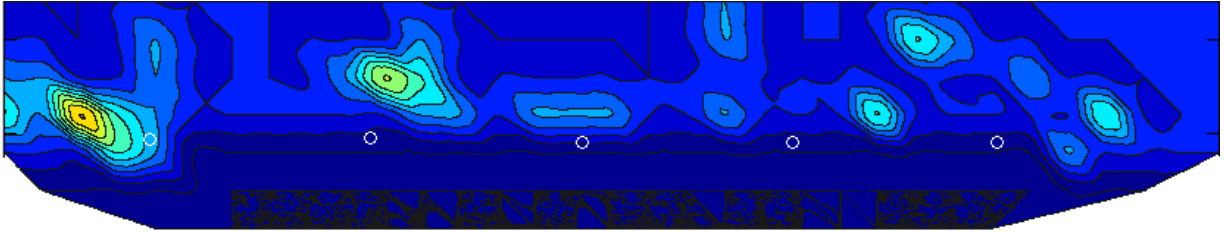


Figure VI.5: Intersection damage map. Slice surface 1. Block CH02B01

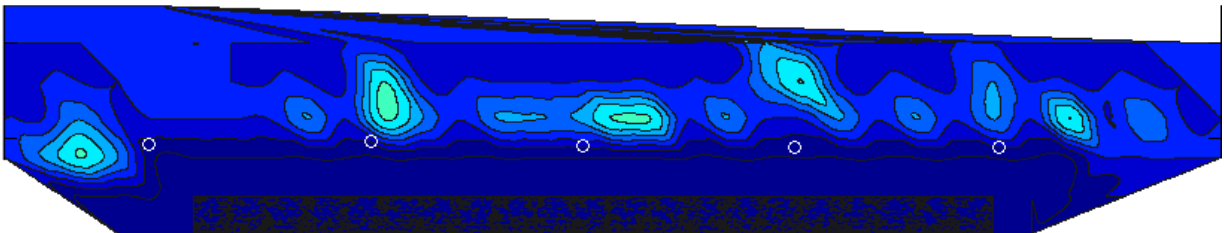


Figure VI.6: Intersection damage map. Slice surface 2. Block CH02B01

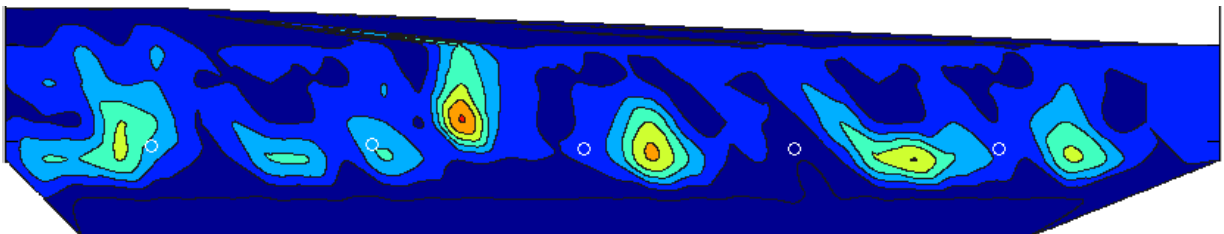


Figure VI.7: Intersection damage map. Slice surface 3. Block CH02B01

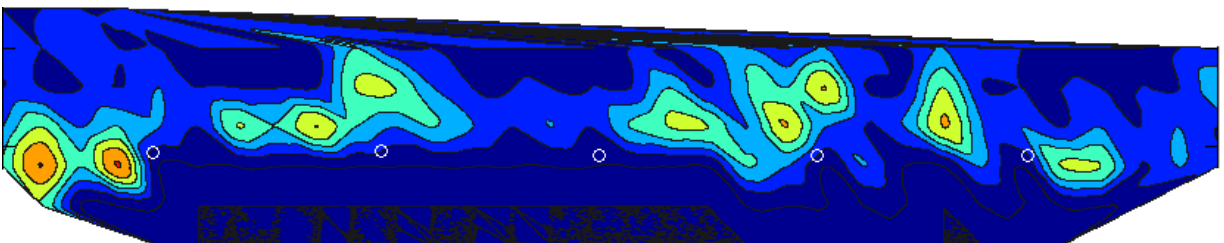


Figure VI.8: Intersection damage map. Slice surface 4. Block CH02B01



Block CH02B01

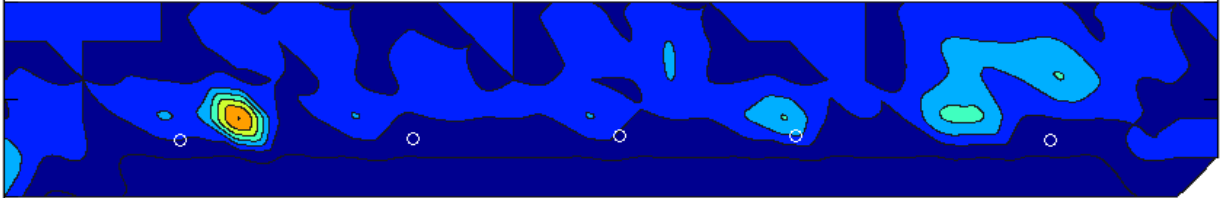


Figure VI.9: Intersection damage map. Slice surface 1. Block CH02B02

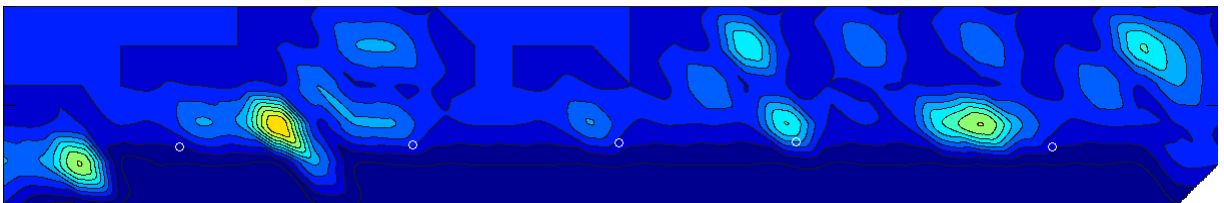


Figure VI.10: Intersection damage map. Slice surface 2. Block CH02B02

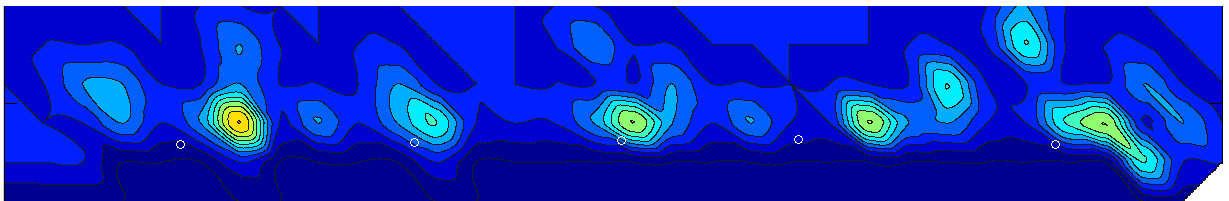


Figure VI.11: Intersection damage map. Slice surface 3. Block CH02B02

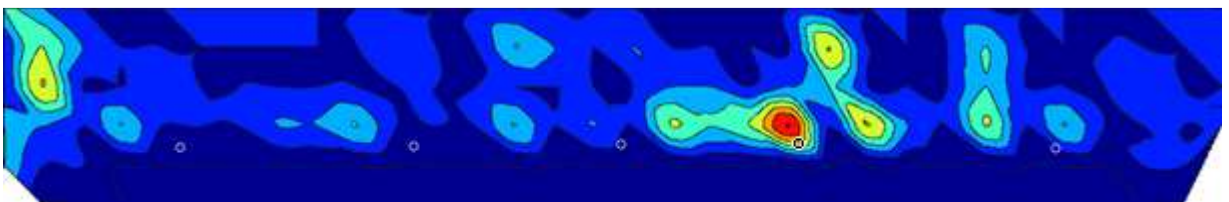


Figure VI.12: Intersection damage map. Slice surface 4. Block CH02B02



Block CH02B02

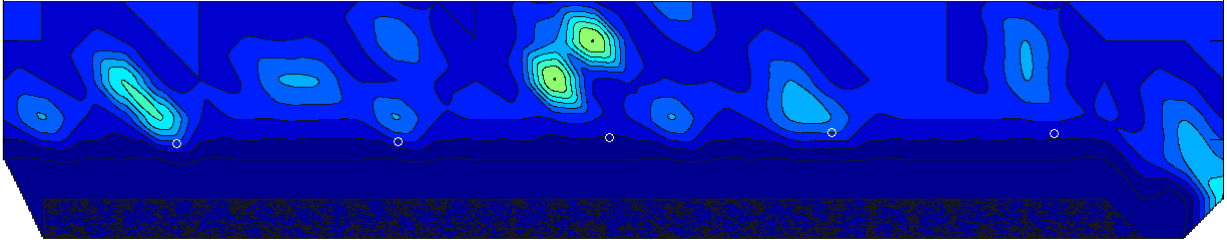


Figure VI.13: Intersection damage map. Slice surface 1. Block CH02B03

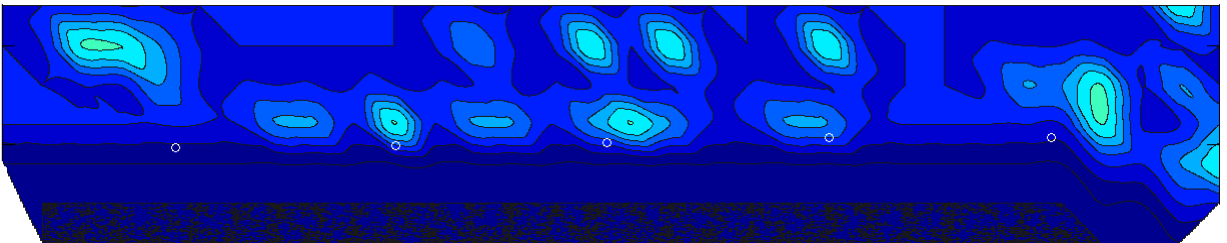


Figure VI.14: Intersection damage map. Slice surface 2. Block CH02B03

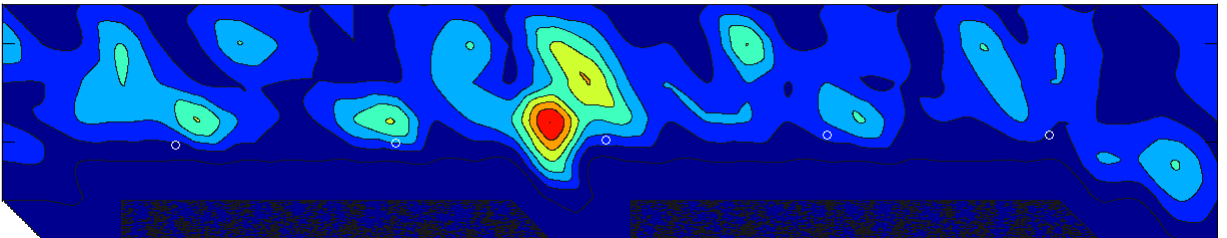


Figure VI.15: Intersection damage map. Slice surface 3. Block CH02B03

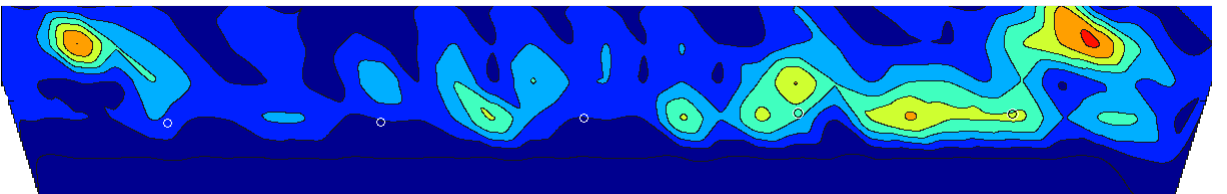


Figure VI.16: Intersection damage map. Slice surface 4. Block CH02B03



Block CH02B03

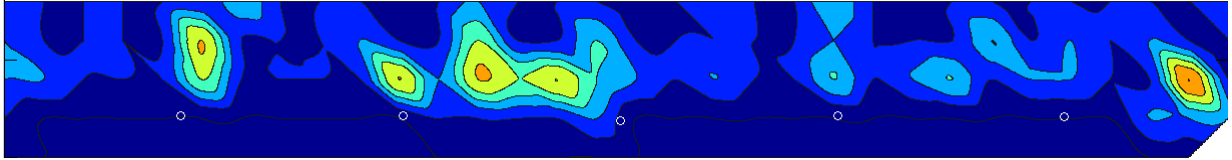


Figure VI.17: Intersection damage map. Slice surface 1. Block CH02B04

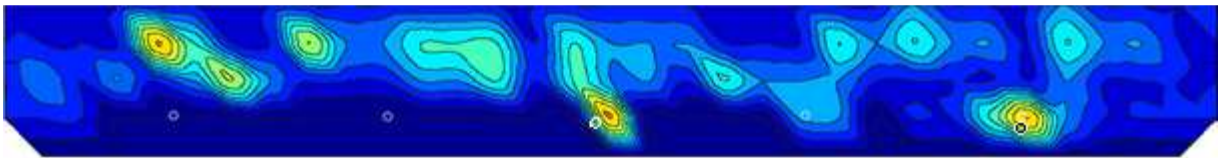


Figure VI.18: Intersection damage map. Slice surface 2. Block CH02B04

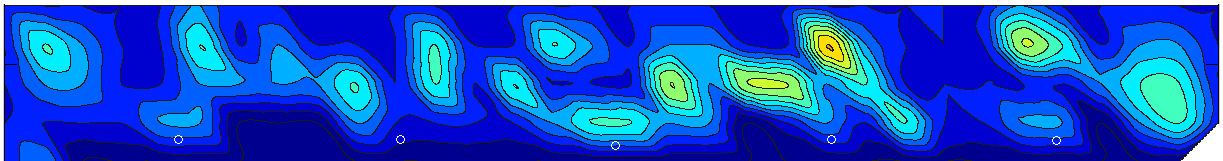


Figure VI.19: Intersection damage map. Slice surface 3. Block CH02B04

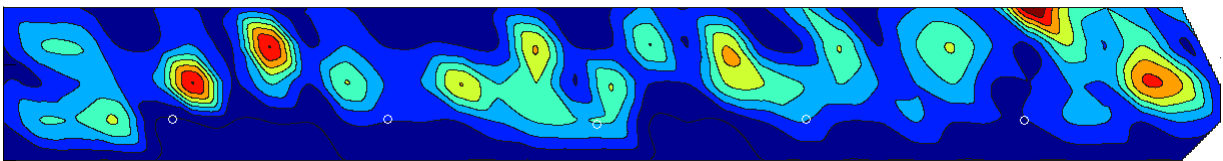


Figure VI.20: Intersection damage map. Slice surface 4. Block CH02B04



Block CH02B05

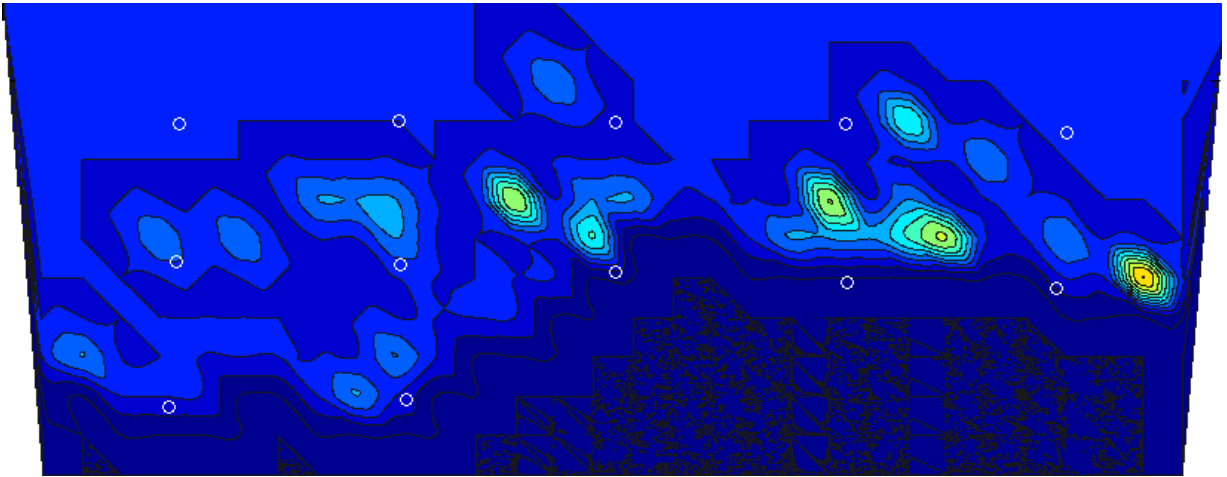


Figure VI.21: Intersection damage map. Slice surface 1. Block CH02B05

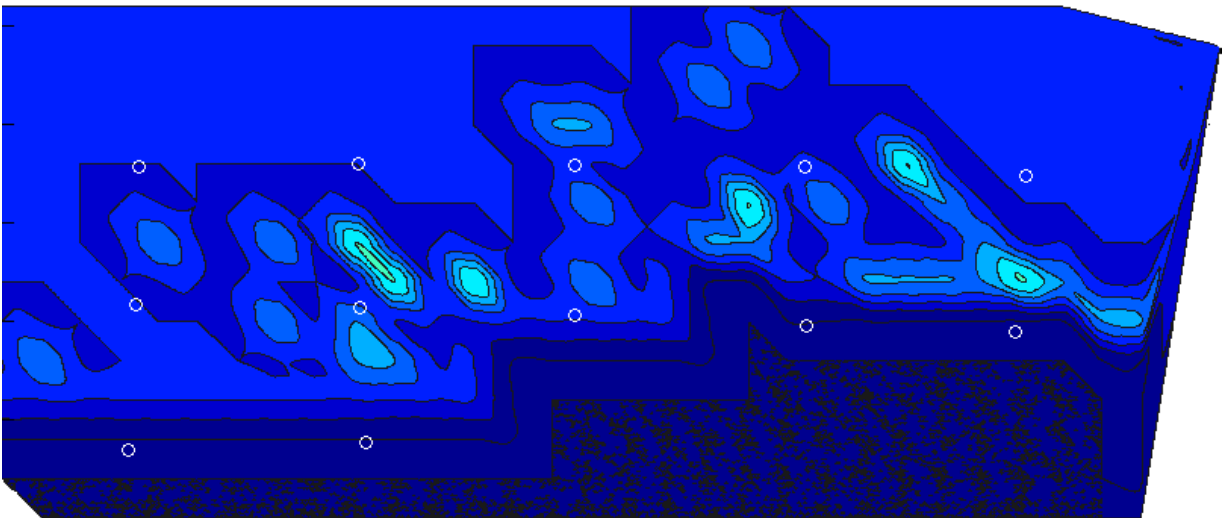


Figure VI.22: Intersection damage map. Slice surface 2. Block CH02B05

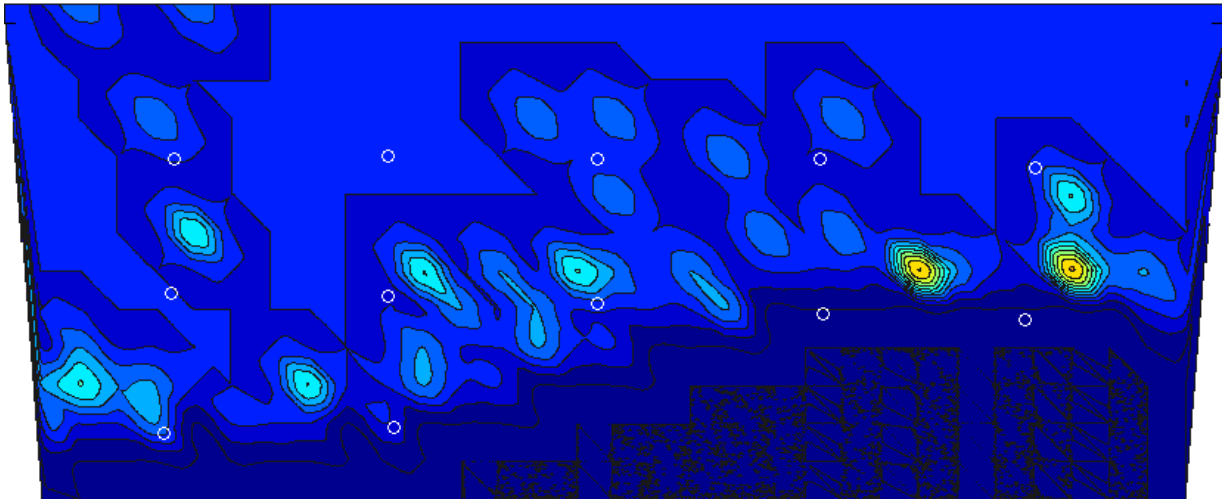


Figure VI.23: Intersection damage map. Slice surface 3. Block CH02B05

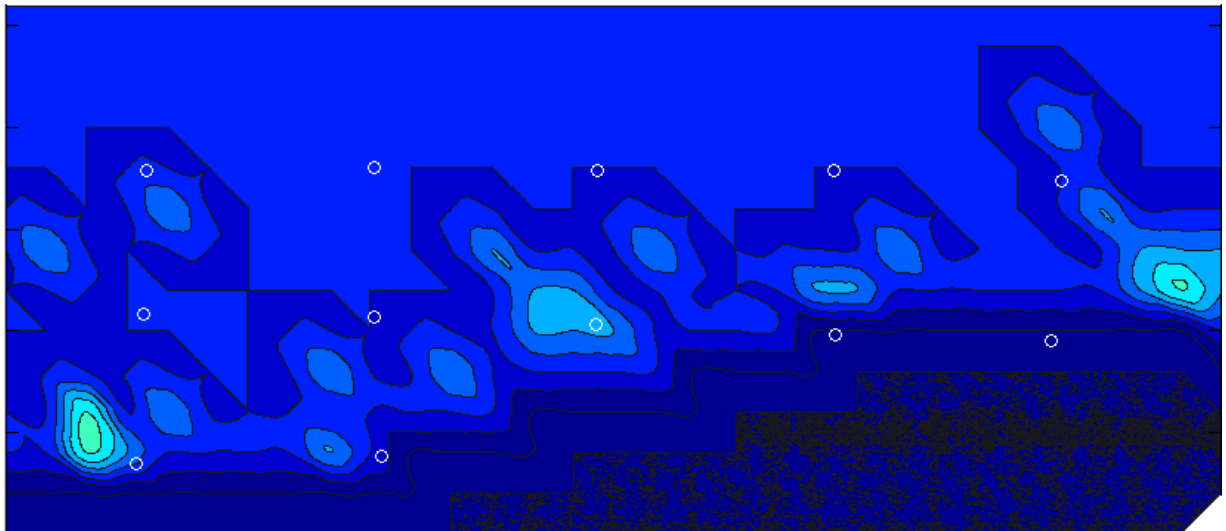
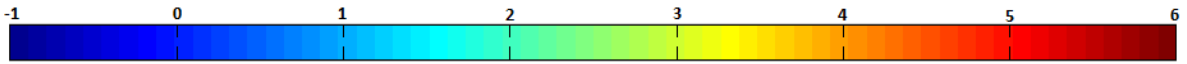


Figure VI.24: Intersection damage map. Bottom. Block CH02B05



Block CH03B04

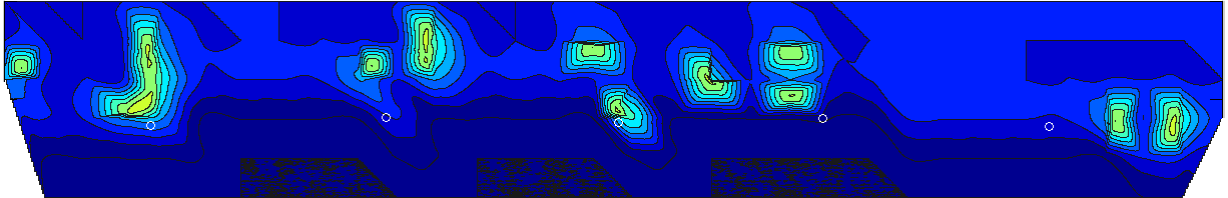


Figure VI.25: Intersection damage map. Slice surface 1. Block CH03B04



Figure VI.26: Intersection damage map. Slice surface 2. Block CH03B04

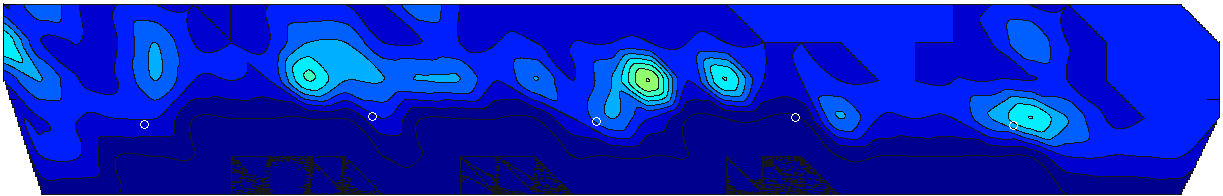


Figure VI.27: Intersection damage map. Slice surface 3. Block CH03B04

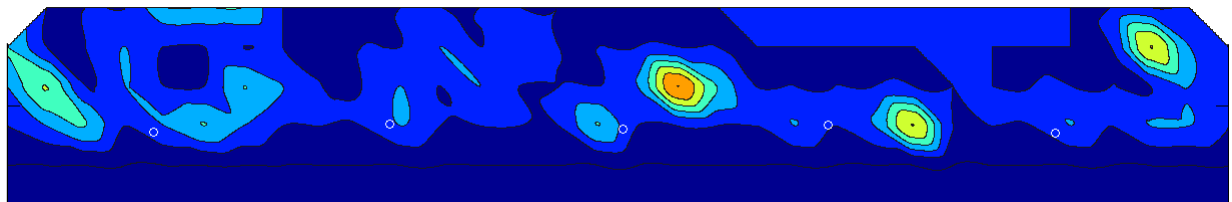


Figure VI.28: Intersection damage map. Slice surface 4. Block CH03B04



Block CH03B05

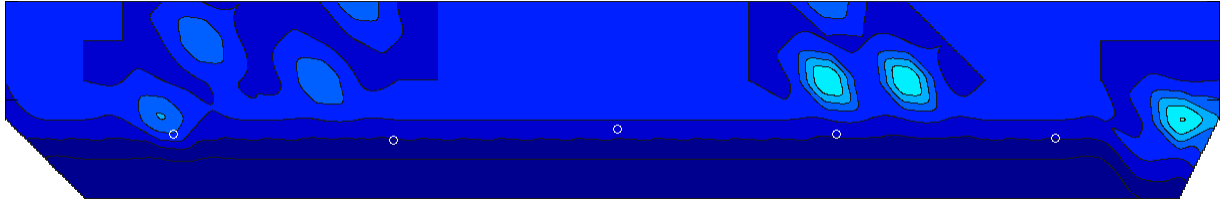


Figure VI.29: Intersection damage map. Slice surface 1. Block CH03B05

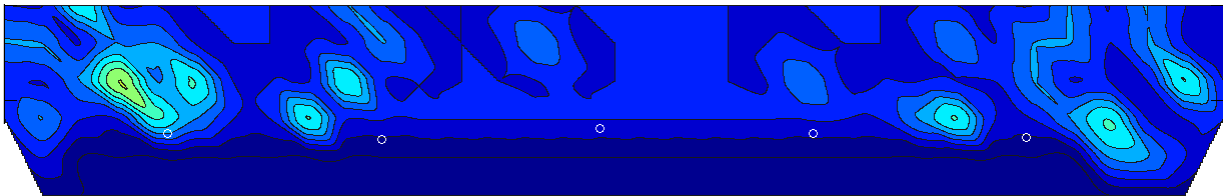


Figure VI.30: Intersection damage map. Slice surface 2. Block CH03B05

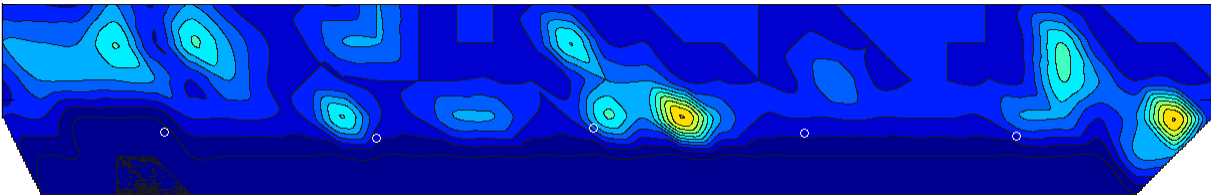


Figure VI.31: Intersection damage map. Slice surface 3. Block CH03B05

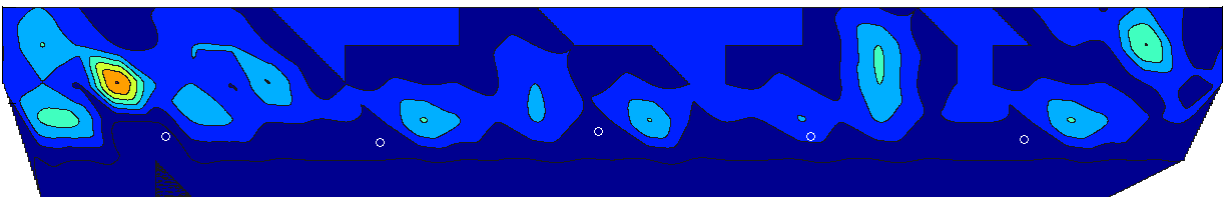


Figure VI.32: Intersection damage map. Slice surface 4. Block CH03B05

ANNEX VII: ANOVA F-Test an Kruskal Wallis methods

One Way ANOVA F-Test

As explained by Lane (onlinestatbook.com), “analysis of variance is a method for testing differences among means by analyzing variance. The test is based on two estimates of the population variance (σ^2). One estimate is called the mean square error (MSE) and is based on differences among scores within the groups. MSE estimates σ^2 regardless of whether the null hypothesis is true (the population means are equal). The second estimate is called the mean square between (MSB) and is based on differences among the sample means. MSB only estimates σ^2 if the population means are equal. If the population means are not equal, then MSB estimates a quantity larger than σ^2 . Therefore, if the MSB is much larger than the MSE, then the population means are different. On the other hand, if the MSB is about the same as MSE, then the data are consistent with the null hypothesis that the population means are equal”.

The following assumptions made by ANOVA must be considered:

1. Homogeneity of variance: the populations have the same variance.
2. The populations are normally distributed.
3. Each value is sampled independently from every other value. In this way, each subject provides only one value. If a subject provides two scores, then the values are not independent.

These assumptions are the same as for a t-test of differences between groups except that they apply to two or more groups, not just to two groups.

Step 1) Sample sizes

The first step is to assume that there are an equal number of observations in each group. The number of observations in each group is called n and the total number of observations N .

Step 2) Calculation of MSE

According to the assumption of homogeneity of variance states, the variance within each of the populations (σ^2) must be the same. This variance (σ^2) is the quantity estimated by MSE and is calculated as the mean of the sample variances.

Step 3) Calculation of MSB

The MSB is calculated as the variance of the sampling distribution of the mean:

$$\sigma_M^2 = \frac{\sigma^2}{n}$$

where n is the sample size of each group and σ_M^2 is the variance of the means. Rearranging this formula, the variance (σ^2) can be calculated as:

$$\sigma^2 = n \cdot \sigma_M^2$$

In case that the variance of the sampling distribution of the mean is not known, it can be estimated with the variance of the sample means.

In this way, if the population means are equal, then both MSE and MSB are estimates of σ^2 and should be about the same, but not exactly the same, since they are estimated and are based on different aspects of the data: The MSB is computed from the sample means and the MSE is computed from the sample variances.

On the other hand, if the population means are not equal, then MSE will still estimate σ^2 because differences in population means do not affect variances. However, differences in population mean will affect MSB since they are associated with differences among sample means. Therefore the larger the differences among sample means, the larger the MSB.

Step 4) Comparing MSE and MSB

The critical step in the ANOVA test is comparing MSE and MSB. As explained by Lane (onlinestatbook.com), *“since MSB estimates a larger quantity than MSE only when the population means are not equal, a finding of a larger MSB than an MSE is a sign that the population means are not equal. But since MSB could be larger than MSE by chance even if the population means are equal, MSB must be much larger than MSE in order to justify the conclusion that the population means differ”*.

In this way, the probability of getting that big a difference or a bigger difference if the population means were all equal must be known. The standard method for

determining this probability is based on the ratio of MSB to MSE. This ratio is named after Fisher and is called the F_{ratio} (Lane: onlinestatbook.com):

$$F_{ratio} = \frac{MSB}{MSE}$$

The shape of the F distribution depends on two degrees of freedom (df) parameters: one for the numerator (MSB) and one for the denominator (MSE). As said by Lane (onlinestatbook.com), “*the degrees of freedom for an estimate of variance are equal to the number of observations minus one. Since the MSB is the variance of k means, it has k - 1 df. The MSE is an average of k variances, each with n - 1 df. Therefore, the df for MSE is k (n - 1) = N - k, where N is the total number of observations, n is the number of observations in each group, and k is the number of groups*”. To summarize:

$$df_{numerator} (dfn) = k-1$$

$$df_{denominator} (dfd) = N-k$$

Step 5) Sources of variation

In ANOVA, the term sum of squares (SSQ) is used to indicate variation. The total variation is defined by Lane (onlinestatbook.com) as “*the sum of squared differences between each score and the mean of all subjects*”. The mean of all subjects is called the grand mean (GM). In this way, when there are an equal number of subjects in each condition, the GM is the mean of the condition means. The total sum of squares is calculated by subtracting the GM from each score (X), squaring the difference and finally summing up the obtained values:

$$SSQ_{total} = \sum (X - GM)^2$$

The sum of squares condition is calculated as shown below.

$$SSQ_{condition} = n[(M_1 - GM)^2 + (M_2 - GM)^2 + \dots + (M_k - GM)^2]$$

where n is the number of scores in each group, k is the number of groups, M_1 is the mean for Condition 1, M_2 is the mean for Condition 2, and M_k is the mean for Condition k.

If there are unequal sample sizes, then the formula is used for the sum of squares condition:

$$SSQ_{condition} = n_1 \cdot (M_1 - GM)^2 + n_2 \cdot (M_2 - GM)^2 + \dots + n_k \cdot (M_k - GM)^2$$

where n_i is the sample size for each condition. SSQ_{total} is calculated in the same way as shown above.

The sum of squares error is the sum of the squared deviations of each score from its GM. This can be written as:

$$SSQ_{error} = \sum (X_{i1} - M_1)^2 + \sum (X_{i2} - M_2)^2 + \dots + \sum (X_{ik} - M_k)^2$$

where X_{i1} is the score in group 1 and M_1 is the mean for group 1, X_{i2} is the score in group 2 and M_2 is the mean for group 2, etc.

Once the sums of squares have been done, the mean squares (MSB and MSE) can be calculated according to the following formulas:

$$MSB = \frac{SSQ_{condition}}{dfn}$$

$$MSE = \frac{SSQ_{error}}{dfd}$$

The probability value (P-value) is finally obtained by testing against the F-distribution with the degrees of freedom associated with the numerator and denominator of the ratio. The P-value is the probability of getting such an F_{ratio} . Larger F_{ratio} give smaller P-values.

For a given alpha (α = significance level), usually 0.05, the $F_{critical}$ value is the F value which 100 % of the null sampling distribution occurs. If the statistic is smaller than the critical value ($F_{critical}$), the null hypothesis is retained because the P-value must be bigger than α , but if the statistic is equal to or bigger than the critical value, the null hypothesis is rejected because the P-value must be equal to or smaller than α . When the null hypothesis is rejected, we say that there are significant differences between the group means (crack families).

Kruskal Wallis

As is explained in the *Graham Hole Research Skills Kruskal-Wallis handout, version 1.0*, “the Kruskal-Wallis H test is a rank-based nonparametric test that can be used to determine whether there are statistically significant differences between two or more groups of an independent variable on a continuous or ordinal dependent variable. It is considered the nonparametric alternative to the one-way ANOVA, and an extension of the Mann-Whitney U test to allow the comparison of more than two independent groups”.

The Kruskal-Wallis H test is a test statistic and cannot tell which specific groups of the independent variable are statistically significantly different from each other; it only tells that at least two groups are different.

Some characteristics of the Kruskal-Wallis test are the following:

- No assumptions are made about the type of underlying distribution.
- It is assumed that all groups have a distribution with the same shape.
- No population parameters are estimated.

The Kruskal Wallis test is calculated following the steps below:

- 1) Rank all of the values, ignoring the group to which they belong. The procedure for ranking is as followed: the lowest value gets the lowest rank. If two or more values are the same then they are "tied". Each "tied" value gets the average of the summed ranks that all the tied values would have obtained.
- 2) Calculate total of the ranks for each group by just adding together all of the ranks for each group in turn.
- 3) Find the value of “H”:

$$H = \left[\frac{12}{N(N+1)} \cdot \sum \frac{T_c^2}{n_c} \right] - 3 \cdot (N + 1)$$

where:

N is the total number of data (all groups combined);

T_c is the rank total for each group; and

n_c is the number of data in each group.

- 4) The degrees of freedom (d.f.) are the number of groups minus one.

- 5) Assessing the significance of H that depends on the number of data and the number of groups. H is statistically significant if it is equal to or larger than the critical value of Chi-Square (X^2) for a particular d.f. and the alpha (α) value.

ANNEX VIII: Data crack detection families

CHO2B01							
Family	Length	Slice 1	Slice 2	Slice 3	Slice 4	Total	
CB 90-80	long	4	4	4	1	13	13
	short	0	0	0	0	0	
CB 80-30	long	2	1	2	3	8	15
	short	0	5	1	1	7	
CB 30-0	long	6	7	9	9	31	42
	short	1	4	4	2	11	
SCB	long	1	1	2	2	6	12
	short	0	2	0	4	6	
Parallel	long	1	0	1	2	4	9
	short	0	3	0	2	5	
Connections		3	4	3	3	13	
Dir 90-80	long	0	2	0	1	3	5
	short	0	0	0	2	2	
Dir 80-30	long	2	2	3	1	8	25
	short	3	4	4	6	17	
Dir 30-0	long	1	1	0	0	2	10
	short	3	1	3	1	8	
Short cracks	short	8	5	7	4	24	

Table VIII.1: Data crack detection. Block CH02B01

CHO2B02							
Family	Length	Slice 1	Slice 2	Slice 3	Slice 4	Total	
CB 90-80	long	4	4	3	4	15	18
	short	1	1	1	0	3	
CB 80-30	longg	6	5	2	1	14	23
	short	2	2	4	1	9	
CB 30-0	long	3	4	5	6	18	33
	short	7	2	4	2	15	
SCB	long	0	3	5	4	12	28
	short	3	4	3	6	16	
Parallel	long	1	0	0	2	3	4
	short	1	0	0	0	1	
Connections		2	2	3	2	9	
Dir 90-80	long	2	0	0	1	3	6
	short	1	1	1	0	3	
Dir 80-30	long	3	1	1	2	7	31
	short	7	6	3	8	24	
Dir 30-0	long	0	0	0	0	0	17
	short	6	2	6	3	17	
Short cracks	short	4	2	5	7	18	

Table VIII.2: Data crack detection. Block CH02B02

CHO2B03							
Family	Length	Slice 1	Slice 2	Slice 3	Slcie 4	Total	
CB 90-80	long	3	3	3	2	11	11
	short	0	0	0	0	0	
CB 80-30	long	1	2	5	1	9	20
	short	3	3	0	5	11	
CB 30-0	long	2	1	10	8	21	34
	short	2	5	5	1	13	
SCB	long	2	3	4	3	12	19
	short	1	1	4	1	7	
Parallel	long	5	2	4	6	17	31
	short	4	4	6	0	14	
Connections		0	1	3	2	6	
Dir 90-80	long	0	0	0	1	1	12
	short	1	3	4	3	11	
Dir 80-30	long	2	2	2	2	8	25
	short	6	5	2	4	17	
Dir 30-0	long	1	0	0	2	3	20
	short	3	6	2	6	17	
Short cracks	short	4	2	7	3	16	

Table VIII.3: Data crack detection. Block CH02B03

CHO2B04							
Family	Length	Slice 1	Slice 2	Slice 3	Slcie 4	Total	
CB 90-80	long	5	4	4	2	15	16
	short	0	1	0	0	1	
CB 80-30	long	7	5	6	4	22	37
	short	2	2	5	6	15	
CB 30-0	long	4	8	2	3	17	26
	short	0	1	5	3	9	
SCB	long	3	3	1	3	10	24
	short	1	5	3	5	14	
Parallel	long	3	4	4	2	13	33
	short	4	4	5	7	20	
Connections		2	3	2	2	9	
Dir 90-80	long	0	0	1	0	1	6
	short	1	0	2	2	5	
Dir 80-30	long	1	0	5	2	8	30
	short	2	4	9	7	22	
Dir 30-0	long	0	1	0	1	2	12
	short	1	1	0	8	10	
Short cracks	short	0	3	3	7	13	

Table VIII.4: Data crack detection. Block CH02B04

CHO3B04							
Family	Length	Slice 1	Slice 2	Slice 3	Slice 4	Total	
CB 90-80	long	5	5	4	2	16	17
	short	0	0	1	0	1	
CB 80-30	long	1	1	1	5	8	21
	short	2	3	5	3	13	
CB 30-0	long	2	3	5	4	14	28
	short	2	4	3	5	14	
SCB	long	0	4	0	1	5	8
	short	1	1	0	1	3	
Parallel	long	1	1	1	1	4	14
	short	1	4	2	3	10	
Connections		2	3	2	3	10	
Dir 90-80	long	0	0	0	0	0	3
	short	1	0	0	2	3	
Dir 80-30	long	2	2	4	2	10	21
	short	2	2	4	3	11	
Dir 30-0	long	1	2	1	0	4	12
	short	1	3	0	4	8	
Short cracks	short	6	3	0	4	13	

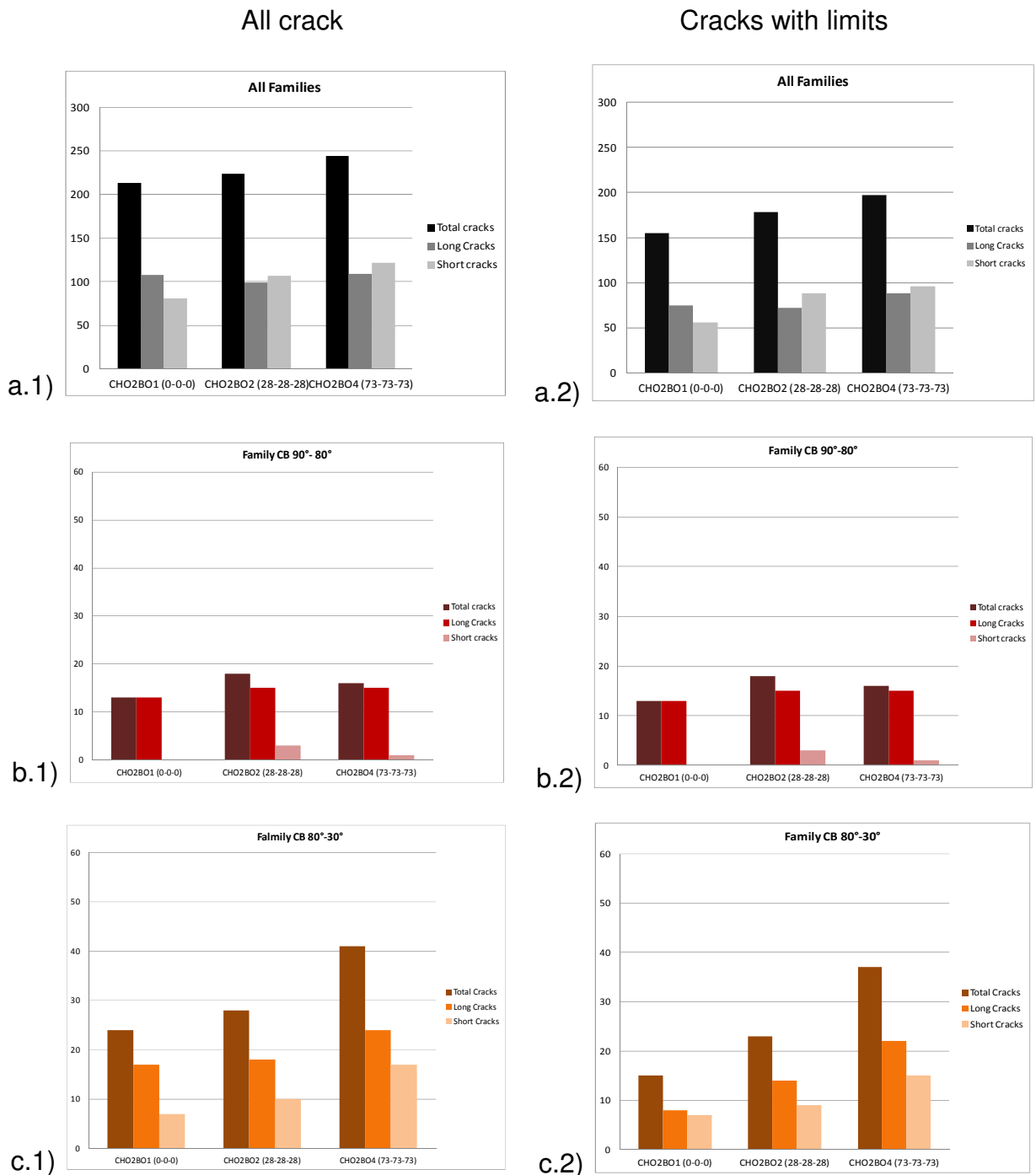
Table VIII.5: Data crack detection. Block CH03B04

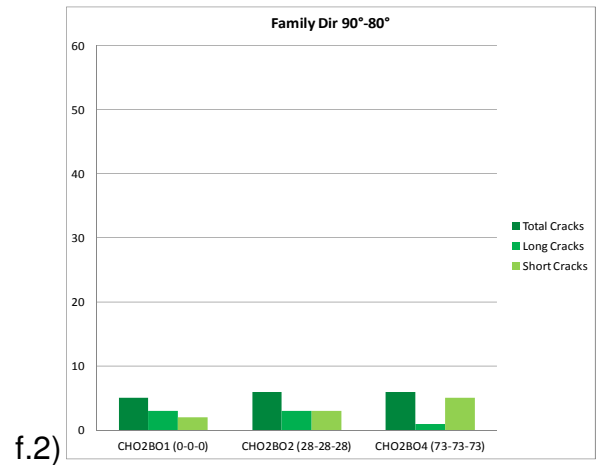
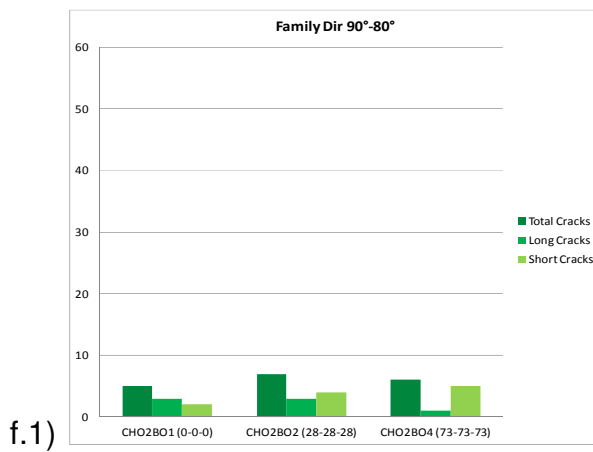
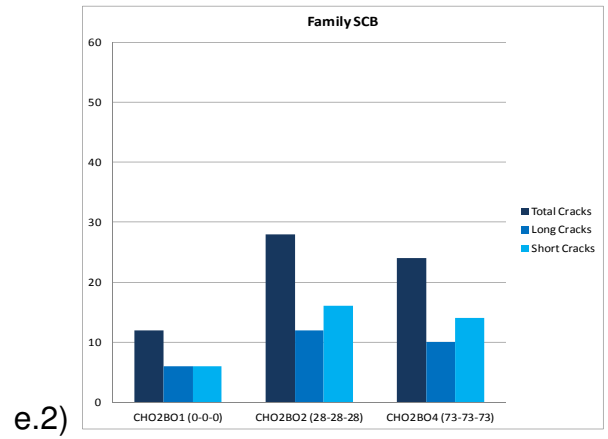
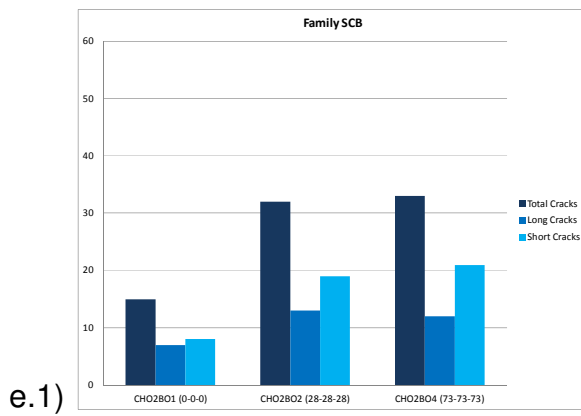
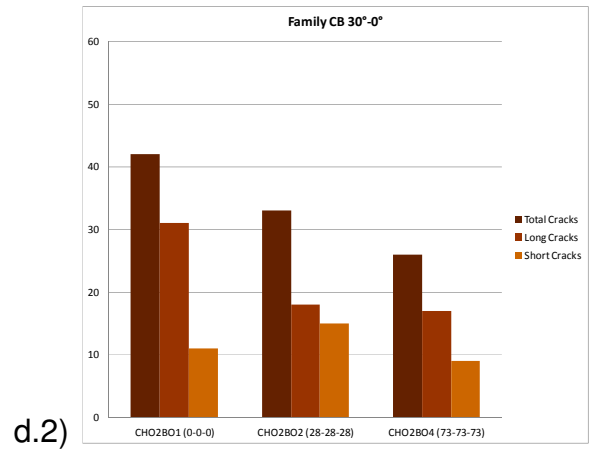
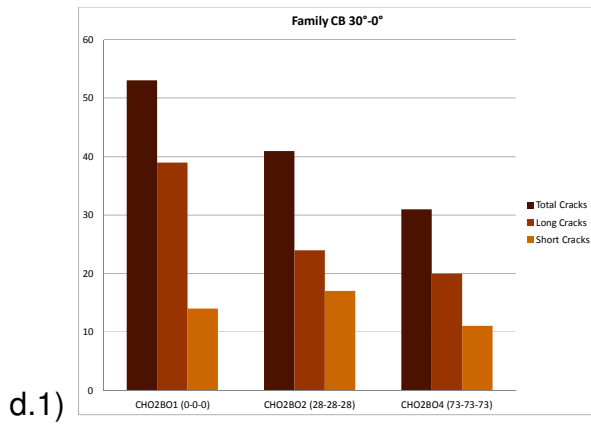
CHO3B05							
Family	Length	Slice 1	Slice 2	Slice 3	Slcie 4	Total	
CB 90-80	long	5	5	5	3	18	19
	short	0	0	0	1	1	
CB 80-30	long	1	1	4	2	8	17
	short	1	2	3	3	9	
CB 30-0	long	2	4	6	2	14	21
	short	2	1	1	3	7	
SCB	long	3	0	1	2	6	10
	short	0	1	1	2	4	
Parallel	long	1	1	0	2	4	12
	short	1	3	3	1	8	
Connections		2	2	2	1	7	
Dir 90-80	long	0	2	0	0	2	7
	short	0	1	3	1	5	
Dir 80-30	long	0	0	2	0	2	14
	short	4	2	6	0	12	
Dir 30-0	long	1	1	0	0	2	12
	short	2	1	4	3	10	
Short cracks	short	5	4	5	7	21	

Table VIII.6: Data crack detection. Block CH03B05

ANNEX IX: Comparison between data when using all the crack information from the slice and when using only cracks inside the edges

Comparison 1: 0-0-0 vs 28-28-28 vs 73-73-73





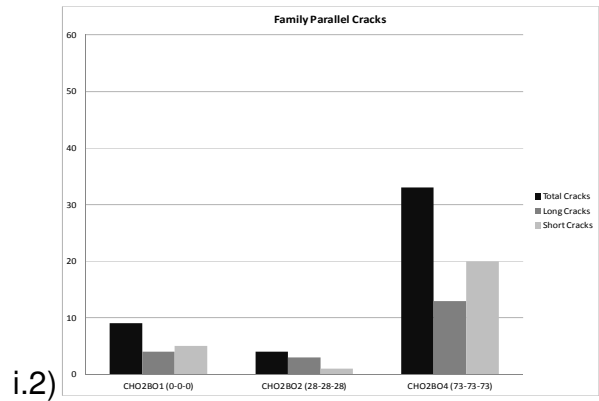
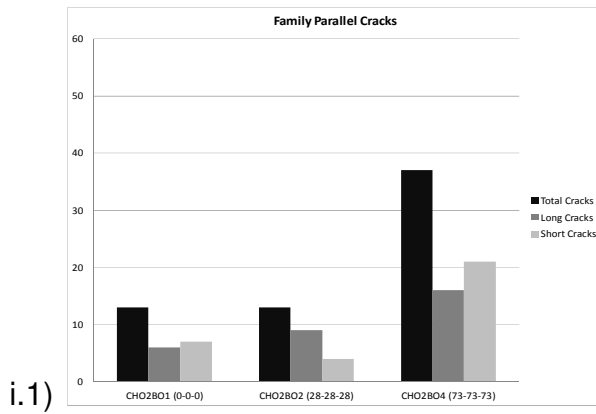
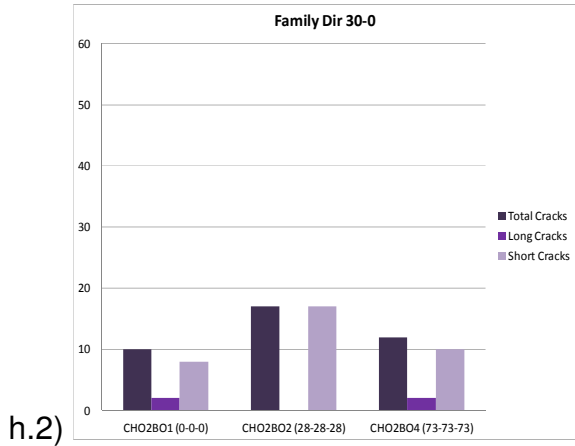
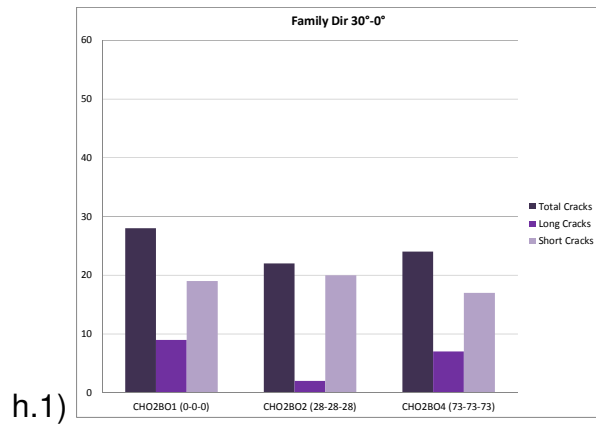
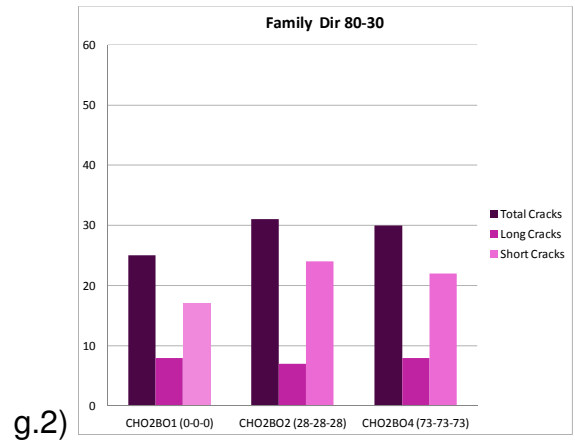
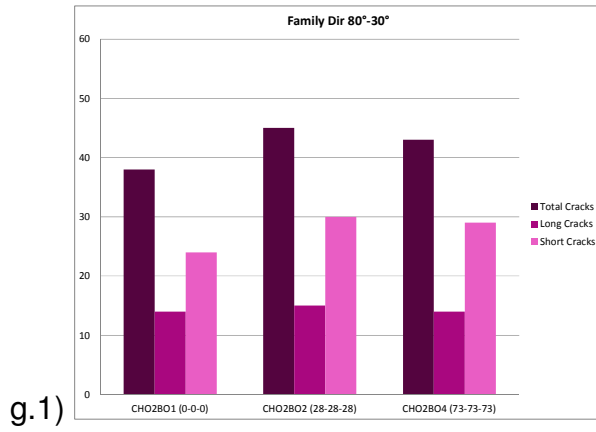
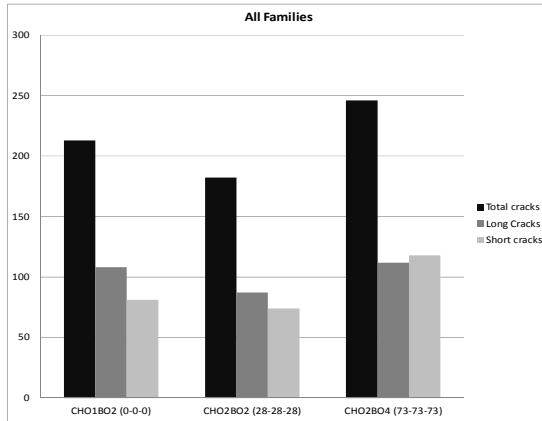


Figure IX.2: Comparison 1: 0-0-0 vs 28-28-28 vs 73-73-73:

a) All Families; b) Family CB 90-80; c) Family CB 80-30; d) Family 30-0; e) Family SCB; f) Family Dir 90-80; g) Family Dir 80-30; h) Family Dir 30-0; i) Family Parallel Cracks

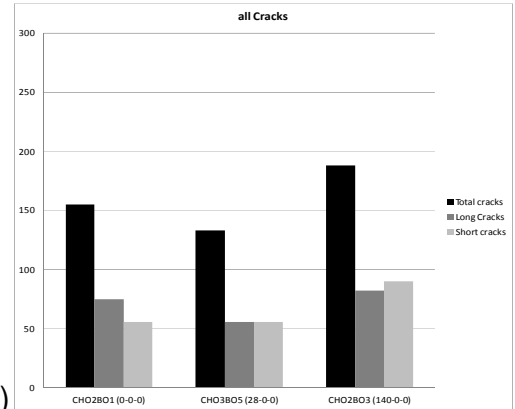
Comparison 2: 0-0-0 vs 28-0-0 vs 140-0-0

All cracks

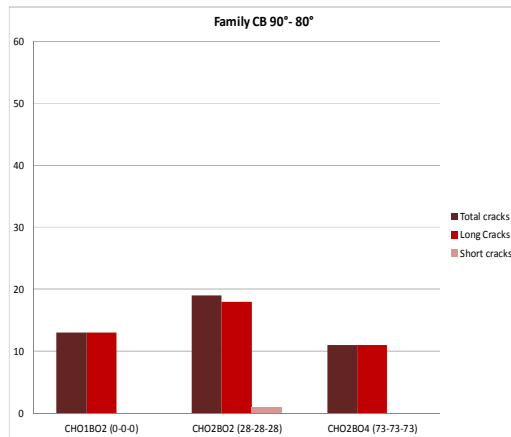


a.1)

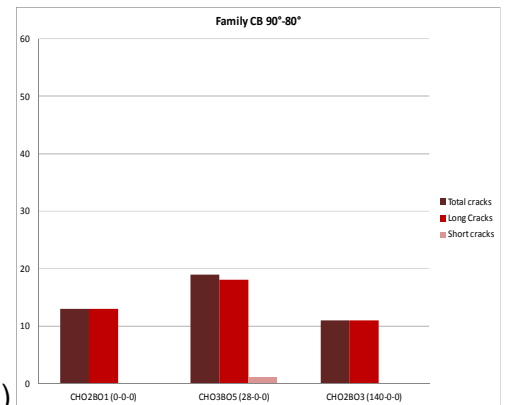
Cracks with limits



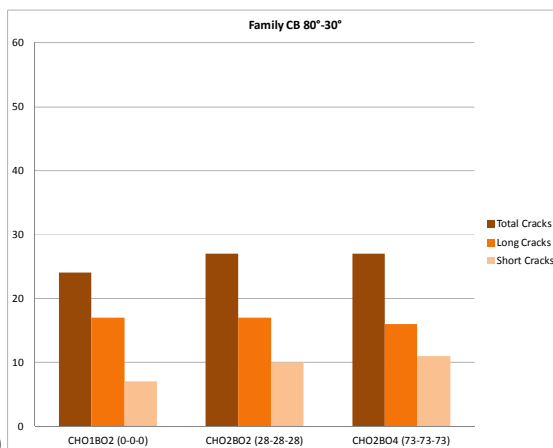
a.2)



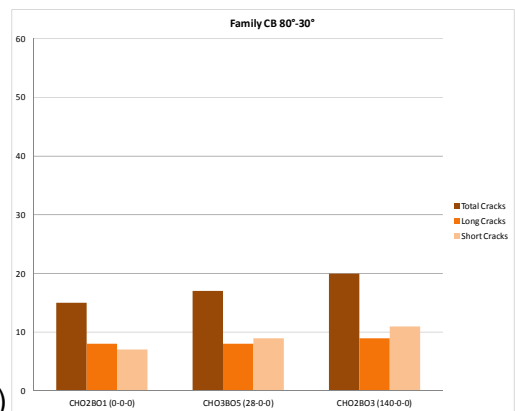
b.1)



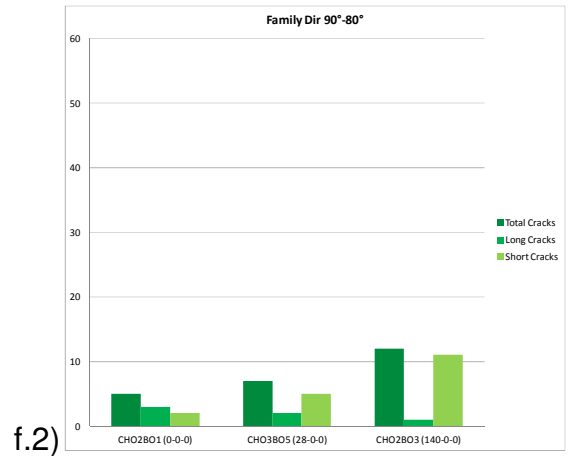
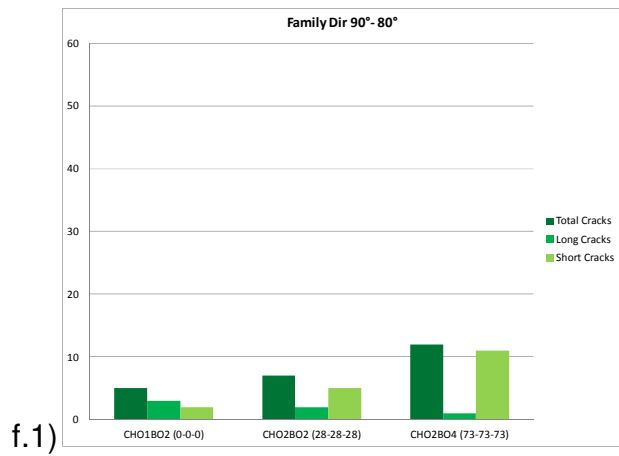
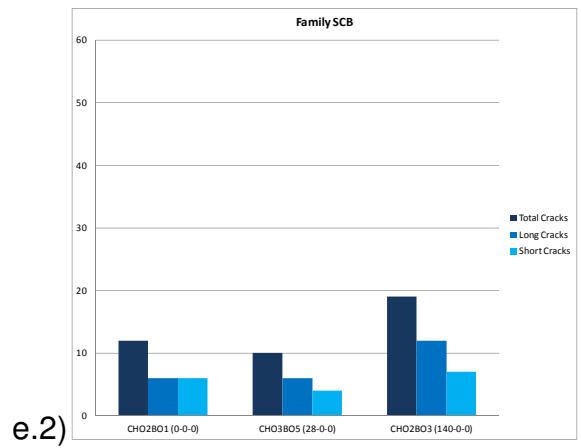
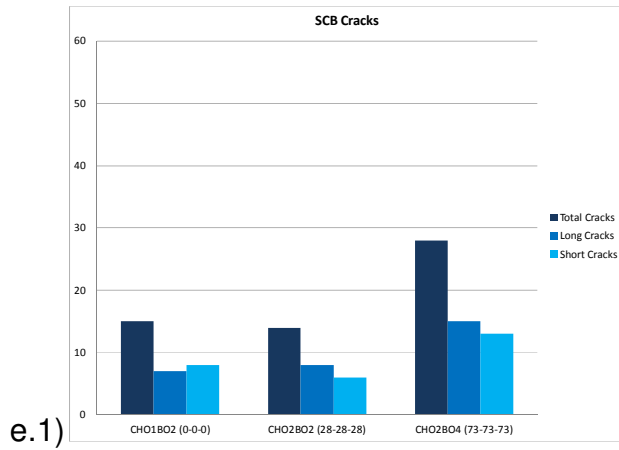
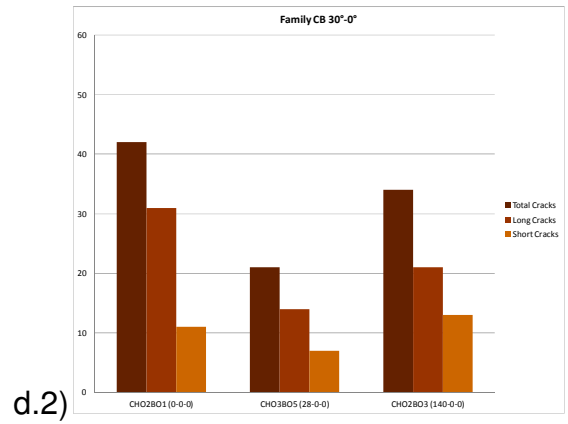
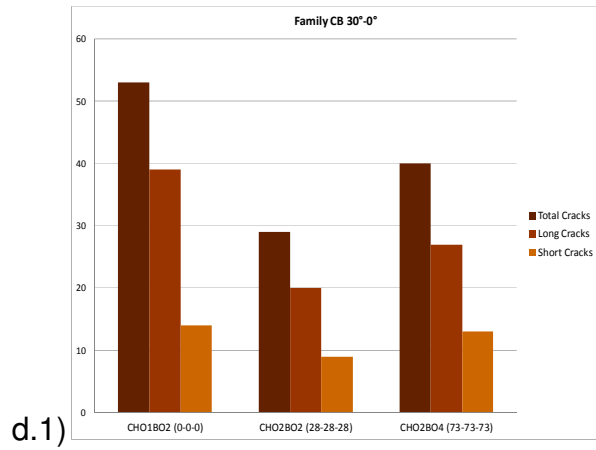
b.2)



c.1)



c.2)



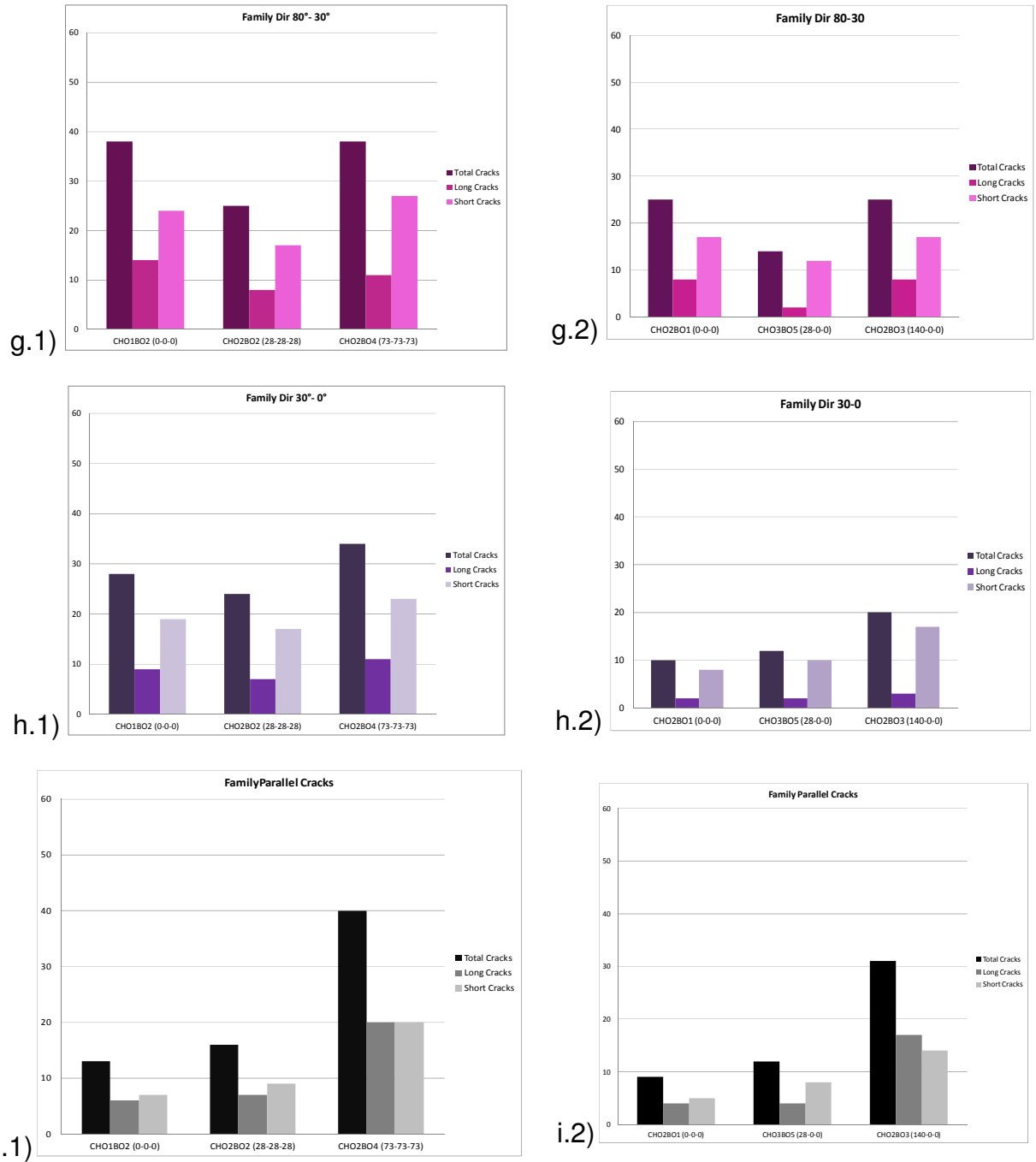
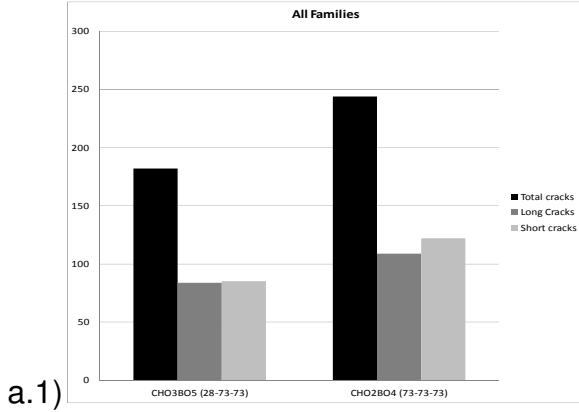


Figure IX.2: Comparison 2: 0-0-0 vs 28-0-0 vs 140-0-0:

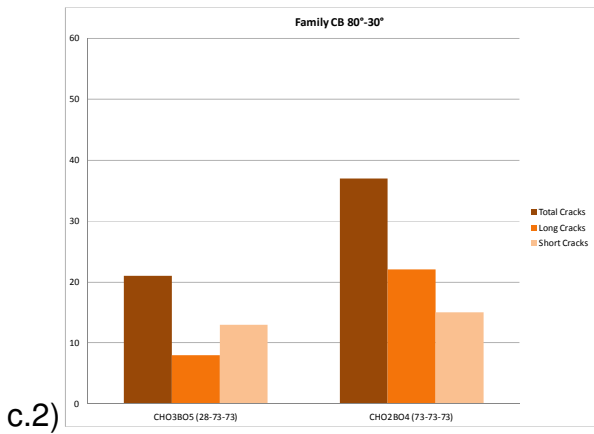
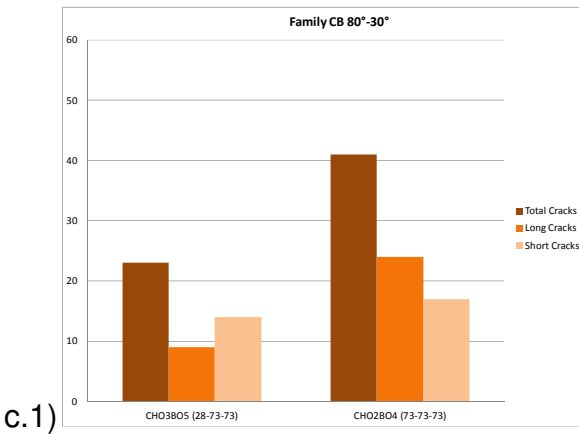
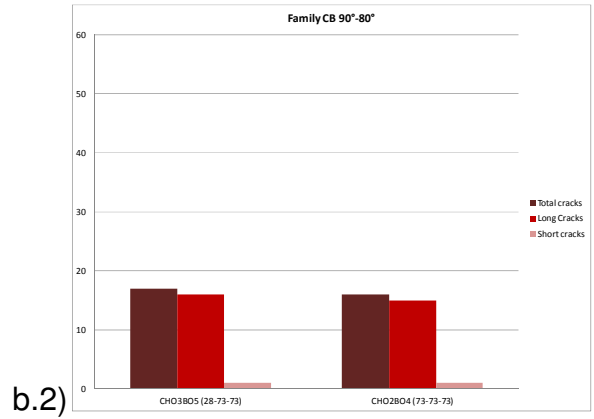
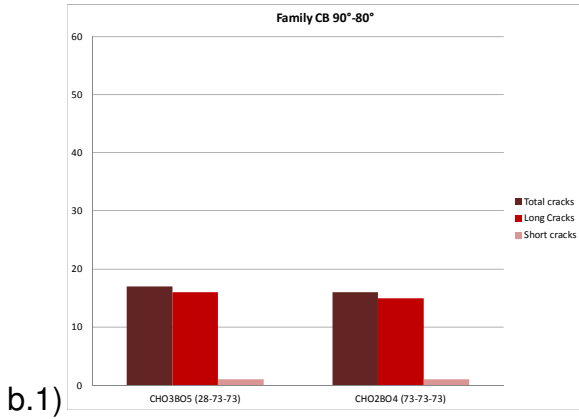
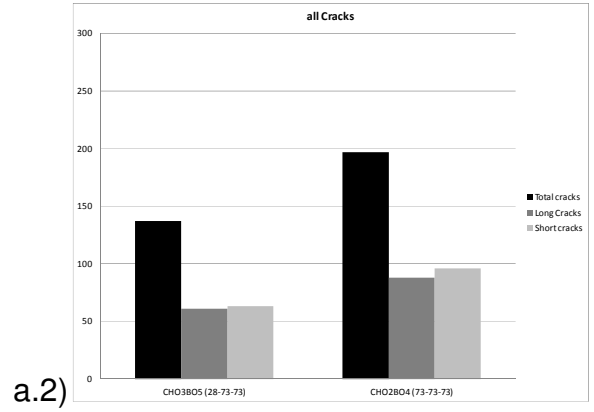
a) All Families; b) Family CB 90-80; c) Family CB 80-30; d) Family 30-0; e) Family SCB; f) Family Dir 90-80; g) Family Dir 80-30; h) Family Dir 30-0; i) Family Parallel Cracks

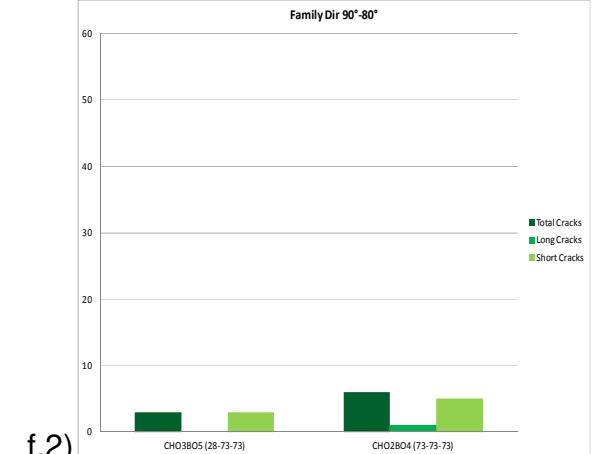
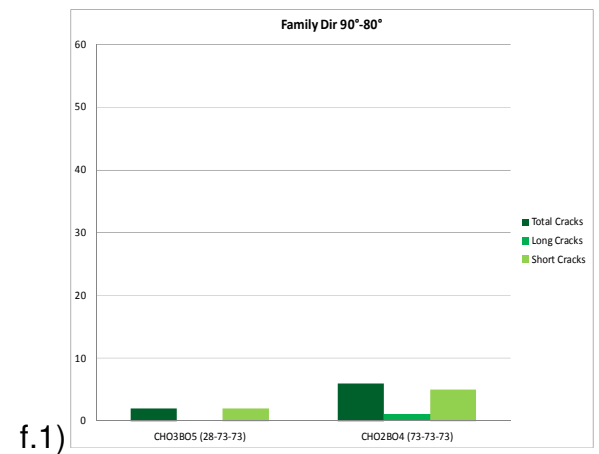
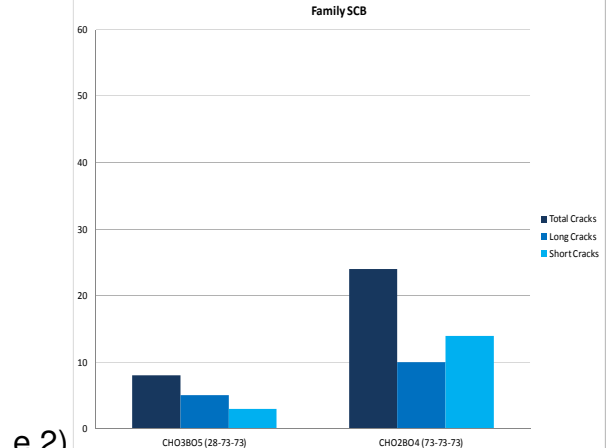
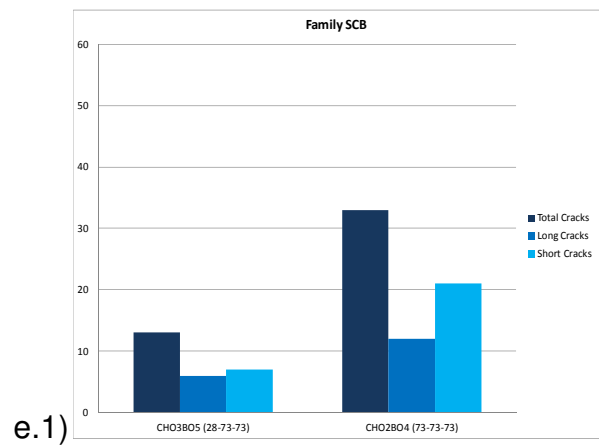
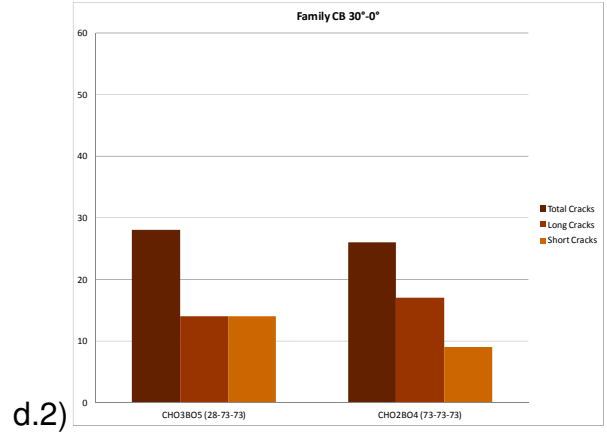
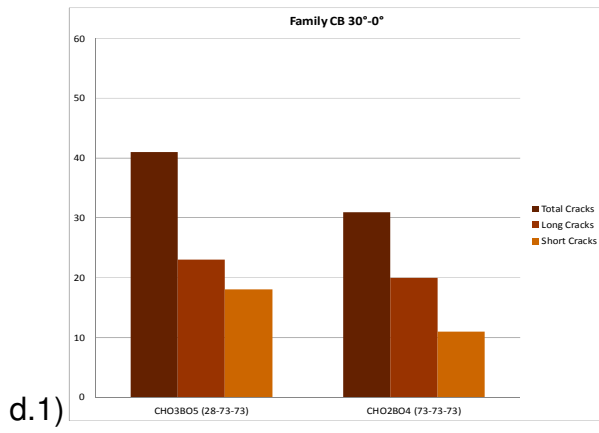
Comparison 3: 28-73-73 vs 73-73-73

All cracks



Cracks with limits





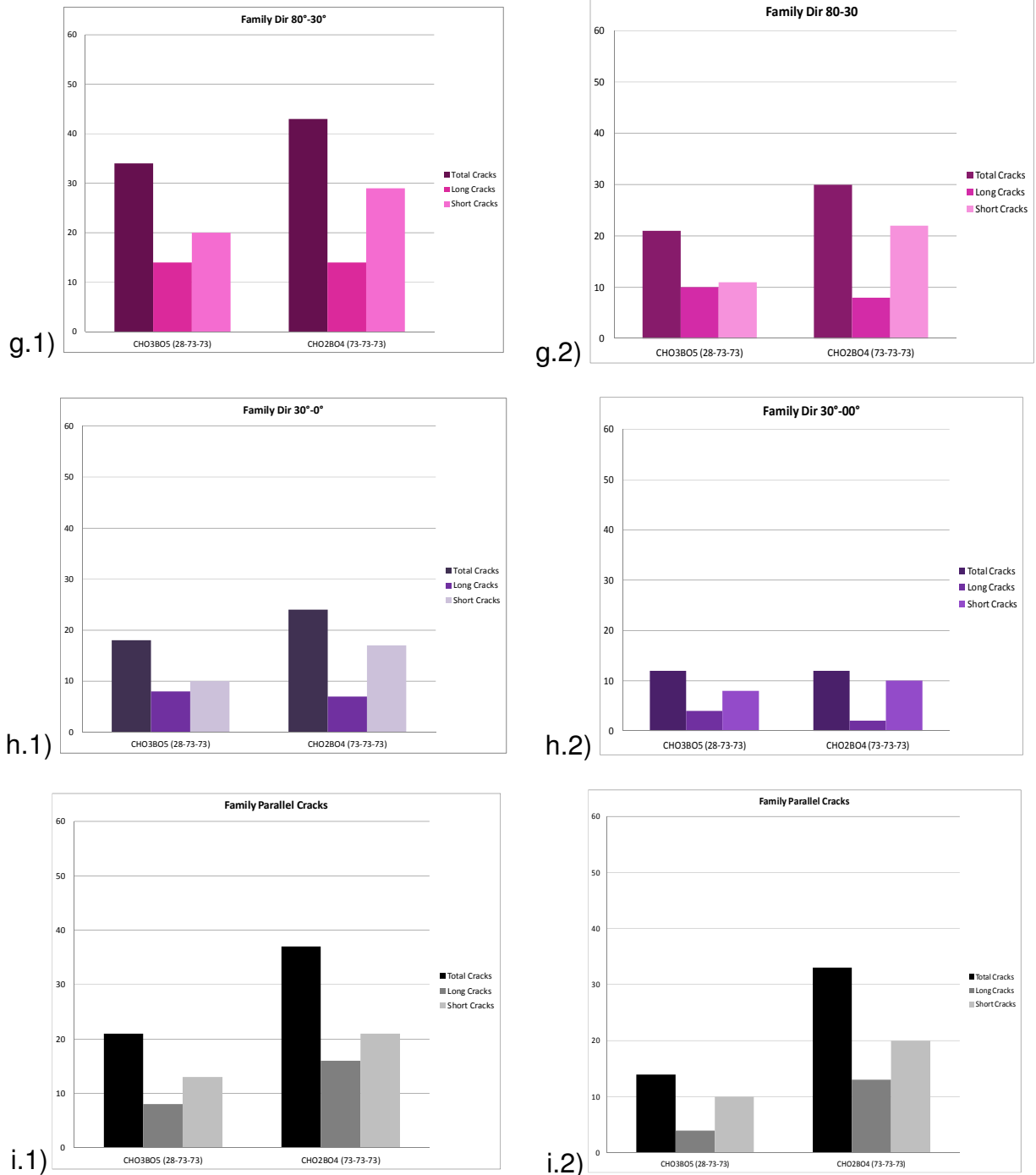


Figure IX.3: Comparison 3: 28-73-73 vs 73-73-73

a) All Families; b) Family CB 90-80; c) Family CB 80-30; d) Family 30-0; e) Family SCB; f) Family Dir 90-80; g) Family Dir 80-30; h) Family Dir 30-0; i) Family Parallel Cracks